

Award Number: DAMD17-01-1-0084

TITLE: Prostate Cancer Detection Using Near Infrared Spectral Polarization Imaging

PRINCIPAL INVESTIGATOR: Robert Alfano, Ph.D.  
Dr. W. B. Wang

CONTRACTING ORGANIZATION: City College of New York  
New York, NY 10031

REPORT DATE: July 2005

TYPE OF REPORT: Final Addendum

PREPARED FOR: U.S. Army Medical Research and Materiel Command  
Fort Detrick, Maryland 21702-5012

DISTRIBUTION STATEMENT: Approved for Public Release;  
Distribution Unlimited

The views, opinions and/or findings contained in this report are those of the author(s) and should not be construed as an official Department of the Army position, policy or decision unless so designated by other documentation.

# REPORT DOCUMENTATION PAGE

Form Approved  
OMB No. 0704-0188

Public reporting burden for this collection of information is estimated to average 1 hour per response, including the time for reviewing instructions, searching existing data sources, gathering and maintaining the data needed, and completing and reviewing this collection of information. Send comments regarding this burden estimate or any other aspect of this collection of information, including suggestions for reducing this burden to Department of Defense, Washington Headquarters Services, Directorate for Information Operations and Reports (0704-0188), 1215 Jefferson Davis Highway, Suite 1204, Arlington, VA 22202-4302. Respondents should be aware that notwithstanding any other provision of law, no person shall be subject to any penalty for failing to comply with a collection of information if it does not display a currently valid OMB control number. **PLEASE DO NOT RETURN YOUR FORM TO THE ABOVE ADDRESS.**

1. REPORT DATE (DD-MM-YYYY) 01-07-2005		2. REPORT TYPE Final Addendum		3. DATES COVERED (From - To) 1 Jul 2004 – 30 Jun 2005	
4. TITLE AND SUBTITLE Prostate Cancer Detection Using Near Infrared Spectral Polarization Imaging				5a. CONTRACT NUMBER	
				5b. GRANT NUMBER DAMD17-01-1-0084	
				5c. PROGRAM ELEMENT NUMBER	
6. AUTHOR(S) Robert Alfano, Ph.D. Dr. W. B. Wang  E-mail: rmaster@sci.ccny.cuny.edu				5d. PROJECT NUMBER	
				5e. TASK NUMBER	
				5f. WORK UNIT NUMBER	
7. PERFORMING ORGANIZATION NAME(S) AND ADDRESS(ES) City College of New York New York, NY 10031				8. PERFORMING ORGANIZATION REPORT NUMBER	
9. SPONSORING / MONITORING AGENCY NAME(S) AND ADDRESS(ES) U.S. Army Medical Research and Materiel Command Fort Detrick, Maryland 21702-5012				10. SPONSOR/MONITOR'S ACRONYM(S)	
				11. SPONSOR/MONITOR'S REPORT NUMBER(S)	
12. DISTRIBUTION / AVAILABILITY STATEMENT Approved for Public Release; Distribution Unlimited					
13. SUPPLEMENTARY NOTES Original contains color plates: ALL DTIC reproductions will be in black and white					
14. ABSTRACT Abstract follows.					
15. SUBJECT TERMS Prostate tumor, invasive optical detection, tissue absorption, emission and scattering, NIR spectral polarization imaging, prostate-cancer-receptor-targeted contrast agents					
16. SECURITY CLASSIFICATION OF:			17. LIMITATION OF ABSTRACT	18. NUMBER OF PAGES	19a. NAME OF RESPONSIBLE PERSON
a. REPORT	b. ABSTRACT	c. THIS PAGE			19b. TELEPHONE NUMBER (include area code)
U	U	U	UU	72	

## ABSTRACT

**Specific aims:** The objective of this grant is to develop a near infrared (NIR) spectral polarization imaging technique for prostate cancer detection. The technique is based on the spectral and polarization properties of light scattered, absorbed and emitted from prostate cancerous and normal tissues, and contrast agents targeted to the prostate cancers.

**Results of finding and their significance:** All of the six specific tasks listed in the revised work statement were performed successfully: (1) NIR spectral polarization imaging measurements were performed on human rectum-membrane-prostate tissue samples (task #1), and the results show that small objects hidden inside host prostate tissues can be imaged and identified through a rectum-and-membrane tissues; (2) imaging measurements of in-vitro prostate cancerous-normal tissue samples (task #2) based on water absorption, and a cancer-receptor-targeted contrast agent (Cybesin) were performed. The results show that the water content may be used for prostate cancer detection, and prostate cancerous tissues takes up more Cybesin agent than that of normal tissues that makes Cybesin a potential candidate maker for prostate cancer detection; (3) a breadboard rectal optical probe used for the prostate NIR scanning imaging unit was designed, built and tested (task #3); (4) the absorption spectra of prostate cancerous and normal tissues were measured (task #4), and the results show that prostate cancerous tissue has less absorption than that of normal tissue at water absorption peaks indicating cancer tissue has less water content than that of normal tissue; (5) preliminary integrating sphere measurements were performed to investigate the difference of scattering length between prostate cancerous and normal tissue (task #5); and (6) steady-state and time-resolved spectral measurements for Cybesin (Task #6) were performed, and results show that Cybesin has polarization preservation property that can be used to improve the contrast between prostate cancerous and normal tissue areas, and to enhance the ability for prostate cancer detection. A number of publications and a patent have been produced.

---

## Table of Contents

Cover.....	
SF 298.....	
Introduction.....	4
Body.....	5
Key Research Accomplishments.....	20
Reportable Outcomes.....	21
Publications .....	22
Presentations.....	22
Patents .....	22
Ph.D. Degree supported.....	23
Conclusions.....	23
References.....	24
Appendices.....	25

**For Army AMRMC Grant DAMD17-01-1-0084**  
(CUNY RF 47462-00-01)

## **Introduction**

The objective of this AMRMC (U. S. Army Medical Research and Materiel Command) research project (DAMD17-01-1-0084) is to develop a novel near infrared (NIR) spectral polarization imaging technique for early detection of prostate cancer. The technique is based on the spectral and polarization properties of light scattered, absorbed and emitted from normal and cancerous prostate tissues, and contrast agents targeted to the prostate cancer receptors.

The research project started on 7/1/2001 for three-years plus an additional one-year no-cost extension. The research was carried in the steps based on the work statement. The revised work statement includes six specific tasks: (1) image model rectum-membrane-prostate tissue samples with and without contrast agents; (2) image in-vitro prostate cancerous-and- normal tissue samples with and without contrast agents; (3) design and build a rectal optical probe for the NIR spectral polarization imaging unit; (4) spectral investigation of water content in prostate cancerous and normal tissues; (5) measure scattering lengths of prostate cancerous and normal tissues using an integrating sphere technique; and (6) spectral measurements of prostate-cancer-receptor-targeted contrast agents.

All of these tasks were performed. A number of papers, presentations, and a patent have been published or to be published, and a breadboard rectal optical probe with a spectral polarization imaging unit has been built and tested.

During the first research year (07/01/01–6/30/02), NIR spectral polarization imaging measurements on several human rectum-membrane-prostate tissue samples (Task #1) obtained from autopsy cases were performed. The results show that small objects hidden inside host prostate tissues can be imaged and identified through a rectum-and-membrane tissues.<sup>1</sup> This indicates that our proposed approach of imaging a prostate gland through rectum using spectral polarization imaging technique is applicable for the prostate screening.

During the second research year (07/01/02–6/30/03), spectral and imaging measurements of in-vitro prostate cancerous-and-normal tissue samples (Tasks #2 & #4) based on the water absorption were performed. The absorption fingerprints of prostate cancerous and normal tissues at water absorption peaks were found, and used to image and detect the prostate cancerous tissues.<sup>2,3</sup> The results show that the water content may be used as a maker for the prostate tissue change.

During the third year (07/01/03–6/30/04), the spectral and imaging studies of in-vitro prostate normal-cancerous tissue samples using a prostate cancer receptor-targeted contrast agent (Tasks #2 & #6), namely Cypate-Bombensin conjugate (called Cybesin) were performed. The absorption and fluorescence spectra of Cybesin were measured. The spectral polarization imaging unit was moved to the Hackensack University Medical Center (HUMC), and the NIR optical imaging measurements on in-vitro prostate tissues were performed, and compared with the pathological results. The taking-up properties of prostate cancerous tissue to prostate-receptor-targeted contrast agents in comparison with that of prostate normal tissue were investigated. The results show that prostate cancerous tissue takes-up more Cybesin agent than that of normal tissues that makes Cybesin a potential candidate maker for prostate cancer detection.<sup>4</sup>

During the fourth year - the no-cost extension year (07/01/04–7/31/05), a breadboard rectal optical probe used for the prostate NIR scanning imaging unit was designed, built and tested (Task #3). The integrating sphere measurements to investigate the difference of scattering length between prostate cancerous and normal tissues (Task #5) were performed. In addition, we carried out the time-resolved fluorescence measurements for prostate cancer receptor-targeted contrast agents (Task # 6) such as Cybesin and Cybesin-stained prostate cancerous and normal tissues. The results show that the Cybesin has polarization preservation property, and the light emitted from the cybesin-stained cancerous tissue shows higher polarization degree than that from the Cybesin-stained prostate normal tissue.<sup>5</sup> These properties can be used to improve the image contrast between the cancerous and normal tissue areas, and to enhance ability to detect prostate cancers.

The details of these accomplishments are described in the next section of “report body”.

## **Report Body**

The following summarizes our major accomplishments during the grant period (7/1/01–7/31/05):

### **(1) Prostate tissue samples studied**

During the 4-year grant period, we have studied two (2) human rectum-membrane-prostate tissue samples from HUMC, forty one (41) prostate normal tissue and fifteen (15) prostate cancerous tissue samples obtained from HUMC (Hackensack University Medical Center), NDRI (National Disease Research Interchange) and CHTN (Cooperative Human Tissue Network – National Cancer Institute) for the proposed spectral and imaging measurements. Table 1 highlights prostate tissue samples studied during the grant period.

All of the spectral and imaging measurements on in-vitro prostate tissue samples were performed under the IRB approvals from both CCNY (City College of New York) and HUMC.

**Table 1. Human prostate tissue samples studied during the grant period**

Sample type	Year 1	Year 2	Year 3	Year 4	Total
Rectum-membrane-prostate tissue	2				2
Prostate normal tissue	5	8	12	16	41
Prostate cancerous tissue	2	3	6	4	15
Supplied sources	HUMC & NDRI	HUMC & NDRI	HUMC & NDRI	HUMC & NDRI & CHTN	

**(2) Imaging measurements on human rectum-membrane-prostate tissue samples (Task # 1)**

Human rectum-membrane-prostate tissue samples were obtained from autopsy cases at HUMC and used for the NIR spectral polarization imaging measurements. The model rectum-membrane-prostate tissue samples were made with a small piece of an object such as an absorber or a tiny piece of prostate tissue stained with a contrast agent (such as indocyanine green) embedded inside a large host piece of prostate tissue in a rectum-membrane-prostate tissue structure as shown in Fig.1. The depth of the object underneath the surface of the rectum-membrane-prostate tissue structure was varied to obtain the depth dependence of the imaging. In the imaging experiments, a white light source was used to illuminate the rectum-membrane-prostate samples, and a CCD camera was used to record the images formed by light scattered or emitted from the samples. The illumination and detection wavelengths were selected in the 550-900 nm range by rotating two sets of wide band filters located on two multiple filter wheels in our NIR spectral polarization imaging unit.<sup>1</sup>

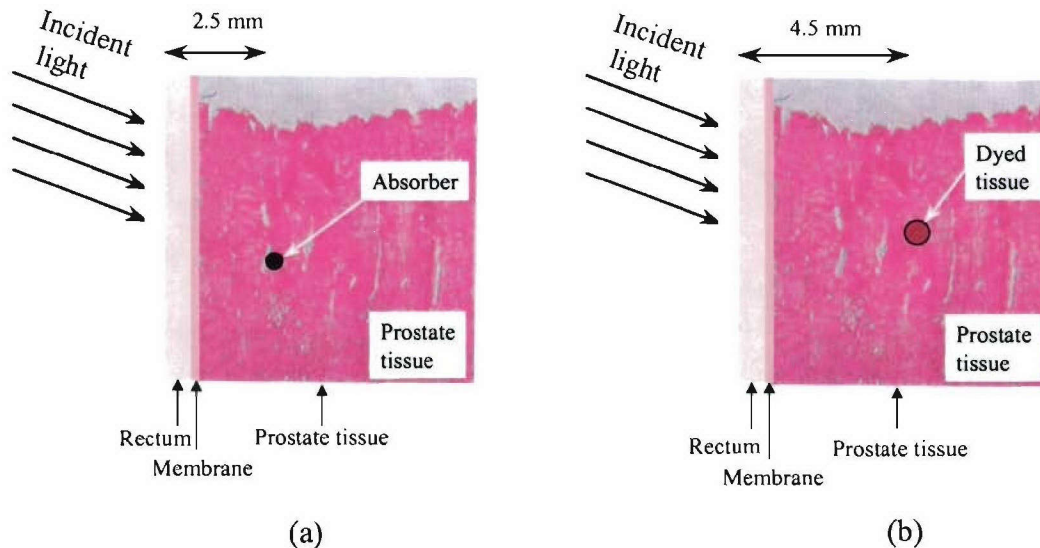


Fig.1 The layer structure of the model rectum-membrane-prostate tissue samples made of (a) a small piece of black absorber, and (b) a tiny piece of prostate tissue dyed with indocyanine green embedded inside larger piece of host prostate tissue in rectum-membrane-prostate structures.

Different spectral polarization imaging methods, including scattered light imaging, tissue emission wing imaging, and contrast agent fluorescence imaging were performed and compared.

The scattered light images for the sample described in Fig.1(a) were recorded at the wavelengths of 600 nm, 700 nm and 800 nm with the detection polarization perpendicular to that of the illumination, and are shown in Figs.2(a) - 2(c). In the images, the object (absorber) can not be distinguished by the 600 nm image, but it can be clearly identified as a dark point by the 800 nm image.<sup>1</sup> As the wavelength increases from 600 nm to 800 nm, the visibility of the object improves. The wavelength dependence of the image quality of the scattered light images can be explained by that the relative absorption of the prostate tissue decreases when the wavelength increases from 400 nm to NIR.<sup>1</sup>

The tissue emission wing images of the sample shown in Fig.1(a) were also investigated. In tissue emission wing imaging measurements, the images recorded by CCD camera were formed by light emitted, not scattered from the prostate tissues at the NIR wing range. The depth for which the object can be identified from the tissue emission wing image was found larger than that for the scattered light imaging. This improvement of detection depth can be understood because the signal light in the tissue emission wing imaging travels shorter distance than that in the scattering light imaging.

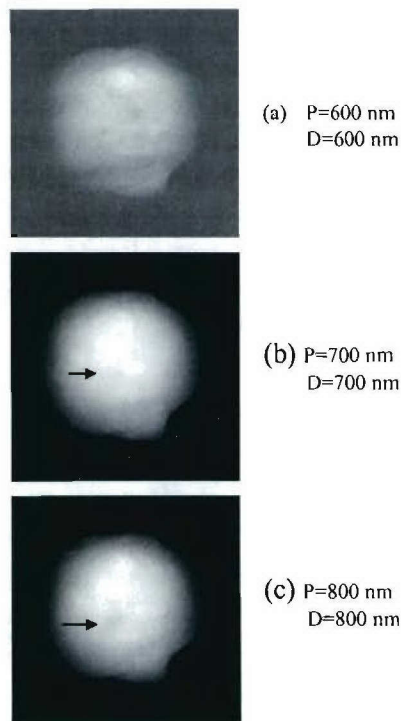


Fig.2 The scattered light images recorded at wavelengths of (a) 600 nm, (b) 700 nm, and (c) 800 nm, respectively, where P: pump, D: detection. The sample consists of a small piece of a black absorber hidden inside a human rectum-membrane-prostate tissue structure at depth of 2.5 mm from the surface of the rectum.

The contrast agent fluorescence light images for the sample described in Fig.1(b) recorded at different pump and detection wavelengths varied from 600 nm to 900 nm are shown in Fig.3. The salient feature of the images is that the dyed object can not be distinguished by images obtained with short wavelength (600 nm and 700 nm) pump, while the object can be clearly identified by the images obtained with longer wavelengths (750 nm and 800 nm) pump. When the pump wavelength increases, the visibility of the dyed object increases dramatically. This pump wavelength dependence can be explained from the relative absorption spectra of prostate tissue and indocyanine green.<sup>1, 6-8</sup> With longer wavelengths (750 nm and 800 nm) pump, the light can penetrate the prostate tissue and reach the dyed object. In addition, the absorption of indocyanine green at 750 nm and 800 nm is strong, and the emission from the dye is much stronger than that of native emission from prostate tissues.<sup>6,7</sup> As a result, the dyed object can be clearly distinguished by the contrast agent fluorescence light images.

The contrast agent fluorescence light imaging measurements were extended to the samples with the dyed tissue embedded at depths of more than 4.5 mm. The results show that the dyed dot tissue with a diameter of  $\sim 1$  mm embedded at 7.5 mm can still be distinguished even the illumination power was only  $\sim 50 \mu\text{w}/\text{cm}^2$ .

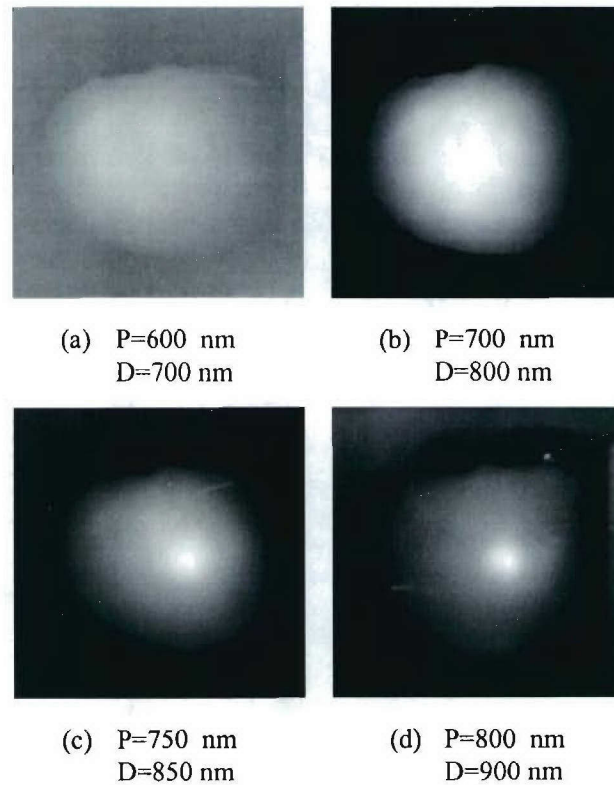


Fig.3 The contrast agent fluorescence images recorded with (a)  $\lambda_{\text{pump}}=600\text{nm}$  and  $\lambda_{\text{detection}}=700\text{nm}$ , (b)  $\lambda_{\text{pump}}=700\text{nm}$  and  $\lambda_{\text{detection}}=800\text{nm}$ , (c)  $\lambda_{\text{pump}}=750\text{nm}$  and  $\lambda_{\text{detection}}=850\text{nm}$ , and (d)  $\lambda_{\text{pump}}=800\text{nm}$  and  $\lambda_{\text{detection}}=900\text{nm}$ , where P: pump, D: detection. The sample consists of a tiny piece of tissue dyed by indocyanine green in a human rectum-membrane-prostate tissue structure at depth of 4.5 mm from the surface of the rectum.

All of these imaging results indicate that even through rectum and membrane tissues, small objects hidden inside the host normal prostate tissues in a human rectum-membrane-prostate tissue structure can still be imaged and identified using the NIR spectral polarization imaging technique, in particular, by the contrast agent fluorescence imaging methods. These results indicate that the NIR spectral polarization imaging technique is a promising noninvasive approach for detecting prostate cancers by imaging prostates through rectum and membrane tissues in real time without removing tissues.

**(3) Spectral and in-vitro imaging measurements based on the absorption fingerprints of prostate cancerous and normal tissues at water absorption peaks (Tasks #2 & # 4)**

The absorption spectra of human prostate normal and cancerous tissues obtained from surgical cases were measured to investigate fingerprints of absorption spectra of prostate cancerous and normal tissues at water absorption peaks.

The results show that there is less absorption in prostate cancerous tissues in comparison with that of normal tissue at the water absorption peaks, which indicates less content of water in the cancerous tissue in comparison with that of prostate normal tissue.<sup>2,3</sup> This difference of water contents and the corresponding absorption spectra between prostate cancerous and normal tissues can be used as fingerprints to distinguish prostate cancerous tissue from the normal tissue.

Fig.4 shows the measured absorption spectra for prostate cancerous and normal tissues in the spectral range of 400 nm to 2400 nm. The salient feature of the curves is that the absorption of prostate cancerous tissue is less than that of normal prostate tissue at several absorption peaks, in particular, at 1195 nm, 1450 nm, and 1930 nm. These peaks are located exactly at the fingerprint absorption peaks of water.<sup>2,3</sup>

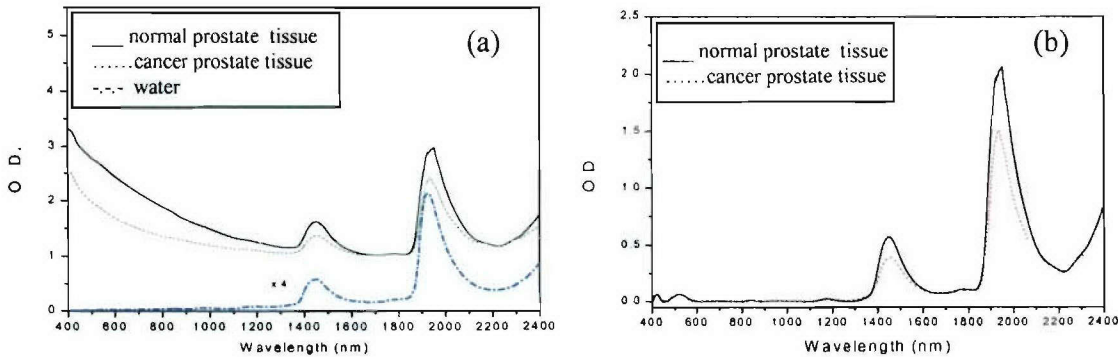


Fig.4 (a) Relative absorption spectra of prostate cancerous tissue (dashed line), normal tissue (solid line) and water (dash-dot-dash line) in the spectral range of 400 nm to 2400 nm, and (b) absorption spectra of prostate cancer tissue (dashed line), and normal tissue (solid line) after removing the scattering contribution by subtracting the scattering wing obtained from the fitting.<sup>2</sup> It can be seen that there is less absorption in prostate cancerous tissue than that in normal tissue at all of the water absorption peaks.

Based on the absorption fingerprints of cancerous and normal tissues found from the spectral measurements, we have performed NIR imaging measurements for in-vitro prostate cancerous and normal tissue samples using an InGaAs NIR CCD imaging system. A model prostate cancerous-normal tissue sample consists of a piece of a prostate cancerous tissue on the right side, and a piece of a prostate normal tissue on the left side. The cancerous tissue cannot be distinguished visually or from a photograph taken using a conventional digital camera as shown in Fig.5(a).

In the imaging measurements, a NIR light source was used to illuminate a model prostate cancerous-normal tissue sample, and an InGaAs NIR CCD camera working in the spectral range of 0.9  $\mu\text{m}$  to 1.7  $\mu\text{m}$  was used to record the images formed by light back-scattered or transmitted from the samples. NIR polarizers and NIR narrow band filters are used to vary the illuminating and detection polarization and wavelengths of the images. Figs.5(b) and 5(c) shows back-scattering images recorded at the fingerprint wavelengths of 1200 nm and 1450 nm, respectively.

In these two NIR back-scattering images, the high intensity areas (right side) correspond to the cancerous tissue areas, while the low intensity areas (left) correspond to the normal tissue areas. The cancerous tissue can be clearly identified from both of these NIR images. The image contrast of the 1450 nm image was found better than that of the 1200 nm image, which can be explained because the difference of absorption between prostate cancerous and normal tissues at the fingerprint wavelength of 1450 nm is much larger than that at 1200 nm.<sup>2</sup>

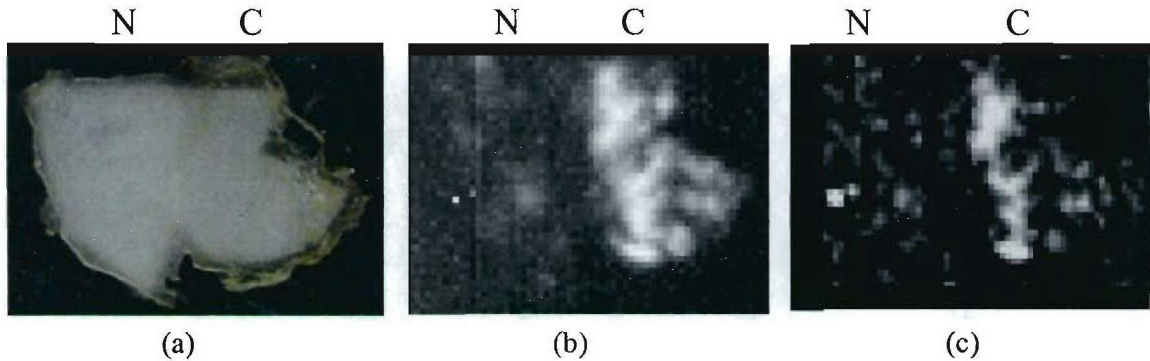


Fig.5 (a) a photograph of a model prostate cancerous and normal tissue sample taken using white light and a conventional digital camera. The sample consists of a piece of prostate normal tissue on the left side and a piece of prostate cancer tissue on the right side. The total sample area is 2x3  $\text{cm}^2$ ; (b) a back-scattering image of the sample recorded at a wavelength of 1200 nm; and (c) a back-scattering image at 1450 nm.<sup>3</sup> The prostate cancerous tissue (right half) are clearly identified by the bright areas from both of the two NIR images.

These imaging results clearly indicate that there is less water content in prostate cancerous tissues (less absorption) than that in normal tissues (more absorption). The NIR imaging using the fingerprint wavelengths of water absorption of prostate cancerous and normal tissues is a potential approach for monitoring the physiological change of the prostate tissues,<sup>9</sup> and identifying the prostate cancer tissue from the surrounding normal tissue.

#### **(4) Spectral investigation of prostate-cancer-receptor-targeted contrast agents, and imaging measurements on in-vitro prostate cancerous and normal tissues (Tasks # 2 & # 6)**

In order to improve image contrast between cancerous and normal tissue areas, and detection ability for prostate cancers, we have investigated prostate cancer-receptor-targeted contrast agents, namely Cypate-Bombesin conjugate (Cybesin) for prostate cancer detection. The previous investigation<sup>10</sup> shows that this Cypate-Bombesin conjugate can be used for pancreas cancer detection, and may be good for other organs and muscle. Our interest is to investigate whether Cybesin can be used for the prostate cancer detection.

The Cybesin is solvable in Dimethyl Sulfoxide (DMSO). The absorption and fluorescence spectra of Cybesin in 20% aqueous Dimethyl Sulfoxide solution were investigated, and the results are shown in Figs. 6(a) and 6(b), respectively. The absorption band of Cybesin covers from 680 nm to 830 nm with a small peak at 720 nm and a strong peak at 792 nm. The fluorescence spectrum covers from 800 nm to 950 nm with a main peak at 825 nm and a weak peak at 925 nm.<sup>4</sup> For the fluorescence measurements, the sample was excited with a 680 nm diode laser.

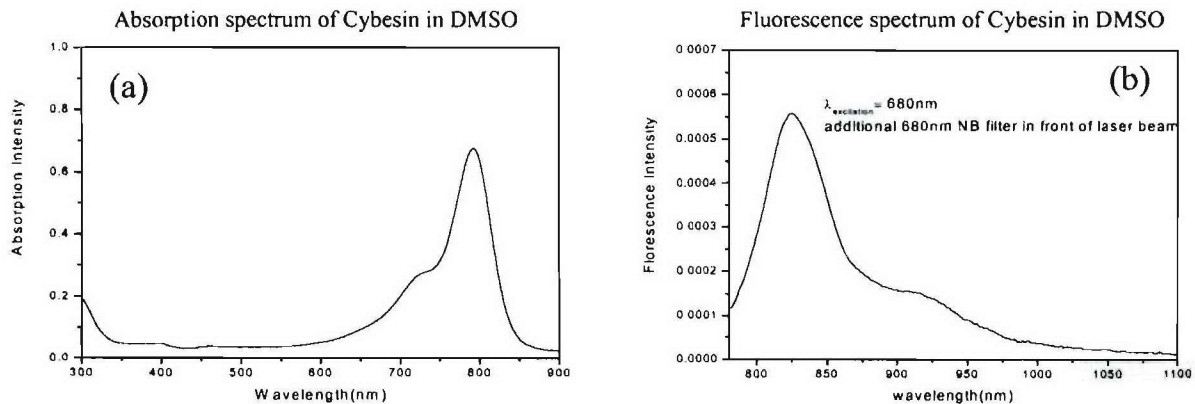


Fig.6 (a) absorption and (b) fluorescence spectra of Cybesin in 20% aqueous Dimethyl Sulfoxide.

Based on the absorption band and fluorescence spectrum of Cybesin, we have selected the pump and detection wavelengths for imaging, and performed contrast agent emission imaging measurements on prostate cancerous and normal tissue samples using a Si-based CCD imaging system. In order to collaborate with urologists and pathologists at HUMC, we moved our spectral polarization imaging unit to HUMC for in-vitro imaging measurements. Eight (8) patients have signed consent forms before their operation, and agreed to allow the researchers using the prostate tissue obtained from their surgeries after completing the pathological section measurements. Six (6) in-vitro prostate cancer-and-normal tissue samples obtained from the surgical cases at HUMC were provided for optical imaging measurements using the prostate cancer targeted contrast agent, Cybesin. The results of pathological section measurements performed at the Pathology Department at HUMC were used as a guide to indicate the locations

of the cancerous and normal tissue areas. The optical imaging measurements were used to compare with the pathological results in collaboration with a pathologist, Dr. S. R. Peters (MD), at HUMC.

A typical prostate cancerous-and-normal tissue sample used for the imaging measurements consists of a small piece of prostate cancer tissue and a small piece of prostate normal tissue. These two small tissue pieces were stained in a same Cybesin-DMSO (Dimethyl Sulfoxide) solution for a same period of time, and then sandwiched into several large host pieces of prostate normal tissue. The schematic diagram of a sandwiched prostate cancerous-and-normal tissue sample is shown in Fig.7.

The backscattering fluorescence images of prostate cancerous-normal tissue samples were recorded at different pump and detection wavelengths, and different polarization configuration between the pump and detection. The best images were obtained at  $\lambda_{\text{pump}}=750$  nm and  $\lambda_{\text{detection}}=850$  nm with perpendicular polarization configuration. The sandwiched structure of the prostate tissue samples was used to test the depth for detection. The thickness of the host normal tissue in front of the two stained tissue pieces was varied, and the thickness dependence of images was investigated. Figs.8(a) – 8(c) show the backscattering light images of a pair of two stained cancerous-normal tissue pieces hidden in the different depths in the host normal tissue.<sup>4</sup>

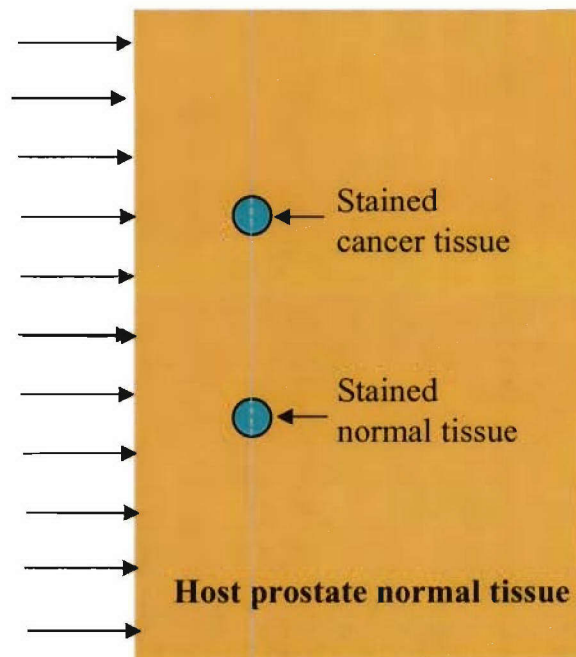


Fig.7. Schematic diagram of a sandwiched prostate cancerous-and-normal tissue sample consisting of a small piece of prostate cancer tissue (left side of the illumination beam) and a small piece of prostate normal tissue (right). These two small tissue pieces were stained in a same Cybesin-DMSO (Dimethyl Sulfoxide) solution for a same period of time, and then sandwiched into several large host pieces of prostate normal tissue which covers the stained cancerous-and-normal tissue pieces.

It can be seen from the images that the cancerous tissue area is much brighter than that of the normal tissue area indicating that the prostate cancer tissue takes-up Cybesin more than normal tissue. This difference can be seen more clearly from the spatial intensity distributions of cross sections of these images at a same row crossing the areas of the stained cancer and normal tissues. Figs. 8(d), 8(e) and 8(f) show the spatial cross section intensity distributions of the images 8(a), 8(b), and 8(c), respectively. The stained cancerous areas are more distinguished than that of the stained normal tissue areas as shown in Figs. 8(d)-8(f). The cancerous areas indicated from these images are in good agreement with the pathological section measurements.<sup>4</sup>

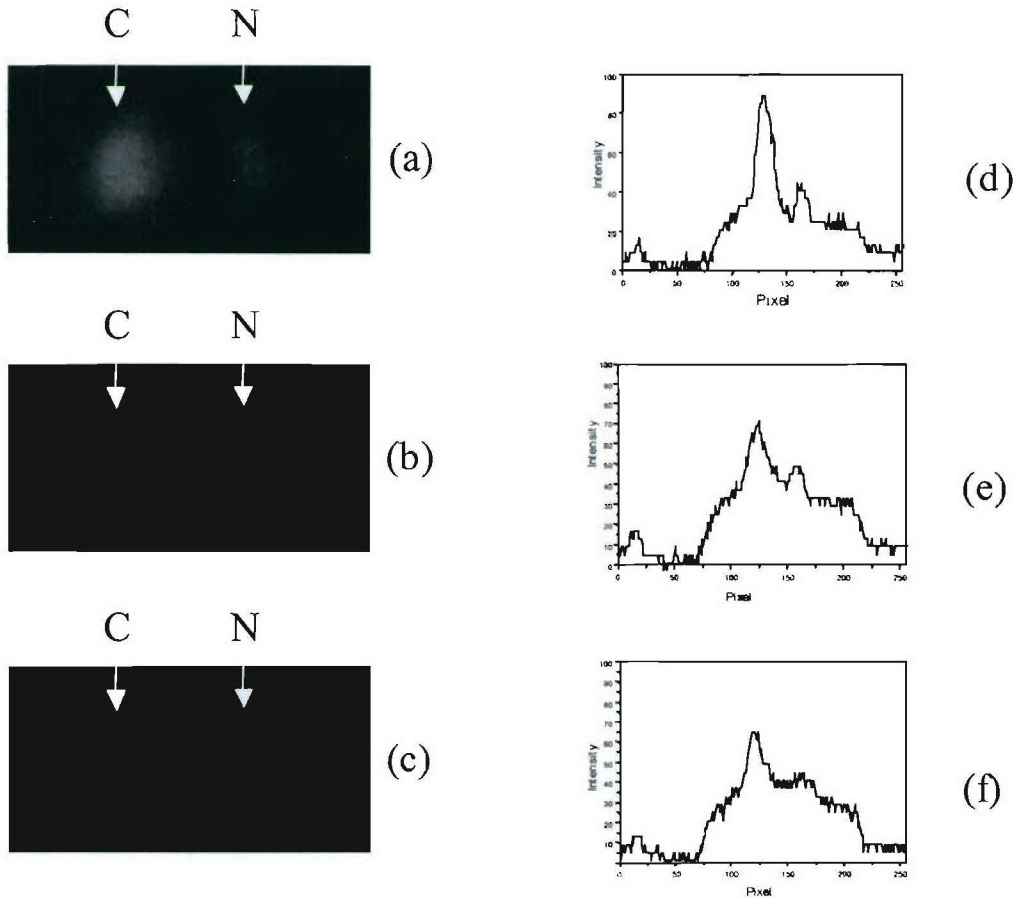


Fig.8. (a), (b), and (c) are fluorescence images of a prostate cancer-and-normal tissue sample recorded with  $\lambda_{\text{pump}}=750\text{nm}$  and  $\lambda_{\text{detection}}=850\text{nm}$  for perpendicular polarization configuration with the stained cancerous (C) and normal (N) pieces hidden in depths of 0, 1 and 2 mm from the surface of the host normal tissue, respectively; (d), (e) and (f) are the spatial intensity distributions of image cross sections at a same row crossing the areas of the stained cancer (C) and normal (N) tissues. The intensity in the cancerous tissue area is much brighter than that of the normal tissue area.

The thickness dependence of the images was investigated by varying the thickness of the host normal tissue in front of the two small pieces of the stained tissue. At a depth of 3 mm, the

difference between cancerous and normal tissues can still be distinguished, and the cancerous areas can still be identified.

The difference of Cybesin agent adsorptions and fluorescence imaging intensities between prostate cancerous (C) and normal (N) tissues shown in Figs. 8 clearly indicate that the Cybesin agent is a promising candidate as a prostate-cancer-receptor-targeted contrast agent for prostate cancer detection.

**(5) Design, build and test a breadboard rectal optical probe for the prostate imaging unit (Task # 3)**

Based on the spectral and imaging investigation on in-vitro prostate cancerous and normal tissues, and the knowledge gained from the research on tasks #1 and #2, we have designed, built and tested a breadboard rectal optical probe for the spectral polarization imaging unit. Fig.9 shows a picture of the breadboard rectal optical probe with scanning imaging system.

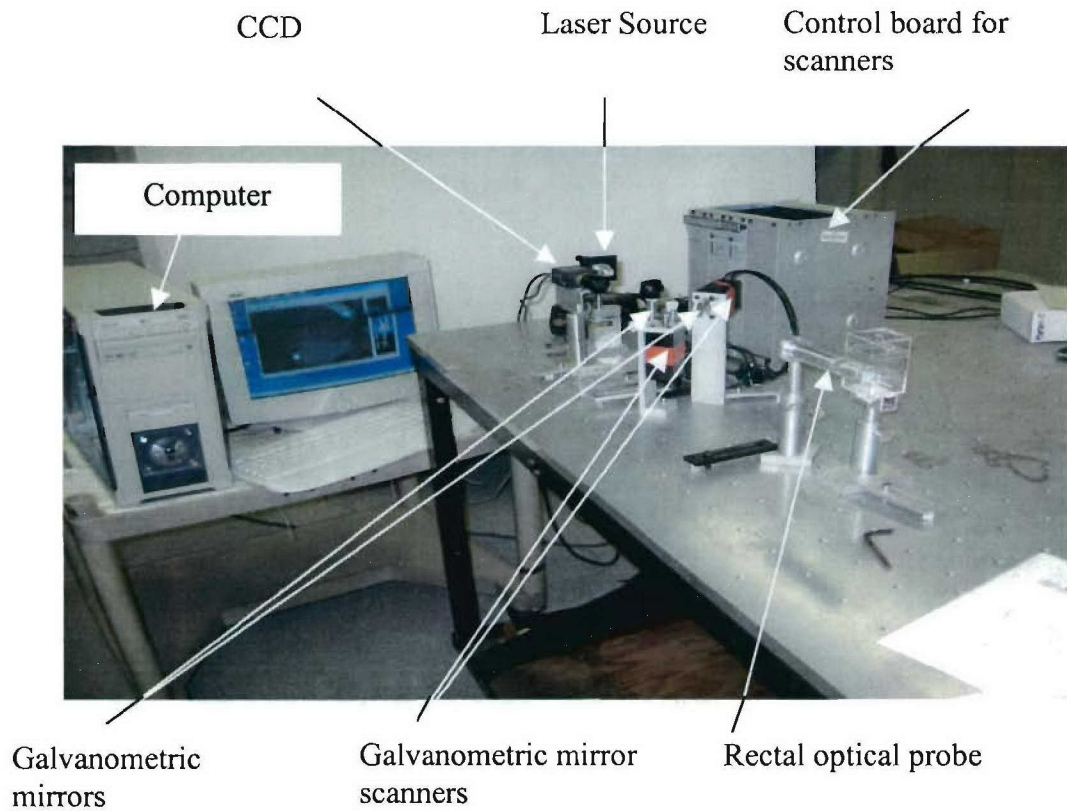


Fig.9 A photograph of the breadboard rectal optical probe with Galvanometric mirrors, scanners, control board for scanners, laser source and CCD for the prostate imaging system.

The probe head is 125 mm long with an outer diameter of 22 mm and an inner diameter of 20 mm. This size is suitable for the rectal probe head to be inserted into rectum and image a prostate

gland through rectum. The focused and polarized laser beam is used to illuminate a prostate sample through two Galvanometric mirrors, an elliptical reflection mirror inside the probe head and an optical window of the probe head. The two reflecting Galvanometric mirrors are used to scan the illumination beam in 2D on the x-y plane of the prostate gland from point-to-point controlled from the outside of the body. The size of the illumination beam, the scan steps and the scan speed can be varied.

The light back-scattered from the prostate sample first passes through the optical window of the probe head and the elliptical reflecting mirror inside the probe head, and is then collected by a lens into a coherent fiber-bundle to form an image of the prostate. A compact CCD camera is used to record the images formed by the backscattered light, and a computer is used to save and analyze the images.

This breadboard rectal optical probe with the spectral polarization imaging unit has been tested for imaging an object embedded inside polystyrene solution. A compact unit will be developed under other and/or future support for in-vivo clinical test.

#### **(6) Integrating sphere measurements for prostate cancerous and normal tissue (Task # 5)**

In order to investigate the difference of scattering coefficient ( $\mu_s$ ) between prostate cancerous and normal tissues, an integrating sphere was used.<sup>11</sup> We added an integrating sphere attachment to our absorption spectrometer, tested it for model scattering media samples, and developed an algorithm to determine  $\mu_s$  from the integrating sphere measurements.

The intensities from prostate cancerous and normal tissues in both transmission and backscattering configurations in the integrating sphere were measured, and an IAD (inverse adding-doubling) program<sup>11</sup> is used to calculate  $\mu_s$  for cancerous and normal tissues using an algorithm. The results were compared with that obtained from two polystyrene solutions whose scattering parameters are known. These two polystyrene solutions have different concentrations of 1/10 and 1/100 of the original polystyrene sphere solution (10%,  $d=0.46 \mu\text{m}$ ). Fig.10 shows preliminary results of scattering coefficients ( $\mu_s$ ) as a function of wavelength for prostate cancerous and normal tissues as well as the two polystyrene solutions. The results show that  $\mu_s$  for prostate cancerous tissue ( $\sim 20 \text{ mm}^{-1}$ ) is less than that of the prostate normal tissue ( $\sim 30 \text{ mm}^{-1}$ ) in the spectral range of 500 nm – 580 nm.

These results indicate that the integrating sphere study has produced a new approach for distinguishing prostate cancerous and normal tissues. To prove this prediction, more prostate cancerous and normal tissues will be investigated under other support. More tissues need to be measured to determine accuracy of  $\mu_s$  for cancerous and normal tissues, and tissues to be tested in the far red and near infrared spectral range of 700 nm to 1200 nm under other and/or future support.

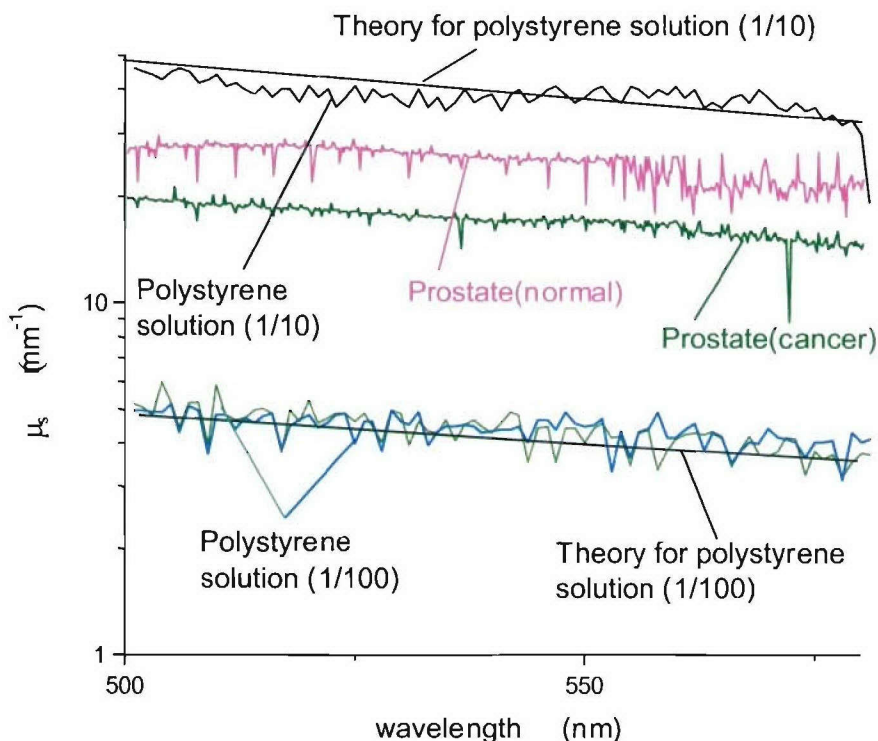


Fig. 10 Scattering coefficient  $\mu_s$  of prostate cancerous (olive) and normal (pink) tissues, and polystyrene sphere solutions with different concentrations of 1/10 (black) and 1/100 (blue and green) of the original polystyrene sphere solution (10%,  $d=0.46 \mu\text{m}$ ) as a function of wavelength, calculated from the data of integrating sphere measurements. As a comparison, the theoretical results of  $\mu_s - \lambda$  calculated based on Mie theory using the known parameters of polystyrene sphere for the two polystyrene solutions are presented (solid lines).

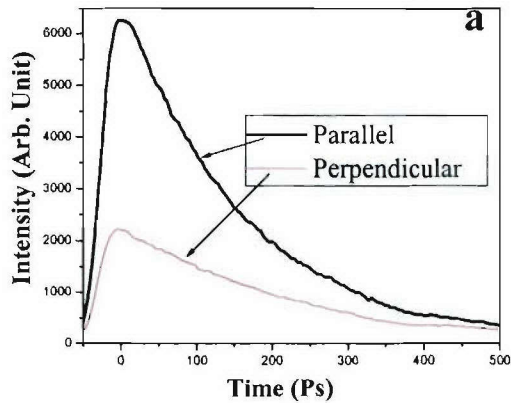
### **(7) Time-resolved and steady-state spectral measurements of prostate-cancer-receptor-targeted contrast agents (Task # 6)**

In order to improve image contrast between prostate cancerous and normal tissue areas, and enhance the ability of optical imaging for prostate cancer detection, we have investigated prostate-cancer-receptor-targeted contrast agents such as Cybesin by time-resolved and steady-state spectral measurements.

The steady-state absorption and fluorescence measurements of Cybesin were performed, and the results were described in section (4) and shown in Fig.6. In order to study the polarization preservation properties, which can be used to further improve the image contrast between prostate cancerous and normal tissue areas,<sup>1,6,7,12</sup> we have performed time-resolved fluorescence spectral measurements on Cybesin and Cybesin-stained prostate cancerous and normal tissues.

In the time-resolved fluorescence measurements, femtosecond Ti-Sapphire laser pulses were used to excite the Cybesin agent and a streak camera system was used to record the temporal polarization profiles of the fluorescence. The measured temporal profiles of the fluorescence emitted from Cybesin solution for two polarization orientations parallel and perpendicular to the polarization direction of the excitation at 800 nm are shown in Fig. 11 (a).<sup>5</sup> The thick- and thin-line profiles are  $I_{\parallel}(t)$  the parallel and  $I_{\perp}(t)$  the perpendicular component, respectively. The main difference for these two components is that  $I_{\parallel}$  is greater than  $I_{\perp}$  at all of the decay time, in particular, at the peak position. The parallel component  $I_{\parallel}(0)$  is almost three times stronger than that of the perpendicular one  $I_{\perp}(0)$  at peak position. This indicates the polarization preservation nature of Cybesin.

**Time Resolved Fluorescence Intensity of Cybesin**



**Time Resolved Polarization Anisotropy of Cybesin**

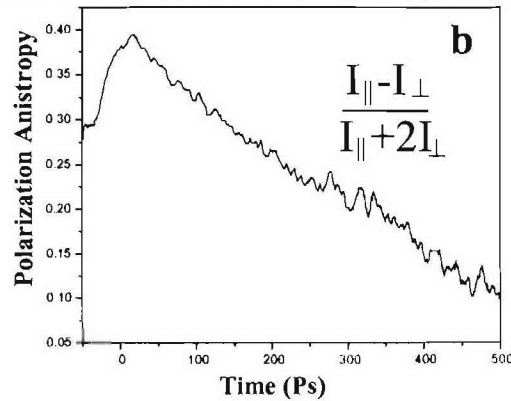


Fig.11. Temporal polarization profiles and polarization anisotropy of fluorescence emitted from Cybesin in 20% aqueous DMSO under a linear polarized 800 nm laser illumination. (a) The profiles of the time-resolved emission components with polarization directions parallel (thick line) and perpendicular (thin line) to the polarization direction of excited light. (b) Calculated time-dependent polarization anisotropy using the measured data shown in (a) and equation (1) as described in the text.

The time-dependent polarization anisotropy is defined as <sup>13,14</sup> :

$$r(t) = \frac{I_{\parallel}(t) - I_{\perp}(t)}{I_{\parallel}(t) + 2I_{\perp}(t)} = r(0)e^{-t/\tau_{\text{rot}}} \quad (1)$$

The temporal profile of the polarization anisotropy  $r(t)$  of Cybesin was calculated using the measured  $I_{\parallel}(t)$  and  $I_{\perp}(t)$ , and shown in Fig. 11 (b). The polarization anisotropy profile shown in Fig. 11 (b) gives  $r(0)=0.39$  at the peak position, that is very close to the theoretical value of 0.4, and a rotation time  $\tau_{\text{rot}} \sim 360$  ps. This indicates that the transitions dipole moments of Cybesin molecules in solution are randomly oriented.

The decay behavior of  $r(t)$  reflects the type of the dipole reorientation of the excited Cybesin molecules in a solvent. From the decay behavior of the  $r(t)$  curve, the reorientation time of the Cybesin solution was found to be  $\sim 360$  ps. This polarization preservation property of Cybesin shown in our time-resolved polarization fluorescence measurements indicates that it can be used as a contrast agent for the FPDI (fluorescence polarization difference imaging) technique to enhance the image quality.<sup>7</sup>

The measured temporal profiles of the fluorescence emitted from the Cybesin-stained prostate cancerous and normal tissues are displayed in Fig.12 (a). The thick-solid (black)- and thin-dash (red)-line profiles are the parallel and perpendicular components emitted from Cybesin-stained cancerous tissue, respectively, while the thin-solid (green)- and thin-dot (blue)-line profiles show the parallel and perpendicular components emitted from Cybesin-stained normal tissue, respectively.

The most important feature of Fig.12 (a) is that the emission intensities from Cybesin-stained cancerous tissue is larger than those of stained normal tissue within all the life time of Cybesin emission. The emission peak of dyed cancerous tissue is much stronger than that of the dyed normal tissue. Under parallel polarization configuration, the ratio of peak fluorescence intensity of the Cybesin-stained cancerous tissue to that of the Cybesin-stained normal tissue is found to be  $\sim 3.67$ , while under perpendicular configuration, the ration is  $\sim 3.23$ . These results indicate that the prostate cancerous tissue takes-up more Cybesin than the prostate normal tissue.

Another important feature shown in Fig.12 (a) is that  $I_{\parallel}$  is greater than  $I_{\perp}$  for both Cybesin-stained cancerous and normal tissues. At the peak position,  $I_{\parallel}^{\text{cancer}}(0)$  is  $\sim 1.45$  times stronger than  $I_{\perp}^{\text{cancer}}(0)$ . The ratio of  $I_{\parallel}^{\text{normal}}(0) / I_{\perp}^{\text{normal}}(0)$  is  $\sim 1.30$ . This indicates the measured fluorescence emitted from Cybesin-stained prostate cancerous and normal tissue still show the polarization preservation property. Because of this property, fluorescence polarization difference imaging technique can be applied to enhance the contrast of images<sup>7</sup>.

The temporal profile of the polarization anisotropy  $r(t)$  of Cybesin-stained cancerous and normal tissues were calculated using the measured profile data of  $I_{\parallel}^{\text{cancer}}(t)$ ,  $I_{\perp}^{\text{cancer}}(t)$ ,  $I_{\parallel}^{\text{normal}}(t)$  and  $I_{\perp}^{\text{normal}}(t)$  shown in Fig.12 (a). The calculated results show  $r^{\text{cancer}}(0)=0.18$  and  $\tau_{\text{rot, cancer}} \sim 750$  ps for

Cybesin-stained cancerous tissue, and  $r^{\text{normal}}(0)=0.13$  and  $\tau_{\text{rot, normal}} \sim 600$  ps for Cybesin-stained normal tissue. This indicates that the rotation time of the Cybesin-stained cancerous tissue is longer than that of the Cybesin-stained normal tissue. The Cybesin motion is more restrictive in the cancerous tissue than that in the normal tissue.

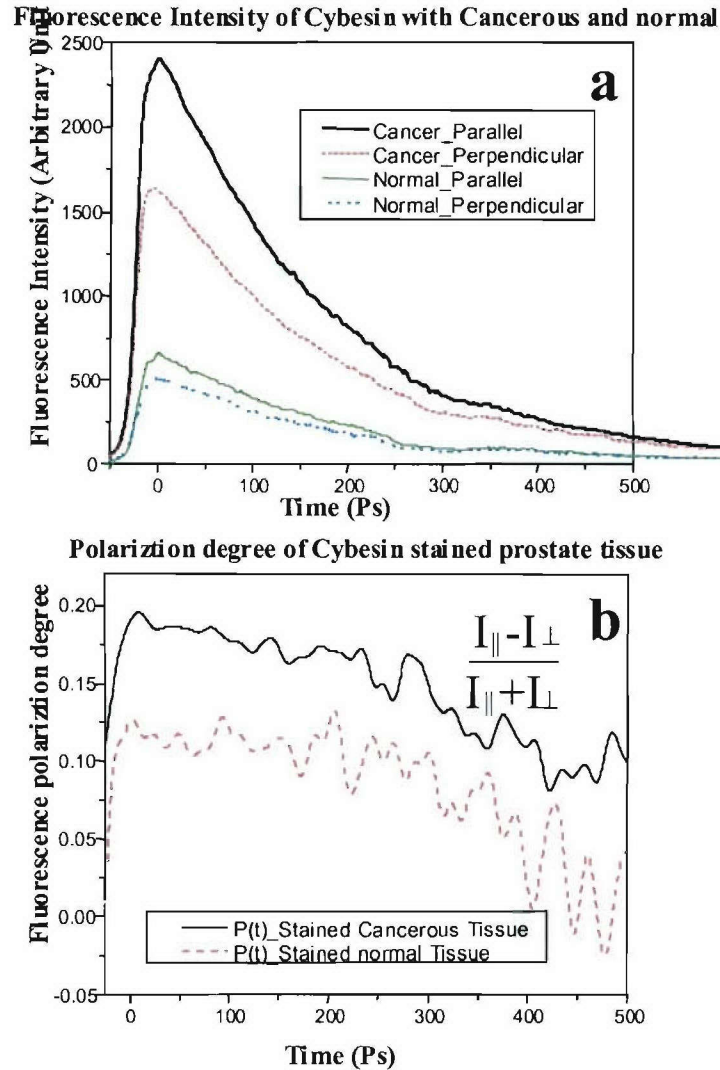


Fig.12. (a) The time-resolved fluorescence intensity emitted from the Cybesin-stained cancerous (thick solid line) and normal (thin solid line) prostate tissues when the detection polarization direction is parallel, and cancerous (thin dash line) and normal (thin dot line) prostate tissues when the detection polarization direction is perpendicular to that of excited light at  $\lambda_{\text{pump}}=800$  nm. (b) Calculated time-dependent polarization degree using equation (2) as described in the text and the measured data of temporal polarized fluorescence intensity emitted from the cancerous (solid line) and normal (dot line) prostate tissues stained by Cybesin under a linear polarized 800 nm laser illumination.

Another valuable feature is that the polarization degree of the Cybesin-stained cancerous tissue is larger than that of the Cybesin-stained normal tissue. The time-resolved polarization degrees of

fluorescence emitted from Cybesin-stained cancerous and normal tissue are calculated using equation of:

$$P(t) = \frac{I_{\parallel}(t) - I_{\perp}(t)}{I_{\parallel}(t) + I_{\perp}(t)} \quad (2)$$

and measured data of  $I_{\parallel}(t)$  and  $I_{\perp}(t)$  shown in Fig.12(a). The calculated temporal profiles of the polarization degree  $P(t)$  of the fluorescence emitted from Cybesin-stained prostate cancerous and normal tissues are displayed in Fig.12 (b).

The salient features of  $P(t)$  curves shown in Fig.12 (b) is that the values of polarization degree of the stained cancerous tissue are always larger than that of stained normal tissue at all the decay time. The larger fluorescence polarization degree of Cybesin-stained cancerous tissue can be used with FPDI technique to further improve the image contrast between Cybesin-stained cancerous and normal tissue areas, and enhance the ability of prostate cancer detection.

In addition to the work on Cybesin, we have initiated a collaboration with Merck & Co. Inc. to develop new efficient prostate-cancer-targeted contrast agents based on the Indocyanine Green (ICG) dye and SSTR (somatostatin receptor) antagonists #1-5 for optical imaging. These antagonists #1-5 investigated by Merck are used to target the prostate cancer receptors SSTR #1-5, respectively.<sup>15</sup>

Merck have sent 5 types of SSTR antagonists to CCNY. We have initiated absorption and fluorescence spectral measurements for the SSTR agonists. We found that the development of this new prostate-cancer-receptor-targeted contrast agent is important but beyond the scope of this grant support. We will complete the spectral investigation of these agonists, and attempt to connect ICG and SSTR agonists to develop new contrast agents under other and/or future support. Since ICG is sensitive for NIR imaging (NIR light can penetrate larger distance in tissues), and antagonist #1-5 are good targeting conjugates for prostate receptors, the new contrast agents consisting of ICG and antagonists #1-5 should be useful for prostate cancer detection.

#### **(8) Specific personnel supported by this grant:**

Dr. W. B. Wang, Senior Research Associate, Project Leader.

Mr. Yang Pu, Ph.D. Student,

Dr. J. H. Ali, former Ph. D. Student, graduated in October, 2004.

Mr. G. C. Tang, Research Associate,

Mr. F. Zeng, Research Associate, and

Dr. V. Sriramoju (MD), Research Associate.

#### **Key Research Accomplishments**

- Performed NIR spectral polarization imaging measurements on rectum-membrane-prostate tissue samples.

- Performed absorption measurements on prostate cancerous and normal tissues, and found that prostate cancerous tissue contains less water than that of prostate normal tissue;
- Performed imaging measurements for in-vitro human prostate cancerous and normal tissues based on the absorption fingerprints of prostate cancerous and normal tissues at water absorption peaks;
- The absorption and fluorescence spectra of a prostate-cancer-receptor-targeted contrast agent, Cybesin, were measured and shown to exist in the NIR tissue “optical window”.
- Performed time-resolved fluorescence polarization profiles of Cybesin solution, and Cybesin-stained prostate cancerous and normal tissues, and the results show that Cybesin has fluorescence polarization preservation properties that can be used to improve the image contrast between prostate cancerous and normal tissue areas, and enhance the ability for prostate cancer detection;
- Determined initial polarization anisotropy values and rotation times for Cybesin solution, and Cybesin-stained prostate cancerous and normal tissues based on the time-resolved fluorescence polarization measurements. They are:  $r^{\text{cybesin solution}}(0)=0.39$  and  $\tau_{\text{rot, cybesin solution}} \sim 360$  ps for Cybesin solution,  $r^{\text{cancer}}(0)=0.18$  and  $\tau_{\text{rot, cancer}} \sim 750$  ps for Cybesin-stained cancerous tissue, and  $r^{\text{normal}}(0)=0.13$  and  $\tau_{\text{rot, normal}} \sim 600$  ps .
- Performed optical imaging measurements for in-vitro human prostate cancerous-and-normal tissues using a prostate-cancer-receptor-targeted contrast agent, Cybesin, and compared the optical imaging results with the pathological measurements. The results show that prostate cancerous tissue takes-up more Cybesin than that of normal tissue making the Cybesin a potential marker for prostate cancer detection.
- Developed a collaboration with Merck & Co. Inc. to investigate better prostate- cancer-receptor-targeted contrast agents based on ICG dye and SSTR antagonists. Received SSTR antagonist samples from Merck, and started spectral measurements for the SSTR antagonist samples.
- Designed, built and tested a breadboard rectal optical probe for the spectral polarization imaging unit. The optical probe head is suitable to be inserted into rectum to image a prostate gland through rectum.
- Performed integrating sphere measurement to investigate scattering coefficients of prostate cancerous and normal tissues.

### Reportable Outcomes

- Five (5) papers have been produced from the research supported by this grant.
- Three (3) presentations have been given from the research supported by this grant.
- A provisional patent disclosure was submitted, and the corresponding patent application was filed.
- A breadboard rectal optical probe with a spectral polarization imaging unit was designed, built and tested.

- A Ph.D. student supported by this grant graduated in 10/2004, and a second Ph.D. student supported by this grant has completed most of his research work toward his Ph.D. thesis (expected to graduate in 2006).

The following lists the publications, presentations, a patent application, and Ph.D. degrees supported by this grant:

**(1) Publications:**

1. Y. Pu, W. B. Wang, G. C. Tang, F. Zeng, S. Achilefy, J. H. Vitenson (M.D.), I. Sawczuk (M.D.), S. Peters (M.D.), J. M. Lombardo (M.D.), and R. R. Alfano, "Spectral polarization imaging of human prostate cancer tissue using near-infrared receptor-targeted contrast agent", *TCRT (Technology in Cancer Research and Treatment)*, **4**, 429-436 (2005).
2. J. H. Ali, W. B. Wang, M. Zevallos, and R. R. Alfano, "Near infrared spectroscopy and imaging to probe differences in water content in normal and cancer human prostate tissues", *TCRT (Technology in Cancer Research and Treatment)*, **3**, 491-498 (2004).
3. W. B. Wang, J. H. Ali, J. H. Vitenson, J. M. Lombardo, and R. R. Alfano, "Spectral polarization imaging of human rectum-membrane-prostate tissues", *IEEE Journal of Selected Topics in Quantum Electronics*, **9**, No. 2, 288-293 (2003).
4. W. B. Wang, J. H. Ali, M. Zevallos, and R. R. Alfano, "Near infrared imaging of human prostate cancerous and normal tissues based on water absorption", in *OSA 2004 Biomedical Optics Topical Meetings on CD-ROM (The Optical Society of American, Washington, DC, 2004)*, MF 38.
5. Y. Pu, W. B. Wang, B. B. Das, G. C. Tang, S. Achilefy, and R. R. Alfano, "Time-resolved fluorescence polarization dynamics and optical imaging of Cybesin: a prostate cancer receptor-targeted contrast agent", a manuscript to be submitted for publication.

**(2) Presentations**

1. Y. Pu, W. B. Wang, G. C. Tang, F. Zeng, S. Achilefy, J. H. Vitenson (M.D.), I. Sawczuk (M.D.), S. Peters (M.D.), J. M. Lombardo (M.D.), and R. R. Alfano, "Optical imaging of human prostate cancer tissue using near-infrared receptor-targeted contrast agent", presented in the "Student Research Conference of 'Einstein in the City'", held in New York, NY, on April 11-12, 2005. Technical Program, P 12.11.
2. W. B. Wang, J. H. Ali, M. Zevallos, and R. R. Alfano, "Near infrared imaging of human prostate cancerous and normal tissues based on water absorption", presented in the *OSA 2004 Biomedical Optics Topical Meetings*, Miami, FL, April 14-17, 2004.
3. W. B. Wang, J. H. Ali, J. H. Vitenson, J. M. Lombardo, and R. R. Alfano, "Spectral polarization imaging of prostate and rectum-membrane-prostate tissues", presented in the *Symposium of Frontiers of Photonics*, New York, NY, on November 5, 2001.

**(3) Patent application:**

1. R. R. Alfano, J. H. Ali, W. B. Wang, and Manuel Zevallos, "Detecting human cancer through spectral optical imaging using key water absorption wavelengths", a patent

disclosure and provisional U. S. patent application filed on 04/17/2003, No. 60/463,352; and U. S. patent application filed on 04/16/2004, No. 10/825,742.

#### **(4) Ph. D. degree supported:**

1. Dr. Jamal H. Ali received his Ph. D. in Physics on 10/12/2004. His thesis research entitled “Light propagation in human prostate tissues and paint using visible-to-mid-IR spectroscopy and imaging techniques” was mainly supported by this grant.
2. Mr. Yang Pu is a Ph. D. student currently working on “prostate cancer detection using spectral polarization imaging and cancer-receptor-targeted contrast agents” toward his Ph. D. thesis under the support of this grant (expected to graduate in 2006).

#### **Conclusions:**

1. The NIR spectral polarization imaging measurements on rectum-membrane-prostate tissue samples show that even through rectum and membrane tissues, small objects hidden inside the host prostate tissues in a human rectum-membrane-prostate tissue structure can still be imaged and identified. This result indicates that our spectral polarization imaging technique is a promising noninvasive approach for detecting prostate cancers by imaging prostate gland through rectum and membrane tissues in real time without removing tissues.
2. Absorption spectra of prostate cancerous and normal tissues show that prostate cancerous tissue have less water content and less absorption at water absorption peak wavelengths in comparison with that of prostate normal tissue. The imaging measurements for in-vitro prostate cancerous and normal tissues show that the absorption fingerprints of prostate cancerous and normal tissues can be used to monitor physiological changes of prostate tissues, and detect prostate cancers.
3. Spectral measurements of a prostate-cancer-receptor-targeted contrast agent, namely Cypate-Bombensin conjugate (Cybesin), show that the absorption and fluorescence spectra of Cybesin exist in the NIR tissue “optical window” making Cybesin a sound contrast agent for the application of tissue imaging.
4. Optical imaging measurements of in-vitro prostate cancerous-and-normal tissues samples using Cybesin show that prostate cancerous tissue takes-up more Cybesin than that of normal tissues, indicating Cybesin is a promising candidate contrast agent for targeting prostate cancer receptors, and can be used as a marker of prostate cancers.
5. The time-resolved fluorescence polarization spectral measurements of Cybesin and Cybesin-stained prostate cancerous and normal tissues show that Cybesin in both solution and tissue has polarization preservation properties that can be used to further improve the image contrast between cancerous and normal tissue areas, and enhance the ability for prostate cancer detection.
6. The initial polarization anisotropy values and rotation times for Cybesin solution, and Cybesin-stained prostate cancerous and normal tissues were determined:  $r^{\text{cybesin solution}}(0)=0.39$  and  $\tau_{\text{rot, cybesin solution}} \sim 360$  ps for Cybesin solution,  $r^{\text{cancer}}(0)=0.18$  and  $\tau_{\text{rot, cancer}} \sim 750$  ps for Cybesin-stained cancerous tissue, and  $r^{\text{normal}}(0)=0.13$  and  $\tau_{\text{rot, normal}} \sim 600$  ps from the time-resolved fluorescence polarization measurements.

## References

1. W. B. Wang, J. H. Ali, J. H. Vitenson, J. M. Lombardo, and R. R. Alfano, "Spectral polarization imaging of human rectum-membrane-prostate tissues", *IEEE Journal of Selected Topics in Quantum Electronics*, **9**, No. 2, 288-293 (2003).
2. J. H. Ali, W. B. Wang, M. Zevallos, and R. R. Alfano, "Near infrared spectroscopy and imaging to probe differences in water content in normal and cancer human prostate tissues", *TCRT (Technology in Cancer Research and Treatment)*, **3**, 491-498 (2004).
3. W. B. Wang, J. H. Ali, M. Zevallos, and R. R. Alfano, "Near infrared imaging of human prostate cancerous and normal tissues based on water absorption", in *OSA 2004 Biomedical Optics Topical Meetings on CD-ROM (The Optical Society of American, Washington, DC, 2004)*, MF 38.
4. Y. Pu, W. B. Wang, G. C. Tang, F. Zeng, S. Achilefy, J. H. Vitenson (M.D.), I. Sawczuk (M.D.), S. Peters (M.D.), J. M. Lombardo (M.D.), and R. R. Alfano, "Spectral polarization imaging of human prostate cancer tissue using near-infrared receptor-targeted contrast agent", *TCRT (Technology in Cancer Research and Treatment)*, **4**, 429-436 (2005).
5. Y. Pu, W. B. Wang, B. B. Das, G. C. Tang, V. Sriramoju, S. Achilefu, and R. R. Alfano, "Time-resolved fluorescence polarization properties of Cybesin: a prostate cancer receptor-targeted contrast agent", a manuscript to be submitted.
6. W. B. Wang, J. H. Ali, J. H. Vitenson, J. M. Lombardo, and R. R. Alfano, "Spectral polarization imaging of human prostate tissues", in *Proceedings of Optical Biopsy III, SPIE, Vol. 3917*, 75 (2000).
7. W. B. Wang, S. G. Demos, J. Ali, R. R. Alfano, "Imaging fluorescent objects embedded inside animal tissues using polarization difference technique", *Optics Communications*, **142**, 161 (1997).
8. W. B. Wang, S. G. Demos, J. Ali, Gang Zhang, and R. R. Alfano, "Visibility enhancement of fluorescent objects hidden in animal tissues using spectral fluorescence difference method", *Optics Communications*, **147**, 11 (1998).
9. Gleason DF, Mellinger GT, "Prediction of prognosis for prostatic adenocarcinoma by combined histological grading and clinical staging", *J. Urol*, **111**, 58-64 (1974).
10. J. E. Bugaj, S. Achilefu, R. Dorshow, and R. Rajagopalan, "Novel fluorescence contrast agents for optical imaging of in-vivo tumors based on a receptor-targeted dye-peptide conjugate platform", *J. of Biomedical Optics*, **6**, 122 (2001).
11. S. A. Prahl, M. J. C. Van Gemert, and A. J. Welch, "Determining the optical properties of turbid media using the adding-doubling method", *Applied Optics*, **32**, 559-568 (1993).
12. W. B. Wang, J. H. Ali, R. B. Dorshow, M. A. McLoughlin, and R. R. Alfano, "Time-resolved fluorescence polarization dynamics and imaging of fluorescein dye attached to different molecular weight chains", *SPIE, Vol. 3600*, 227 (1999).

13. G. R. Fleming, J. M. Morris and G. W. Robinson, "Direct observation of rotational diffusion by picosecond spectroscopy", *Chemical Physics*, 17, 91-100, (1976).
14. G. Porter, P. J. Sadkowski and C. J. Tredwell, "Picosecond rotational diffusion in kinetic and steady state fluorescence spectroscopy", *Chemical Physics Letter*, 49, 416-420, (1977).
15. Susan P. Rohrer, Elizabeth T. Birzin, Ralph T. Mosley, Scott C. Berk et al., "Rapid identification of subtype-selective agonists of the somatostatin receptor through combinatorial chemistry", *Science*, 282, 737 (1998).

## Appendix

The reprints or copies of the following papers and a patent abstract produced from the research supported by this grant are attached:

1. Y. Pu, W. B. Wang, G. C. Tang, F. Zeng, S. Achilefy, J. H. Vitenson (M.D.), I. Sawczuk (M.D.), S. Peters (M.D.), J. M. Lombardo (M.D.), and R. R. Alfano, "Spectral polarization imaging of human prostate cancer tissue using near-infrared receptor-targeted contrast agent", *TCRT (Technology in Cancer Research and Treatment)*, 4, 429-436 (2005).
2. J. H. Ali, W. B. Wang, M. Zevallos, and R. R. Alfano, "Near infrared spectroscopy and imaging to probe differences in water content in normal and cancer human prostate tissues", *TCRT (Technology in Cancer Research and Treatment)*, 3, 491-498 (2004).
3. W. B. Wang, J. H. Ali, J. H. Vitenson, J. M. Lombardo, and R. R. Alfano, "Spectral polarization imaging of human rectum-membrane-prostate tissues", *IEEE Journal of Selected Topics in Quantum Electronics*, 9, No. 2, 288-293 (2003).
4. R. R. Alfano, J. H. Ali, W. B. Wang, and Manuel Zevallos, "Detecting human cancer through spectral optical imaging using key water absorption wavelengths", a patent disclosure and provisional U. S. patent application filed on 04/17/2003, No. 60/463,352; and U. S. patent application filed on 04/16/2004, No. 10/825,742.

## Spectral Polarization Imaging of Human Prostate Cancer Tissue Using a Near-infrared Receptor-targeted Contrast Agent

www.tcr.org

The Cypate-Bombesin Peptide Analogue Conjugate (Cybesin) was used as a prostate tumor receptor-targeted contrast agent. The absorption and fluorescence spectra of Cybesin were measured and shown to exist in the NIR tissue "optical window". The spectral polarization imaging of Cybesin-stained prostate cancerous and normal tissues shows that prostate cancerous tissue takes-up more Cybesin than that of prostate normal tissue, making Cybesin a potential marker of prostate cancer.

Keywords: Prostate cancer; Receptor-targeted; Peptide analogue conjugate; Contrast agent; Spectral polarization imaging; Near-infrared; Absorption; and Fluorescence.

### Introduction

The increasing incidence and mortality rate of prostate cancers in men makes early tumor detection research a challenge for oncological specialists. The region of the highest incidence is in the western world, where there are 10-11% chances for a man to develop prostate cancer, and 3-4% chances of dying from the disease (1). Conventional oncology imaging methods for prostate cancer diagnosis, still depend on bulk physical properties of cancer tissue and are not effective for early-stage primary tumors (2). It is well known that diagnosis of a small premalignant lesion is critical for the success of cancer therapy and a key to increase survival rates. Scientists have been looking for methods that emphasize gene-specific or receptor-specific, minimally invasive diagnosis for early-stage tumors (2).

Near-infrared (NIR) optical imaging is a powerful tool in cancer research that relies on activating endogenous chromophores or applying contrast agents that can target cancer cells. The use of intrinsic chromophores to differentiate the optical properties of diseased and healthy human tissues has been reported in some studies using fluorescence and absorption (3, 4). The most attractive advantage of optical imaging is the high sensitivity, which can be superior to other *in vivo* imaging techniques (2). Over the past decade, cyanine dyes have been investigated by several groups (5, 6) as contrast agents for optical detection of tumors. In order to observe fluorescence from a substantial distance within the body, the emission wavelength must be in the NIR wavelength window in which light passing through tissue is less likely to be absorbed or scattered (7). Researchers are interested in cyanine dyes because their emission range of 700 nm to 900 nm is in the tissue "optical window" (8). Indocyanine Green (ICG, also called cardio-green), a clinically approved NIR dye by FDA, is one of the most investigated cyanine dyes. Its fluorescence range is between 775 nm and 850 nm, that avoids the

Y. Pu, B.S.<sup>1</sup>  
W. B. Wang, Ph.D.<sup>2</sup>  
G. C. Tang, M.S.<sup>2</sup>  
F. Zeng, B.S.<sup>2</sup>  
S. Achilefu, Ph.D.<sup>3</sup>  
J. H. Vitenson, M.D.<sup>4</sup>  
I. Sawczuk, M.D.<sup>6</sup>  
S. Peters, M.D.<sup>5</sup>  
J. M. Lombardo, M.D.<sup>5</sup>  
R. R. Alfano, Ph.D.<sup>2,\*</sup>

<sup>1</sup>Department of Electrical Engineering

<sup>2</sup>Department of Physics

The City College of the City Univ. of NY  
Convent Avenue at 138th Street  
New York, NY 10031

<sup>3</sup>Washington University School of Medicine  
4525 Scott Avenue  
St. Louis, Missouri 63110

<sup>4</sup>Department of Urology

<sup>5</sup>Department of Pathology  
Hackensack University Medical Center  
30 Prospect Avenue  
Hackensack, NJ 07601

<sup>6</sup>Department of Urology  
Hackensack University Medical Center  
Adjunct Professor of Urology  
College of Physicians and Surgeons  
Columbia University  
Professor of Surgery (Urology)  
UMDNJ Newark Medical School

\* Corresponding Author:  
R. R. Alfano, Ph.D.  
Email: alfano@sci.cuny.edu

absorption bands at 950nm and 1195nm due to water which is the main chromophore component in human tissue (4, 9).

The investigations of receptor expression in normal and cancer tissue suggest that small peptide-dye conjugates can be used to target over-expressed receptors on tumors contrary to the traditional approach of dyes conjugated to large proteins and antibodies (5, 10, 11). As a small ICG-derivative dye-peptide, Cypate-Bombesin Peptide Analogue Conjugate (Cybesin) was synthesized and used as a contrast agent to detect pancreas tumors in an animal model a few years ago (5). The prior experimental results of Cybesin for tumor detection indicated that Cybesin preferentially localized for over 24 hours in tumors known to over-express bombesin receptors in a small animal model (5). In this study, Cybesin was used to target over-expressed bombesin receptors in human prostate cancer tissue. Bombesin belongs to a family of brain-gut peptides that play an important role in cancer development (12). It was observed that human primary tumors can synthesize bombesin (12), and the bombesin receptor can also be over-expressed on the membranes of human prostate cancer cells (12). All of these results motivated us to apply Cybesin to human prostate cancer detection.

In this paper, we report our NIR spectral polarization imaging study using Cybesin as an optical contrast agent marker to differentiate human prostate cancerous and normal tissues. The absorption and fluorescence spectra of Cybesin were studied in the wavelength region from 650 nm to 900 nm. The model prostate samples consisting of a small piece of normal prostate tissue and a small piece of prostate cancer tissues stained with Cybesin were imaged. The results indicate that this receptor-targeted Cybesin was preferentially taken up by prostate cancerous tissue compared to prostate normal tissues.

## Materials and Methods

### Experimental Method and Sample

The schematic diagram of the experimental set-up for our NIR spectral polarization imaging is shown in Figure 1. Light from a white light source is used to illuminate the prostate tissue sample with average power of about  $50 \mu\text{W}/\text{cm}^2$ , which is much lower than the critical illumination level given by FDA. The illumination wavelengths are selected by wide-band pass filters varying from 550 nm to 900 nm with FWHM=40 nm placed on a multiple filter wheel, which can be rotated to the desired filter position by computer control. A CCD camera records images formed by light emitted from the sample. The detection wavelength is selected by rotating a similar set of band pass filters placed on the second multiple filter wheel located in front of the detector. Polarizer  $P_1$  used to ensure linear polarization of the illumination and polarizer  $P_2$  is placed in the front of the

CCD for selecting the detection polarization. Images are recorded when the detection polarization is parallel or perpendicular to the illumination polarization (7). For emission light imaging, the wavelengths of the band pass range of the detection (imaging) filter is longer than that of the illumination so that the pump light is blocked, and only the light emitted from the sample is collected by the CCD camera (7).

Eight [8] *in vitro* prostate cancer-and-normal tissue samples obtained from Hackensack University Medical Center (HUMC) and the National Disease Research Interchange (NDRI) were used for optical imaging measurements. The results of histological section measurements performed at the Pathology Department of HUMC were used as a guide to indicate the locations of the cancerous and normal tissue areas. The prostate normal tissues were cut into a number of large slices with thicknesses of 1.0 mm to 4.5 mm and used as host tissue. The experiments were performed under IRB approvals at HUMC and CCNY (City College of New York).

A typical prostate cancerous-normal tissue sample used for the imaging measurements consists of a small piece of prostate cancer tissue and a small piece of prostate normal tissue. Both of them have a similar size and were soaked in the same Cybesin-DMSO (in 20% aqueous Dimethyl Sulfoxide) solution with a Cybesin concentration of  $\sim 3.2 \times 10^{-6} \text{ M}$  for the same period of time. Then the samples were put into sodium phosphate buffer (Sigma-Aldrich) to wash off the unbound Cybesin. The stained normal and cancer tissues were then sandwiched between large pieces of prostate normal tissue. The depth of the stained tissue underneath the surface of the host prostate normal tissue was varied to obtain the detectable imaging depths. The schematic diagram of a sandwiched prostate cancerous-and-normal tissue sample is shown at the sample position in Figure 1.

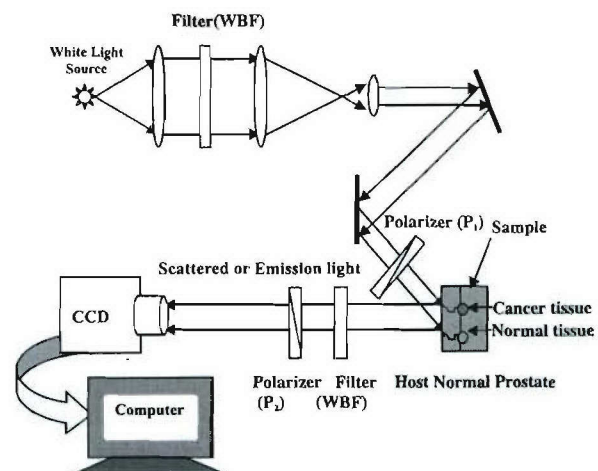


**Figure 1:** Schematic diagram of our spectral polarization imaging set-up. The structure of a sandwiched prostate cancerous-and-normal tissue sample is schematically shown in the sample position.

The prostate tissue from which the stained normal and cancerous tissue pieces were taken was cut into a number of slides with a thickness of 250  $\mu\text{m}$  at HUMC for microscopy study. The microscope images were taken using a digital electro-microscope (Mel Sobel Microscopes Ltd) and compared with the results obtained from the optical imaging. Figures 2(a) and (b) show the low power ( $\times 40$ ) microscope images of the normal and cancerous areas of prostate tissue, respectively.

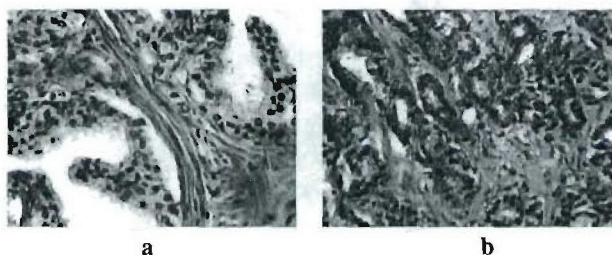


**Figure 2:** (a) 40 times magnified microscope image of the normal area in a prostate tissue sample and (b) 40 times magnified microscope image of the cancerous area in a prostate tissue sample. The cancer is estimated as Gleason grade 3+4.

#### The Absorption and Fluorescence Spectra of Cybesin

Cybesin was prepared by Achilefu's group at the Washington University School of Medicine. The molecular structure of Cybesin is shown in Figure 3. It is mainly composed of ICG and the bombesin receptor ligand, which delivers the ICG to the receptor presented in the tumor (5). The synthesis of this contrast agent was reported elsewhere (5). The previous investigation shows that Cybesin can be used for effectively targeting a bombesin-rich tumor in the animal model because of the high affinity of Cybesin for the bombesin receptor (5). The schematic for Cybesin targeting the bombesin receptor on a tumor is also shown in Figure 3.

In this study, we investigated the over-expressed bombesin receptor status in human prostate cancer cells. A variety of tumor tissues have been found to express bombesin receptors, for instance prostate, lung, breast, and pancreas tumors

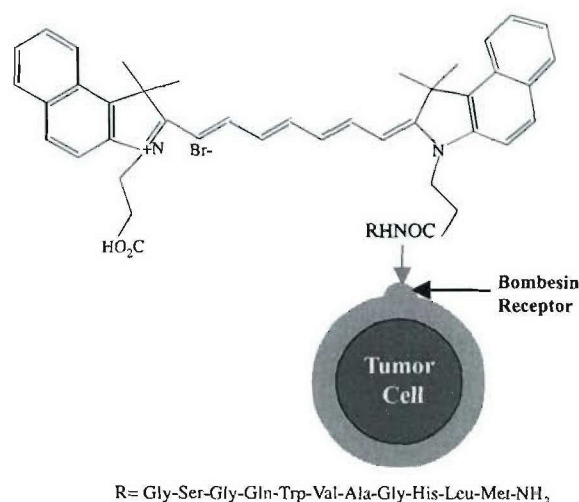
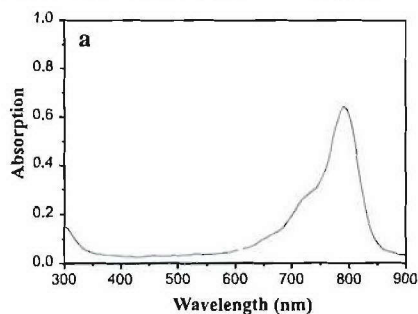


**Figure 3:** Molecular structure of the Cybate-Bombesin Peptide Analogue Conjugate (Cybesin), and schematic diagram of Cybesin targeting to the bombesin receptor on prostate tumor cells.

(12, 13). The optical imaging for human prostate cancer detection using this contrast agent depends on the two factors: (i) The high affinity of Cybesin for the bombesin receptor (5) and (ii) the over-expressed bombesin receptor status of human prostate cancer cells (12, 13).

In our study, Cybesin was solvated in 20% aqueous Dimethyl Sulfoxide (DMSO). The absorption spectrum of Cybesin in DMSO solution was investigated using a Perkin-Elmer Lambda 9 UV/VIS/NIR Spectrophotometer in the spectral range of 300 nm to 900 nm. The fluorescence spectrum was measured using a far-red to NIR spectral setup excited by modulated excitation with a 680 nm diode laser. Fluorescence light from the sample after passing through lenses was focused on the entrance slit of a SPEX Minimate 0.25-m monochromator (spectrometer) and detected by a Hamamatsu P394A PbS detector mounted at the exit slit of the monochromator. Signals from the detector were recorded by a PAR Model HR-8 lock-in amplifier connected to a computer.

Absorption spectrum of Cybesin in 20% aqueous DMSO



Fluorescence Spectrum of Cybesin in 20% aqueous DMSO

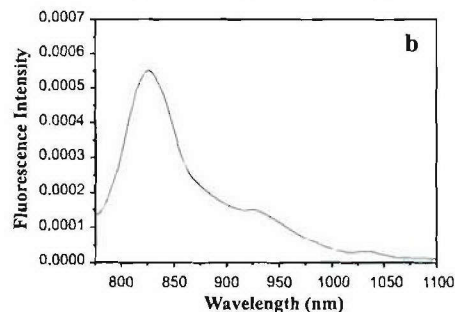


**Figure 4:** (a) Absorption and (b) fluorescence spectra of Cybesin in 20% aqueous DMSO. The fluorescence was excited by a 680 nm diode laser.

Figure 4(a) and (b) show the measured absorption and fluorescence spectra of Cybesin, respectively. The absorption band of Cybesin ranges from 680 nm to 830 nm with a shoulder peak at 720 nm and a strong peak at 792 nm. The fluorescence spectrum covers from 800 nm to 950 nm with a main peak at 825 nm and a weak peak at 925 nm. Both results show that Cybesin possesses the spectral advantages of ICG that the fluorescence and the absorption ranges are in the NIR range of the "tissue optical window".

### Optical Imaging Result and Discussion

In order to investigate the affinity of Cybesin for prostate cancer tissue and obtain the optimal spectral imaging con-

ditions, the samples were imaged at different wavelengths, polarizations, and depths in which the stained small pieces of the cancerous and normal tissues were embedded inside the host prostate tissue.

The contrast agent emission images of the samples were recorded at different pump and detection wavelengths varying from 650 nm to 850 nm. In order to compare images recorded at different wavelengths in the same polarization configuration, the perpendicular images were recorded. Figure 5 shows perpendicular polarization images of stained cancerous and normal prostate tissue on the host normal prostate tissue recorded at different detection wavelengths of 750 nm to 850 nm. The salient features shown in Figure 5

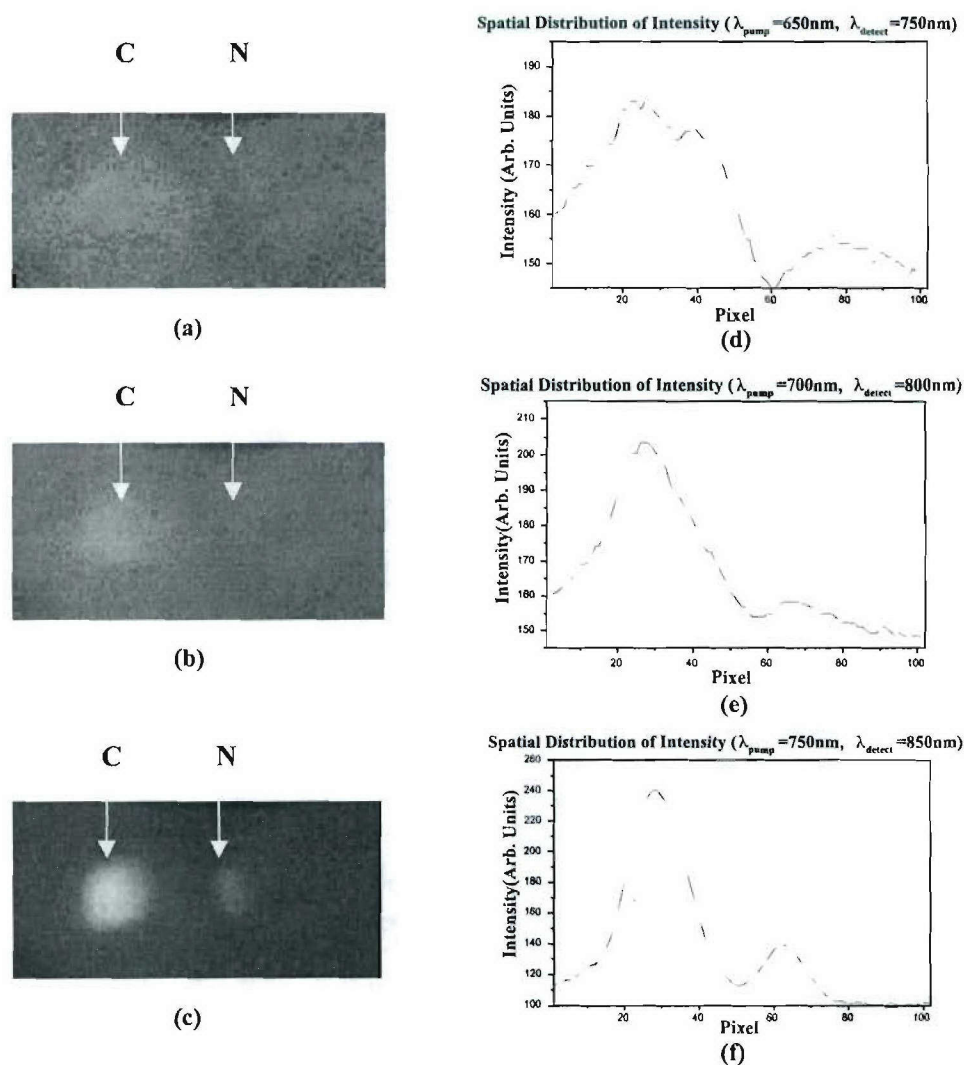


**Figure 5:** Contrast agent emission images of a prostate cancer-and-normal tissue sample recorded at (a)  $\lambda_{\text{pump}}=650\text{nm}$  and  $\lambda_{\text{detection}}=750\text{nm}$ , (b)  $\lambda_{\text{pump}}=700\text{nm}$  and  $\lambda_{\text{detection}}=800\text{nm}$ , and (c)  $\lambda_{\text{pump}}=750\text{nm}$  and  $\lambda_{\text{detection}}=850\text{nm}$ , with a perpendicular polarization configuration; (d), (e), and (f)

are the cross section intensity distributions of the images of (a), (b), and (c) at the same row crossing the areas of the stained cancer (C) and normal (N) tissues, respectively. The intensity in the cancerous tissue area is much greater than that of the normal tissue area.

is that the dyed small pieces of cancer and normal tissues can not be clearly distinguished from the image acquired with short pump and detection wavelengths at  $\lambda_{\text{pump}}=650$  nm and  $\lambda_{\text{detection}}=750$  nm, while the tumor can be recognized by the images obtained with longer pump and detection wavelengths at  $\lambda_{\text{pump}}=750$  nm and  $\lambda_{\text{detection}}=850$  nm. When the wavelength increases, the visibility of the dyed object increases dramatically. The measured results show that the optimized detection wavelength range is from 800 nm to 850 nm, which is exactly the strong fluorescence range of Cybesin. This indicates that the recorded images are indeed formed from the contrast agent emission, not from the tissue's native emission. It can be seen from the images that the cancerous tissue piece is much brighter than that of the normal tissue piece indicating that the prostate cancer tissues adsorb Cybesin more than normal tissues because Cybesin targets the over-expressed bombesin receptors of human prostate cancer cells (12, 13). On the other hand, since malignant tumors are more cell-packed (14), there will be more cells in cancerous area, even for same size, geometry, or weight, and hence more, Cybesin binds to cancerous area versus normal area. We believe that both high adsorption and density of cancer cells contribute to the large fluorescence intensity in the cancerous area, and make Cybesin a good candidate as a marker to differentiate prostate cancerous tissue from the normal tissue.

The difference between cancerous and normal tissue images can be more clearly seen from their spatial intensity distributions at the same pixel row crossing the areas of the stained cancer and normal tissues. Figures 5(d), (e), and (f) show the digital spatial cross section intensity distributions of the images shown in Figures 5(a), (b), and (c), respectively. The image obtained at  $\lambda_{\text{pump}}=750$  nm and  $\lambda_{\text{detection}}=850$  nm shows the best visibility and greatest difference between normal and cancerous tissue. Under this best imaging condition, the ratio of imaging intensity of cancerous tissue area to that of normal tissue area is found to be  $\sim 3.55$ .

As described in our previous study (15, 16), the polarization preservation property of ICG and the fluorescence polarization difference imaging technique can be used to improve the image quality of a fluorescent object embedded in tissues. In order to determine if Cybesin has a polarization preservation property, we studied Cybesin emission images recorded at different polarization configurations. The polarization dependence of fluorescence images of the stained cancerous and normal prostate tissue surrounded by the host normal prostate tissue at  $\lambda_{\text{pump}}=750$  nm and  $\lambda_{\text{detection}}=850$  nm is shown in Figure 6. Figure 6(a) displays the parallel image recorded

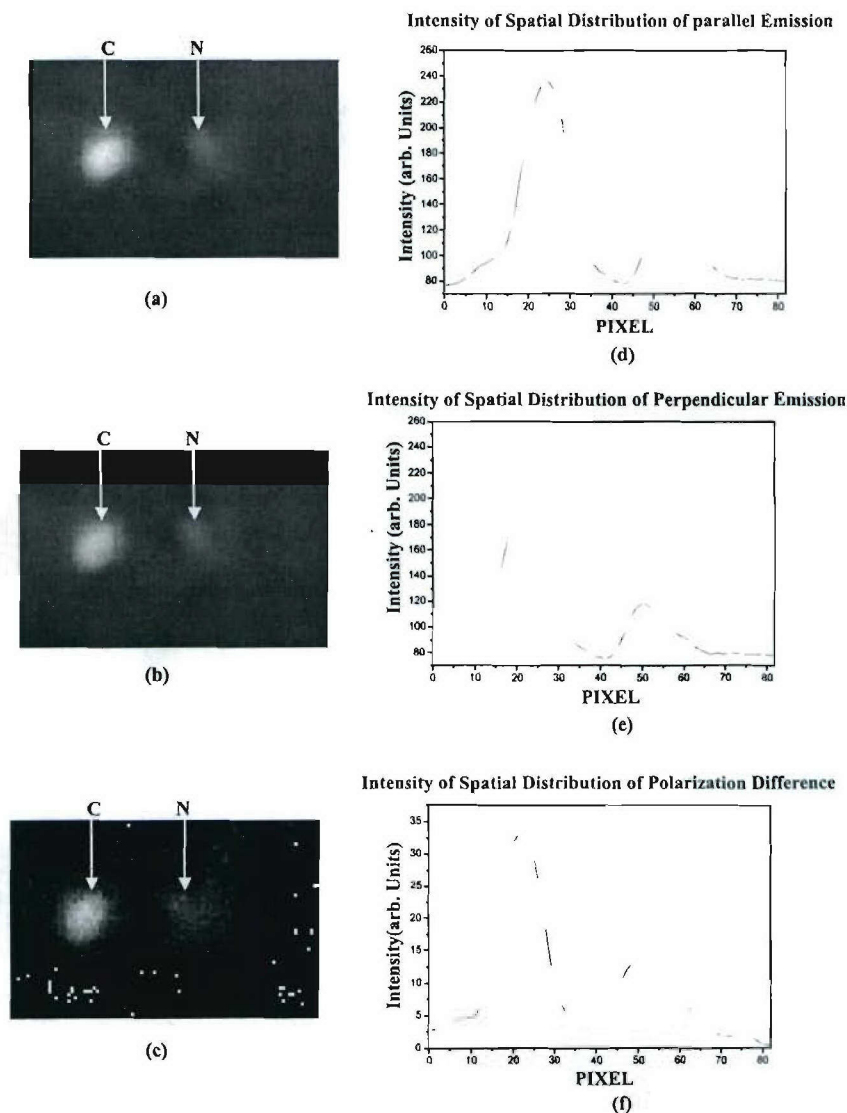


**Figure 6:** Polarization dependence of fluorescence images of a cancerous and normal prostate tissue sample recorded at  $\lambda_{\text{pump}}=750$  nm and  $\lambda_{\text{detection}}=850$  nm when the polarization direction of  $P_2$  is parallel (a) and perpendicular (b) to that of the illuminating light. (c) is the polarization difference image obtained by subtracting (b) from (a). (d), (e), and (f) are the digital spatial cross section intensity distributions of the images shown in (a), (b) and (c), respectively.

when the polarization direction of  $P_2$  in front of the CCD camera is parallel ( $\parallel$ ) to that of the illuminating beam. Figure 6(b) displays the perpendicular image recorded when the polarization direction of  $P_2$  is perpendicular ( $\perp$ ) to that of the illuminating beam. Figure 6(c) displays the difference image obtained by subtracting the perpendicular image [Fig. 6(b)] from the parallel image [Fig. 6(a)]. Figures 6(d), (e), and (f) show the digital spatial cross section intensity distributions of the images shown in Figures 6(a), (b), and (c), respectively.

The salient features of these images and their intensity distributions are: (i) The peak intensity of the cancerous tissue of the parallel image shown in Figure 6(d) is slightly higher than that of perpendicular one shown in Figure 6(e). This difference can be explained because the light reaching the CCD camera is still partially polarized (16). The preferred polarization direction is parallel to that of illuminating beam, and (ii) the relative brightness of the stained cancerous piece in comparison with the stained normal piece for the polarization difference image shown in Figure 6(c) is obviously higher than those of the conventional polarization images shown in Figures 6(a) and 6(b). To quantitatively describe the improvement of the relative brightness of the dyed cancerous area to the dyed normal tissue area for the polarization difference image, the contrasts (C) of the cancerous tissue area relative to the normal tissue area for all of the polarization and difference images were calculated. C is defined as:

$$C = (I_c - I_n) / (I_c + I_n) \quad [1]$$

where  $I_c$  and  $I_n$  are the local maximum values of the cancer-

ous and normal tissue area, respectively. Using the digital data shown in Figures 6(d), (e), and (f), the contrasts for these parallel, perpendicular, and polarization difference images are calculated to be 0.28, 0.26, and 0.45, respective-

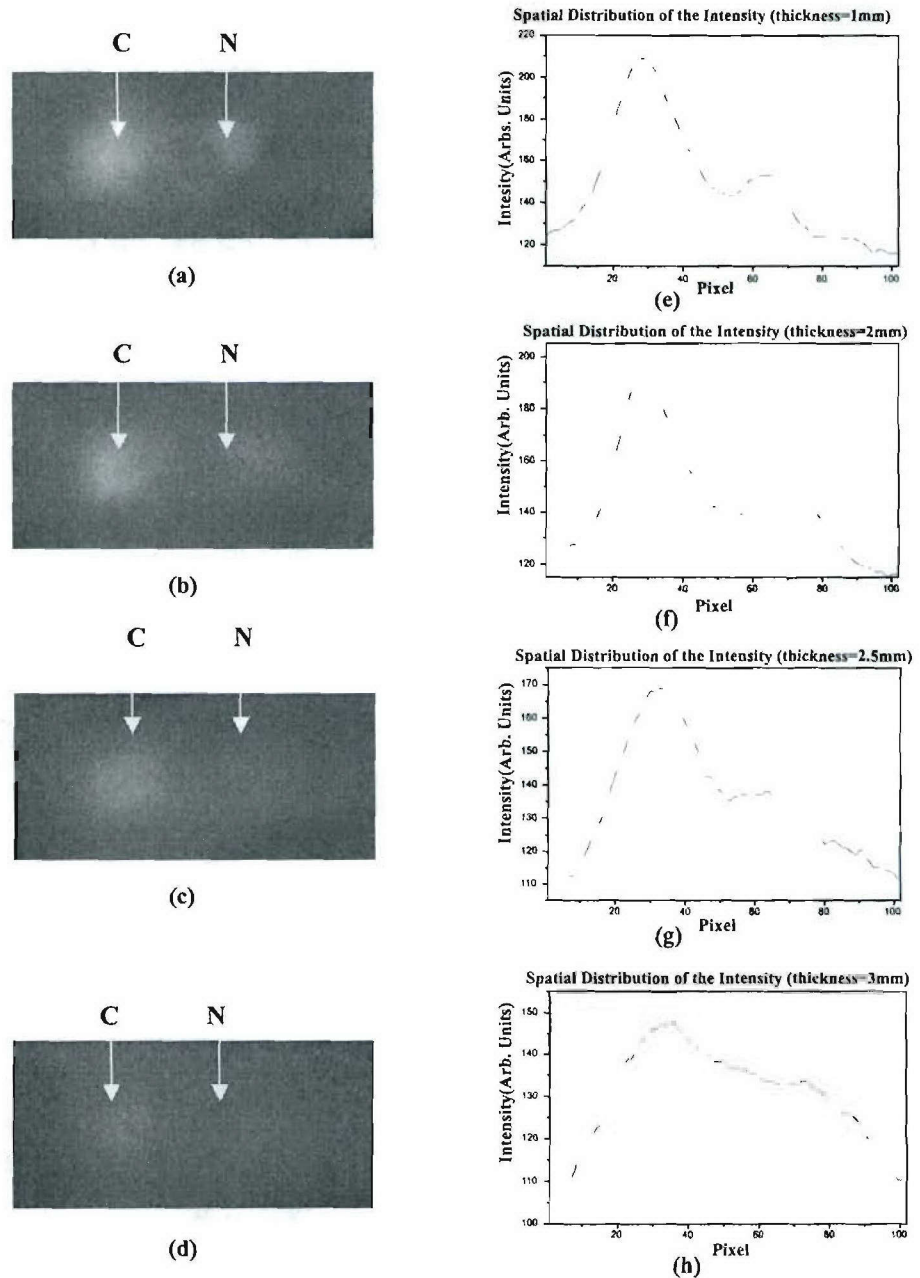


**Figure 7:** Depth-dependence of contrast agent emission images of a prostate cancer-and-normal tissue sample recorded at  $\lambda_{\text{pump}}=750\text{nm}$  and  $\lambda_{\text{detection}}=850\text{nm}$  with a perpendicular polarization configuration for depths of (a)  $\sim 1\text{mm}$ , (b)  $\sim 2\text{mm}$ , (c)  $\sim 2.5\text{mm}$ , and (d)  $\sim 3\text{mm}$  from the surface of the host normal tissue. (e), (f), (g), and (h) are the cross section intensity distributions of the images of (a), (b), (c), and (d) at the same row crossing the areas of the stained cancer (C) and normal (N) tissues. (a) to (c) and (e) to (g) clearly show that the intensity in the cancerous tissue area is much brighter than that of the normal tissue area. From (d) and (g), for a depth of  $\sim 3\text{mm}$ , although the image is blurred, the cancerous region can still be distinguished.

ly. These results indicate that Cybesin has a polarization preservation property similar to ICG, and the polarization difference image shown in Figure 6(c) has a better image contrast than that of the individual polarization images.

The image of the Cybesin dyed prostate cancerous and normal tissues hidden inside the host tissue is formed by photons emitted from Cybesin that have undergone coherent scattering (ballistic photon), less scattering (snake photon), and multiple scattering (diffusive photon) (17). Since most of the photons emitted by the contrast agent undergo multiple scattering, only small percentage of the photons retain their polarization information while they propagate in tissue, the intensities of the two image components  $I_{\parallel}$  and  $I_{\perp}$  have only small difference. When the two image components are subtracted ( $I_{\parallel} - I_{\perp}$ ), the strong diffusive image component is canceled out. Therefore the contrast of the polarization difference image is much better than that of each individual polarization image.

We also investigated the depth dependence of images at  $\lambda_{\text{pump}}=750$  nm and  $\lambda_{\text{detection}}=850$  nm using the sandwiched structure of the prostate tissue samples. The thickness of the host normal tissue in front of the stained cancerous and normal tissue pieces was varied up to 3 mm. In order to compare images of objects at different depths in the same polarization configuration, perpendicular imaging was measured. Figures 7(a) to (d) show the backscattering contrast agent emission images of the pair of stained cancerous-normal tissue pieces hidden by depths of  $\sim 1$  mm,  $\sim 2$  mm,  $\sim 2.5$  mm, and  $\sim 3$  mm, respectively. Figures 7(e), (f), (g), and (h) show the spatial cross section intensity distributions of the images of Figures 7(a), (b), (c), and (d), respectively. The results show that the intensity difference between normal and cancerous tissue can be clearly distinguished up to a depth of  $\sim 2.5$  mm. At a depth of  $\sim 3$  mm, the image is blurred, but the intensities of cancerous tissue are still stronger than that of normal tissue.

### Conclusion

Spectral measurements of a receptor-target contrast agent, Cybesin, and an optical imaging study was performed for human prostate cancerous and normal tissue stained with Cybesin. The experimental results show that prostate cancerous tissue takes up more Cybesin than normal tissue, and Cybesin can be used as a marker of a cancerous region. In addition, Cybesin is a sound contrast agent because its absorption and fluorescence spectra are in the NIR "tissue optical window". The fluorescence-polarization-difference-imaging (FPDI) technique was used to enhance the contrast between cancerous and normal tissue area. The depth dependence of polarization imaging was investigated. With optimum conditions using  $\lambda_{\text{pump}}=750$  nm and

$\lambda_{\text{detection}}=850$  nm, the cancerous prostate tissue can be distinguished at a depth of  $\sim 3$  mm using this contrast agent even for weak illumination of  $\sim 50$   $\mu\text{W}/\text{cm}^2$ .

### Acknowledgement

This research is supported by U. S. Army Medical Research and Materiel Command grant numbered DAMD17-01-1-0084 (CUNY RF 47462-00-01). The authors acknowledge the help of HUMC and NDRI for providing normal and cancer prostate tissue samples for the measurements, in particular, to Ms. Alexandra T. Sawczuk, RN at HUMC for her arrangement of prostate tissue samples.

### References

1. A. Abrahamsson and D. Bostwick. *The Biological Nature of Prostate Cancer – A Basis for New Treatment Approaches*. <http://www.urologi.org/sota/STA026/sta26app.pdf>.
2. D. A. Benaron. The Future of Cancer Imaging. *Cancer Metastasis Rev.* 21, 45-78 (2002).
3. V. G. Peters, D. R. Wyman, M. S. Patterson, G. L. Frank. Optical Properties of Normal and Diseased Human Breast Tissues in the Visible and Near Infrared. *Phys. Med. Biol.* 35, 1317-1334 (1990).
4. J. H. Ali, W. B. Wang, M. Zevallos, R. R. Alfano. Near Infrared Spectroscopy and Imaging to Probe Differences in Water Content in Normal and Cancer Human Prostate Tissues. *Technol Cancer Res Treat* 3, 491-497 (2004).
5. J. E. Bugaj, S. Achilefu, R. B. Dorshow, R. Rajagopalan. Novel Fluorescent Contrast Agents for Optical Imaging of *In Vivo* Tumor Based on a Receptor-targeted Dye-peptide Conjugate Platform. *J Biomed Opt* 6, 122-133 (2001).
6. L. Kai, B. Riefke, V. Ntziachristos, A. Becker, B. Chance, W. Semmler. Hydrophilic Cyanine Dyes as Contrast Agents for Near-infrared Tumor Imaging: Synthesis, Photophysical Properties, and Spectroscopic *In Vivo* Characterization. *Photochem Photobiol.* 72, 392-398 (2002).
7. W. Wang, J. H. Ali, R. R. Alfano, J. H. Vitenson, J. M. Lombardo. Spectral Polarization Imaging of Human Rectum-Membrane-Prostate Tissues. *IEEE Journal of Selected Topics in Quantum Electronics* 9, 288-293 (2003).
8. D. J. Dean, B. J. Korte. Biomedical Imaging and Bioengineering. *Optics & Photonics News*, October 2003 [http://ultra.bu.edu/papers/2003\\_10\\_OPN.pdf](http://ultra.bu.edu/papers/2003_10_OPN.pdf).
9. G. M. Hale, M. R. Querry. Optical Constants of Water in the 200-nm to 200-Mm Wavelength Region. *Applied Optics* 12, 555-563 (1973).
10. S. J. Goldsmith. Receptor Imaging: Competitive or Complementary to Antibody Imaging. *Semin. Nucl. Med.* 27, 85-93 (1997).
11. S. Achilefu, R. B. Dorshow, J. E. Bugaj, R. Rajagopalan. Novel Receptor-targeted Fluorescence Contrast Agent for *In Vivo* Tumor Imaging. *Investigative Radiology* 35, 479-485 (2000).
12. J. C. Reubi, S. Wenger, J. Schmuckli-Maurer, J.-C. Schaefer, M. Gugger. Bombesin Receptor Subtypes in Human Cancers: Detection with the Universal Radioligand ( $^{125}\text{I}$ )-(D-TYR(6), beta-ALA(11), PHE(13), NLE(14)) bombesin(6-14). *Clin Cancer Res* 8, 1139-1146 (2002).
13. M. Langer, A. G. Beck-Sickinger. Peptides as Carrier for Tumor Diagnosis and Treatment. *Curr Med Chem Anti-Canc Agents* 1, 71-93 (2001).
14. E. D. Gotsis. *In Vivo Proton MR Spectroscopy of Brain Lesions*. Institute of High Medical Technology EUROMEDICA, Advanced Research and Therapeutic Institute ENCEPHALOS. <http://users.mland.gr/sgotsis/spectroscopy/mrs.html>.

15. W. B. Wang, S. G. Demos, J. Ali, G. Zhang, R. R. Alfano. Visibility Enhancement of Fluorescent Objects Hidden in Animal Tissue Using Spectral Fluorescence Difference Method. *Optical Communications* 147, 11-15 (1998).
16. W. B. Wang, S. G. Demos, J. Ali, R. R. Alfano. Imaging Fluorescence Objects Embedded Inside Animal Tissue Using Polarization Difference Technique. *Optical Communications* 142, 161-166 (1997).
17. L. Wang, P. P. Ho, C. Liu, G. Zhang, R. R. Alfano. Ballistic 2-D Imaging Through Scattering Wall using an Ultrafast Kerr Gate. *Science* 253, 769-771 (1991).

*Date Received: January 10, 2005*

*Date Accepted: July 4, 2005*

## Near Infrared Spectroscopy and Imaging to Probe Differences in Water Content in Normal and Cancer Human Prostate Tissues

J. H. Ali, M.S.  
W. B. Wang, Ph.D.  
M. Zevallos, Ph.D.  
R. R. Alfano, Ph.D.\*

www.tcr.org

The content of water in cancerous and normal human prostate *in vitro* tissues was shown to be different using near infrared (NIR) spectroscopy. The water absorption peaks at 1444 nm and 1944 nm are observed in both types of prostate tissues. The measurements show that less water is contained in cancerous tissues than in normal tissues. The OH stretching vibrational overtone mode at 1444 nm and other water overtone modes provide key spectroscopic fingerprints to detect cancer in prostate tissue. Transmission and backscattered spectral imaging were measured in cancer and normal prostate tissues. The degree of polarization for 700nm, 800nm, 1200nm, and 1450nm is larger for normal than for cancer tissues. The knowledge about water content offers a potential as a diagnostic tool to better determine and image cancer in prostate and in other tissues types such as breast and cervix using the absorption from vibrational overtones of H<sub>2</sub>O molecules in the NIR.

Key words: Light scattering, Polarization, Prostate cancer detection, Water absorption, Optical imaging, Overtones, Cancer.

### Introduction

The interaction between light and tissues are wavelength dependent. Well-defined wavelengths can be absorbed by chromophores naturally present in tissue such as proteins, water, and adipose. Ever since Alfano and coworkers discovered that fluorescence spectroscopy can be used to detect cancer in tissues (1), optical spectroscopy using absorption, emission and scattering of light has been shown to be a novel way to detect diseases. Typically visible and UV light is used to excite the proteins and other chromophores present in tissues. NIR from 0.7 to 1.3  $\mu\text{m}$  is used to deeply probe tissues such as breast and brain. Since water is the main component of the tissue, water may be important to cancer probing. There are several different grades or stages of cancer, and these may be ranked using a well-known scale that classifies cancerous and precancerous regions into any of five Gleason Grades, usually denoted as Stages 1, 2, 3, 4 and 5 (2). Precancerous stages (denoted as stages 1 and 2) correspond to the early stages of cancer (3). These stages are associated with less amount of water content in these regions than at later stages. Water is one of the main components in the body and helps provide for the conversion of mechanical energy developed by contractile proteins into the chemical energy useful in cell processes. Regulating the water volume within the living cell affect the ability of contractile proteins mechanically control ion selectivity, ion accumulation, and electron transport in mitochondria (4, 5). Within local region in tissue, the amount of water varies very little from site to site. H<sub>2</sub>O is involved in chemical and phys-

Institute for Ultrafast Spectroscopy and Lasers and The New York State Center for Advanced Technology for Ultrafast Photonics Materials and Applications  
Department of Physics  
The City College and Graduate School of the City University of New York  
New York, NY 10031 USA

\* Corresponding Author:  
R. R. Alfano, Ph.D.  
Email: ralfano@sci.ccny.cuny.edu

iological reactions activated by light. The free OH stretching vibration in water has a spectral feature at  $3463\text{ cm}^{-1}$ . The Raman and infrared spectra of water and ice has been investigated (6-9). Bonding of  $\text{H}_2\text{O}$  molecules to other components in tissues give rise to a band at  $3434\text{ cm}^{-1}$  (or shift in OH from  $3463\text{ cm}^{-1}$  to  $3434\text{ cm}^{-1}$  due to hydrogen bonding). Overtones of OH vibrations exist at 1444 nm, 1944 nm and other wavelengths. A great deal of research has focused on nuclear magnetic resonance (NMR) spectroscopy, where the signal is generated by the nuclear spin of the present protons such as in water (10). NMR is used in tomography to yield images of various parts of the body to detect tumors. Optical vibrational spectroscopy and its use to image  $\text{H}_2\text{O}$  offers a new tool for optical diagnosis. It has been shown that the water spectrum of a rat or a mouse's skeletal muscle is broader than in pure water and this is due to the higher order complexes of water. This is due to the water molecules interaction with cellular or other macromolecules. Recently, it has been shown that the water heating via absorption band at 1430 nm is correlated to a higher tensile strength of tissue welded by a laser (11). Optical vibrational spectroscopy of a tissue sample contains information about the biochemical composition and vibrational structure of the tissue. As mentioned earlier, fluorescence and light scattering arising from proteins, nucleic acids, lipids, flavins, NADH, tryptophan, collagen, elastin and other macromolecules have been used to investigate normal, pre malignant, and malignant tissues (1, 12, 13). NIR spectral polarization imaging was used to image absorbers dyed with indocyanine green at different depths inside prostate tissues (14).

Current techniques for detection of prostate cancer have a limited contrast and resolution. These are: digital rectal examination (DRE), ultrasound imaging, and the prostate specific antigen (PSA) blood test. None of the techniques are able to detect early stages of cancer. There are a limited number of spectroscopic studies on the role of water in tissue particularly in tumors. It was shown that there is less water in cancer than normal prostate tissues probably associated with early stages of cancer (15). The water content may be used as a key native spectral marker molecule for cancer for cancer imaging. Water is proposed as a new fingerprint marker to denote changes in the NIR region for prostate, breast, and cervix cancer detection.

In this paper, we investigate near-infrared (NIR) spectral and polarization methods to determine the role of water in neoplastic tissues to detect and image, non-invasively, cancer in prostate tissues. The concept for this new approach to detect tumor is that the amount of water is different for normal and neoplastic tissues.

The NIR absorption is directly related to the concentration of water in the biological samples. From optical density meas-

urements or determination of the attenuation coefficient, water content can be determined in both cancer and normal tissues. The concentration of water may be able to monitor the cancer and normal states of tissue. We found that there is a lack of water in neoplastic tissues in comparison to surrounding normal tissues. The work reported here focuses on understanding the scattering and absorption of light by prostate tissue in the visible and NIR region (400-2400 nm). The difference in water absorption is investigated in cancer and normal human prostate tissues by means of spectroscopy, transmission and backscattering of visible and NIR and is due to the different intermolecular bonding by OH in  $\text{H}_2\text{O}$  in neoplastic and normal tissues. NIR imaging at overtone frequencies is used to distinguish local regions of tissues by their variation in water concentration. Our technique has the advantage over other spectroscopic techniques such as fluorescence and Raman scattering in its being sensitive to chromophores that absorb in the NIR independently of whether these chromophores fluoresce or have a large Raman cross sections. The detected NIR signals in this absorption technique are larger than fluorescence and Raman scattering signals. It is the first time to the best of our knowledge, that cancer can be detected and imaged based on the water content changes in the tissue. Our technique is related to the microstructure detection, measures the optical vibrational frequency of a bonded OH overtone bands in tissues. It describes the state of tissue through its bonding to OH.

### Materials and Methods

Prostate tissue specimens were obtained from the National Disease Research Institute (NDRI) under Institutional Review Board (IRB) at CCNY. A photograph of a typical specimen of human prostate tissue is inserted in Figure 1 using a conventional digital camera. Samples were preserved in saline water. Samples were cut evenly thin. Sample thicknesses were about  $330\text{ }\mu\text{m}$ , and their areas were about  $2 \times 3\text{ cm}^2$ . Samples were arranged such that the right hand side of the specimen was marked as mostly cancerous tissue, while the left hand side was mostly normal tissue. Five different specimens were investigated. For our study, the cancer tissues were harder than normal tissues.

The absorption spectra of normal, cancer prostate tissues, and water were measured using a Perkin-Elmer Lambda 9 UV/VIS/NIR Spectrophotometer with accompanied software. The optical density is defined as

$$O.D. = \ln\left(\frac{I_0}{I}\right) = \ln\left(\frac{1}{T}\right)$$

where  $I_0$  is the incident intensity,  $I$  is the transmitted intensity through the sample, and  $T$  is the transmission ( $T = I/I_0$ ). Images of the scattered light from human prostate samples were measured using the spectral polarization imaging setup

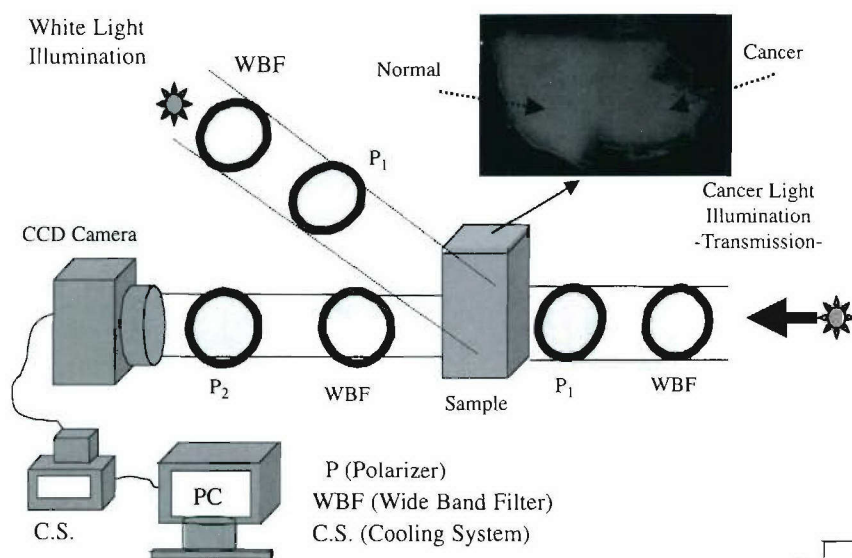


**Figure 1:** Experimental imaging set up for detection of human prostate cancer and normal tissues using a visible and near-infrared polarization technique. The insert shows the photograph of human cancer and normal prostate tissue using a conventional digital camera.

shown in Figure 1. In the imaging measurements, a white light beam of diameter  $\sim 2$  cm was used to illuminate the sample. Wide band filters centered at 700 nm, 800 nm, 1200 nm, and 1450 nm were used to select the desirable spectral range of the illumination and the detected light. The bandwidth of the optical filters is about 60 nm. A polarizer ( $P_1$ ) is located in the incident light beam pathway to obtain a linearly polarized illumination light. The second polarizer ( $P_2$ ) is positioned in front of the CCD camera for selecting the detection polarization direction (parallel and perpendicular relative to the orientation of  $P_1$ ). In the visible and NIR range (600-900 nm) a cooled CCD Silicon camera (Photomatrix CH250) equipped with a zoom lens of 50 mm focal length is used to record the images in the transmission and backscattering geometry. Similarly, images at 1200 nm and 1450 nm were obtained using an InGaAs NIR CCD camera.

### Results and Discussion

The absorption spectra of the five *in vitro* samples studied of thicknesses varying from 300 to 380  $\mu\text{m}$  show very similar results. The absorption spectra of normal and cancer prostate tissues (330  $\mu\text{m}$  thickness), and a water sample with a 200  $\mu\text{m}$  thickness used as a reference between 400 and 2400 nm are shown in Figure 2a. The fingerprints of water absorption in this spectral range are 980 nm (very weak), 1195 nm (weak), 1444 nm (strong), and 1930 nm (very strong). The absorption of water between 400 nm - 800 nm is almost flat and is very small compared to that at longer wavelengths such as 1444 nm and 1930 nm. The absorption at 1444 nm is due to the first overtone of the OH stretching vibration in water. It is well known that the absorption of the stretching vibration of the O-H bond in a non associated (free) alcoholic or phenolic hydroxyl group produces a strong band at 3600 to 3650  $\text{cm}^{-1}$  (2780 - 2740 nm, respec-

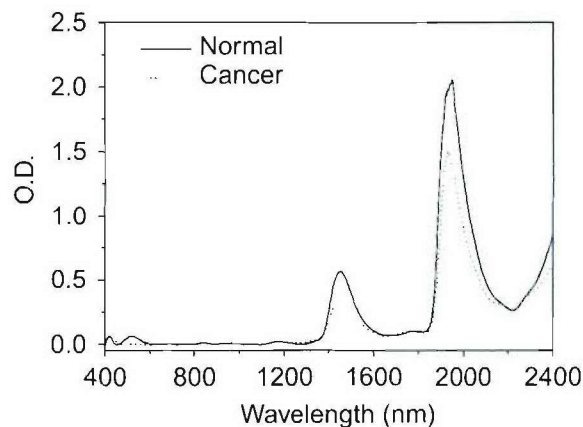
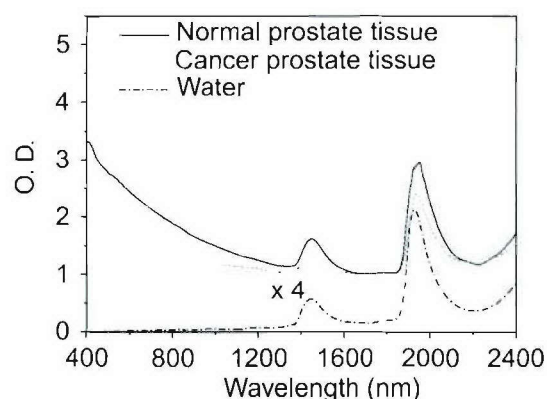


**Figure 2:** (a) Optical density (O.D.) versus wavelength in the 400 - 2400 nm region for (—) normal prostate tissue, (.....) Cancer prostate tissue, and (---) water. (b) Optical density for normal and cancer prostate tissues with scattering wing removed by subtracting the scattering effect in (a) using the scattering wavelength fitting function.

tively) in the fundamental region and near 7100  $\text{cm}^{-1}$  (1410 nm) for the first overtone (16).

It is well known that scattering is a smooth function of wavelength while absorption is represented by peaks in the NIR

spectra (17). The absorption and scattering spectra of cancer and normal prostate tissues shown in Figure 2a is composed of absorption bands superimposed on a smoothly varying background caused by light scattering. Figure 2 shows that scattering dominates in the visible to near infrared optical window (500 to 1200 nm), while the tissues absorption contribution is small in this region. It can be concluded from the optical density data displayed in Figure 2a that scattering from cancer tissue is stronger than the scattering from normal tissue in the forward direction between 400-1200 nm. Both cancer and normal cell nuclei are considered to be large particles (larger than the visible-NIR incident wavelengths) and they obey Mie scattering resulting in a strong forward scattering. Since the nucleus of the cancer cell is larger than that of the normal cell (18), the forward scattering intensity for cancer tissues is larger than that for the normal tissues. So, the transmission of cancer tissue is stronger than that of normal tissue. Absorption will play an important role in NIR at peaks bands ~ 1450 nm and 1940 nm, where the tissue absorption due to H<sub>2</sub>O is strong. At 1444 nm and 1944 nm the absorption dominates, so the absorption is stronger than scattering. The profiles show that absorption of normal tissue is stronger than that for cancer tissue at 1444 nm and 1944 nm, which indicates that the content of water in normal tissues is more than that in cancer tissues. These peaks around 1444 nm and 1944 nm in prostate tissue are due to the water-tissue interaction and are shifted toward longer wavelengths from the stretching frequency of a bonded free OH group (shifts towards the lower wave numbers). This is probably due to the higher order phases of water and their interaction with cellular or other macromolecules in prostate tissues.

We noticed that strong forward scattering is still present for a 330 μm thickness. Since the g factor in tissue is large (~0.9), the scattering is strongly forward. We can estimate the attenuation length in this tissue based on the exponential decay process (proportional to  $e^{-\mu_t x}$ ), where  $\mu_t$  is the attenuation (extinction) coefficient. The calculated extinction coefficients ( $\mu_e$ ) of water at different wavelengths are given in Table I. The extinction coefficient of water at 700 nm is ~0.433 cm<sup>-1</sup> (the attenuation length is about 2.31 cm), 1.29 cm<sup>-1</sup> at 1200 nm, and 9.7 cm<sup>-1</sup> at 1450 nm. The attenuating length at 1450 is ~7.5 times shorter than that at 1200 nm and approximately 22 times shorter than 700 nm in water. To

remove the effect of scattering on the profile shown in Figure 2a, a smooth fitted curve reflecting the contribution of scattering is subtracted from the original curve. The smooth fitted curve is obtained by choosing data points along the scattering curve and fitting that to a high-order polynomial function. The result is shown in Figure 2b. The absorption fingerprints in the visible region at 420 nm and 570 nm are due to the blood in the tissue matrix (Hb and HbO<sub>2</sub>).

In prostate cancer tissue, the attenuation length at 1450 nm is ~1.2 times smaller than that at 1200 nm. In prostate normal tissue, the attenuation length at 1450 nm is ~1.3 times smaller than that at 1200 nm. The total attenuation coefficient of normal tissue is larger than that of cancer (as seen in Table I). The attenuation length (equal to  $1/\mu_t$ ) of normal tissue is shorter than that of cancer tissue. This means that the photons traveling in prostate normal tissue will be absorbed and scattered at a shorter distance than that of cancer tissue. The attenuating length

$$(l_t = \frac{1}{n\sigma})$$

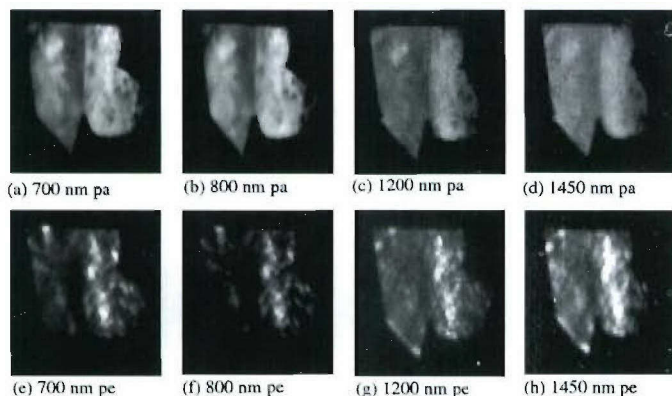
is inversely proportional to the number of particles per unit volume (n) and the cross section of the scatterer ( $\sigma$ ).

Figure 3 shows transmission images of cancer-normal samples at 700 nm, 800 nm, 1200 nm, and 1450 nm for parallel and perpendicular polarization. The left piece of the specimen (mostly normal) has less transmission intensity than that on the right side (mostly cancer) at all wavelengths (700 nm, 800 nm, 1200 nm, and 1450 nm) as shown in Figures 3a-h. Similar results were obtained in normal-cancerous human breast tissues using picosecond temporal time-gated imaging at 800 nm by the use of a Ti:Sapphire pulsed laser (19). In the large particle case (Mie scattering), the intensity for the forward scattering is higher than that for the backscattering. Since the nuclei of cells in cancer tissue are larger than that for normal tissue, the forward scattering for cancer samples are expected to be larger than that for normal samples in the forward direction (18, 20). At 1200 nm the scattering is stronger than absorption. The forward scattering intensity from cancer tissues at 1200 nm is higher than that from normal tissues as shown in Figure 2. As a result the transmission through cancer tissues is more than that for normal as shown

**Table I**

Extinction coefficient ( $\mu_e$ ), optical density (O.D.) and transmission (T) of human prostate normal tissue (N), prostate cancer tissue (C) and water (W) as calculated from the measured results.

$\lambda$ (nm)	O.D.			T			$\mu_e$ (cm <sup>-1</sup> )		
	C	N	W	C	N	W	C	N	W
700	1.50	2.14	0.0062	0.0326	0.0074	0.9858	104	149	0.433
800	1.37	1.89	0.0077	0.0440	0.0132	0.9824	95	131	0.5380
1200	1.10	1.25	0.0185	0.0818	0.0577	0.9583	76	86	1.29
1450	1.36	1.61	0.1394	0.0451	0.0252	0.7254	94	112	9.70



**Figure 3:** Transmission images of human prostate tissue, normal (left) and cancer (right) at different visible and NIR wavelengths for parallel (top images) and perpendicular (bottom images) polarization configurations. The sample thickness is  $\sim 330 \mu\text{m}$  and its area is  $2 \times 3 \text{ cm}^2$ .

in the images in Figures 3c (parallel) and 3g (perpendicular). At 1450 nm wavelength absorption dominates, so the main reason for the higher transmission in a cancer region is due to less  $\text{H}_2\text{O}$  in cancer than in normal regions, which is related to the microscopic bonding of OH in prostate tissues. The transmission intensity through normal tissues is weaker than that of cancer tissues. The tissue that has more water in it will absorb the incoming photons more than that which has less water at the absorption peaks of water. This difference in the concentration of water in tissue will also cause difference in the degree of scattering. The difference in the images displayed in Figures 3d and 3h result mainly from the smaller absorption of water in cancer tissue (first overtone of the OH stretching vibration); in addition, the forward scattering in cancer tissues is larger than that of normal tissues.

From the curves displayed in Figures 2a and 2b, the absorption peak at 1450 nm is stronger than that at 1200 nm. The scattering at 1450 nm is less than that at 1200 nm. Most of the photons at 1450 nm that are incident on the samples get strongly absorbed by water molecules. Photons at 1200 nm get absorbed less. Since cell nuclei are larger than the incident wavelengths they predominantly scatter light in the forward direction. The scattered intensity is related to the population density of the nuclei. For the perpendicular imaging case, the depolarization is due mostly to multiple scattering events. The depolarization is caused by the cell size, shape, and

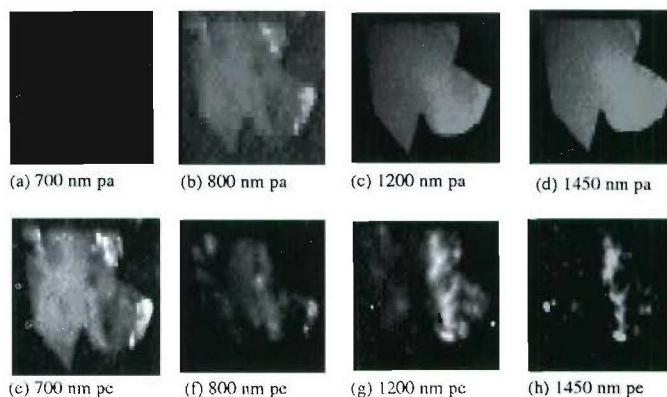
anisotropy, these will cause photons to be more depolarized in cancer tissue. Cancer cells are more randomized in shape and size. The internal structures of the cancer tissue randomize the light more than for normal tissue in the forward direction, which is highly ordered in water as shown in Figure 3.

In the backscattering geometry, images as shown in Figure 4, the light scattering from cancer tissues is stronger than that from normal tissues. It is known that the index of refraction for cancer tissue is higher than that of normal tissue (18). The scattering angle  $\theta_S$  can be written in terms of the scattering wavelength ( $\lambda$ ) and the size of the scatterer ( $a$ ) as

$$\theta_S \sim \frac{\lambda}{a}$$

For objects having small scattering sizes relative to incident wavelength, such as mitochondria (much smaller than normal cell size), scattering in the backward direction is larger, giving a stronger signal for scattering off small structures. The mitochondria index of refraction for cancer tissues is higher than that for normal tissues. This is one of the reasons why small particles such as mitochondria are an important factor in backscattering and for large angle scattering. The index of refraction of tissues is a function of water content varies linearly between 1.33 and 1.50 for water contents between 100 percent and 0 percent, respectively (21). Consequently, it is generally given by:  $n = 1.5 - (1.5 - 1.33) \cdot W$ ,

**Figure 4:** Backscattered images of human prostate normal (left) and cancer (right) tissue at different visible and NIR wavelengths for parallel (top images) and perpendicular (bottom images) polarization configurations. The sample thickness is  $\sim 330 \mu\text{m}$  and had an area of  $2 \times 3 \text{ cm}^2$ .



where  $W$  is the volume fraction of water (21, 22). Accordingly, since cancer tissue has less water than normal tissue it has a higher index of refraction than normal tissue. Due to the following factors: cancer tissue has higher index of refraction than normal tissues, and as a consequence has weak absorption by water in the NIR, it is expected that the backscattering intensity for cancer tissue is larger than that of normal tissue as shown in Figure 4. It is also known that smaller particles in tissues such as mitochondria play a major role in the backscattering geometry (18, 23). Mitochondria from cancer cells has a higher index of refraction than from normal cells. The backscattering signal from tissue is determined mainly by the index of refraction and the particle sizes. The cancer region will be brighter than the normal region due to its higher index of refraction, lower  $H_2O$  absorption, and small particle sizes.

Digitized horizontal scans from left to right at the center of the transmission images displayed in Figures 3a-d were obtained. The digitized images show that the cancer tissue region scatters more than that of the normal tissue region due to the reasons that have been discussed earlier. Linearly polarized light incident on tissue loses its polarization as it traverses the medium. A portion of the incident light is backscattered by the tissue surface, retaining its polarization in this single scattering event. The remaining light propagates in a turbid medium such as prostate tissues and can be viewed as consisting of three components: ballistic, snake and diffusive. Diffusive light is the dominant component consisting of multiple-scattered photons that travel the longest path, and takes the longest time to exit the sample. Ballistic photons traverse the shortest path, retain most of the characteristics of the incident photons, and carry direct information about the interior structure of the scattering medium. Snake photons follow the ballistic light in time and involve in more scattering events; they retain a significant amount of the initial properties and information on structures hidden in the scattering medium. The degree of polarization is determined by using the relationship:

$$D = (I_{\parallel} - I_{\perp}) / (I_{\parallel} + I_{\perp}), \quad [1]$$

where  $I_{\parallel}$  and  $I_{\perp}$  are the intensities for the parallel and perpendicular components of the reflected or scattered light from the object, respectively. The contrast is the difference in light intensity in an object or image, and defined as:

$$C = (I_{\max} - I_{\min}) / (I_{\max} + I_{\min}), \quad [2]$$

where the  $I_{\max}$  and  $I_{\min}$  are the maximum and minimum intensities of light recorded from the object, respectively.

The calculated contrasts between cancer ( $I_{\max}$ ) and normal tissues ( $I_{\min}$ ) are 0.11 at 700 nm and 800 nm, 0.17 at 1200

nm, and 0.15 at 1450 nm. The main difference between the 1200 nm and 1450 nm contrasts is that at 1450 nm the resulting contrast is due to the microscopic OH bonding in prostate tissue while at 1200 nm the difference may be due to the macroscopic scattering size and population density in the prostate tissue.

The calculated degree of polarization ( $D$ ) for normal and cancer tissues at different wavelengths is shown in Table II. The values of  $D$  for normal tissues are higher than that for cancer tissue at all wavelengths (700 nm, 800 nm, 1200 nm, and 1450 nm). This result is expected, arising from the greater randomization (size and shape) of the cancer cells while the normal cells are more ordered than cancer in tissues. The degree of polarization of outgoing light depends on the details of the single scattering by the particle and the number of scattering encountered by light. Light is less depolarized in one scattering event if the scattering is more forward-directed, which is characterized by the anisotropy factor  $g$ . Roughly speaking,  $D$  is related to the ratio of the sample thickness of the slab over the transport length rather than the size of the particle.  $D$  decreases as this ratio increases. Bicout *et al.* (24) show that for small particle size there is a maximum point of polarization, then followed by a decrease in polarization. Tissues, however, have large particles sizes that vary in sizes and shapes that complicate the degree of polarization calculation. Assuming spherical particles for normal and cancer nucleus, it can be derived from Mie calculations that the transport length of the normal tissue is larger than that of the cancer tissue. This results in a slower depolarization for normal tissue than that for cancer tissue. The degree of polarization of the cancer and normal tissues increases as the wavelength increases (see Table II), which suggest that at longer wavelengths the light will be less scattered.

**Table II**  
The degree of polarization of the images in Figures 3a-d.

$\lambda$ (nm)	$D_{\text{Normal}}$	$D_{\text{Cancer}}$
700	0.079	0.059
800	0.100	0.088
1200	0.761	0.435
1450	0.849	0.749

The amount of water in tissues alters the absorption in the NIR from the OH overtone vibrational bands at 1444 nm and 1944 nm. These key spectra fingerprints are used to distinguish between low concentration and high concentration region of water. The local deviations in both the concentration of water and cell size in prostate tissue causes differences in the degree of scattering and overtone absorption. The difference in water content in normal and cancer prostate tissues can be imaged and used for prostate cancer detection. This method can be extended to detect cancer in other organs such

as breast and cervix. It appears that cancer tissues may contain less water than normal tissues at an early stage of cancer (15). It was found that the forward scattering intensity for cancer tissues is larger than that for normal tissues. Due to the higher index of refraction of cancer tissues, and the lower absorption of water in cancer, the backscattering intensity for cancer tissue was found to be larger than that of normal tissue. This information can be used to detect cancer regions in prostate tissue using NIR spectral polarization and difference imaging techniques. Water may also be an important spectral fingerprint marker in other tissue types such as breast and cervix to detect cancer at early stages.

### Acknowledgments

The authors acknowledge the help of NDRI for providing normal and cancer prostate tissues for measurements. This research was supported by U. S. Army Medical Research and Materiel Command grant numbered DAMD17-01-1-0084, (CUNY RF 47462-00-01), and Mediscience Technology Corp. We thank the fruitful discussions with Prof. S. Jacques and also thank Dr. J. Vitenson (MD) from Hackensack University Medical Center (HUMC) for his continued interest, fruitful discussion, and medical insight.

### References

- Alfano, R. R., Tata, D., Cordero, J., Tomashefsky, P., Lonyo, F., and Alfano, M. Laser Induced Fluorescence Spectroscopy from Native Cancerous and Normal Tissue. *IEEE J. Quantum Electron* 20, 1507-1511 (1984).
- Rosai, J. *Ackerman's Surgical Pathology, Vol. 2*. Mosby Incorporated, CA. (1998).
- Gleason, D. F., Mellinger, G. T. Prediction of Prognosis for Prostatic Adenocarcinoma by Combined Histological Grading and Clinical Staging. *J. Urol.* 111, 58-64 (1974).
- Szent-Gyorgyi, A. *Bioenergetics*. Academic Press, New York (1957).
- Minkoff, L. and Damadian, R. Biological Ion Exchanger Resins. *Physiol. Chem. & Physics* 8, 349-387 (1976).
- Ockman, N. and Sutherland, G. B. Infrared and Raman Spectra of Single Crystals of Ice. *Proc. Roy. Soc. Vol. A247*, 434-440 (1958).
- Shin, H. K. Vibrational Relaxation of Water Molecules Near Room Temperature. *J. Chem. Phys.* 69, 1240-1245 (1978).
- Walrafen, G. E. Raman Spectral Studies of the Effect of Temperature on Water and Electrolyte Solution. *J. Chem. Phys.* 44, 1546-1558 (1966).
- Sceats, M., Rice, S. A., and Butler, J. E. The Stimulated Raman Spectrum of Water and Its Relationship to Liquid Structure. *J. Chem. Phys.* 63, 5390-5400 (1975).
- Hazlewood, C. and Nicholas, B. Evidence for the Existences of a Minimum of Two Phases of Ordered Water in Skeletal Muscle. *Nature* 222, 747-750 (1969).
- Tang, J., Zeng, F., Evans, J., Xu, B., Savage, H., Ho, P. P., and Alfano, R. R. A Comparison of Cunyite and Fosterite NIR Tunable Laser Tissue Welding Using Native Collagen Fluorescence Imaging. *J. Clin. Laser Med. Surg.* 18, 117-123 (2000).
- Alfano, R. R., Das, B. B., Cleary, J., Prudente, R., and Celmer, E. Light Sheds Light on Cancer – Distinguishing Malignant Tumors from Benign Tissues and Tumors. *Bull. N.Y. Acad. Med.* 67, 143-150 (1991).
- Liu, C. H., Das, B. B., Sha Glassman, W. L., Tang, G. C., Yoo, K. M., Zhu, H. R., Akins, D. L., Lubicz, S. S., Cleary, J., Prudente, R., Celmer, E., Caron, A., and Alfano, R. R. NIR Raman and Fluorescence Spectroscopies Diagnose Cancer. *J. Photochem. Photobiol.* 1887, 188-194 (1992).
- Wang, W. B., Ali, J. H., Vitenson, J. M., Lombardo, J. M., and Alfano, R. R. Spectral Polarization Imaging of Human Prostate Tissues. *SPIE* 3917, 75-78 (2000).
- Wang, W. B., Ali, J. H., Zevallos, M., and Alfano, R. R. Near Infrared Imaging of Human Prostate Cancerous and Normal Tissues Based on Water Absorption, in *OSA Biomedical Optics Topical Meetings on CD-ROM (The Optical Society of American, Washington, DC), MF 38* (2004).
- Williams, D. Frequency Assignments in Infrared Spectrum of Water. *Nature* 210, 194-195 (1966).
- Marks, F. A. Optical Spectroscopy of Breast Biopsies and Human Breast Cancer Xenografts in Nude Mice. *Frontiers in Bioscience* 3, a1-10 (1998).
- Backman, V., Gurjar, R., Badizadegan, K., Itzkan, I., Dasari, R., Perelman, L., and Feld, M. Polarized Light Scattering Spectroscopy for Quantitative Measurement of Epithelial Cellular Structures *In Situ*. *IEEE J. Select. Topics Q. E.* 5, 1019-1026 (1999).
- Gayen, S. K. and Alfano, R. R. Sensing Lesions in Tissues with Light. *Optics Express* 4, 475-480 (1999).
- Shao, Y., Maximov, A., Ourdev, I., Rozmus, W., and Capjack, C. Spectral Method Simulations of Light Scattering by Biological Cells. *IEEE J. Q. E.* 37, 617-625 (2001).
- Prahl, S. A. *Light Transport in Tissue, Ph.D. Thesis*. University of Texas at Austin (1988).
- Private communication with Prof. Steven Jacques (2003).
- Dunn, A. and Richards-Kortum, R. Three Dimensional Computation of Light Scattering from Cells. *IEEE J. Q. E.* 2, 898-905 (1996).
- Bicout, D., Brosseau, C., A. Martinez, S., and Schmitt, J. M. *Phys. Rev. E* 49, 1767 (1994).

Date Received: May 20, 2004

# Spectral Polarization Imaging of Human Rectum-Membrane-Prostate Tissues

Wubao B. Wang, Jamal H. Ali, Robert R. Alfano, *Fellow, IEEE*, Jack H. Vitenson, and Joseph M. Lombardo

**Abstract**—Human rectum-membrane-prostate tissue samples were studied using near-infrared spectral polarization imaging technique to detect small objects and structural changes inside prostate tissues through the rectum. Four modeling samples were made with a small piece of absorber or prostate tissue dyed with a contrast agent (indocyanine green) embedded inside a large piece of prostate tissue in rectum-membrane-prostate structures. The depth of the foreign objects underneath the surface of the rectum-membrane-prostate structures was varied from a millimeter to a centimeter to obtain the critical imaging distance. Different spectral polarization imaging methods with and without contrast agents were performed and compared. The results show that small objects hidden inside the host prostate tissues in the rectum-membrane-prostate structures at depths of 2.5, 4.0, and 7.5 mm can be imaged and identified using the scattering light imaging, tissue emission wing imaging, and contrast agent fluorescence imaging methods, respectively. Our results indicate the potential of imaging and detecting structural changes and cancers inside prostate tissue through rectum-membrane-prostate tissues using noninvasive spectral polarization imaging technique.

**Index Terms**—Absorption, contrast agent, human prostate cancer, light scattering, spectral and polarization imaging, tissue emission wing, turbid media.

## I. INTRODUCTION

PROSTATE cancer has a high incidence and mortality rate for men [1]. The detection and treatment of early small prostate cancers are most important to prevent death attributable to prostate cancers. Current techniques for detection of prostate cancers have limited accuracy. The common methods for monitoring prostate cancers are the prostate specific antigen (PSA) blood test and a digital rectal examination (DRE). When the PSA level is elevated or when the DRE is abnormal, there is a one-in-three chance that cancer is present. This diagnosis can only be confirmed by a needle biopsy of the prostate. In the biopsy, a number of cores of prostate tissue are taken with a thin needle guided into selected regions of the prostate with an ultrasound probe [1]. Since the ultrasound imaging has poor spatial

resolution and contrast, and the needle biopsy is invasive, better methods are needed to develop high-resolution and noninvasive techniques for early small prostate cancer detection.

Based on spectral and polarization properties of the light scattered, absorbed, and/or emitted from tissues and contrast agents [2]–[7], we have developed near-infrared (NIR) spectral polarization imaging methods to enhance the ability of imaging objects hidden inside turbid media and tissues [4]–[8]. A prototype wide-band NIR spectral polarization imaging instrument was built, and has been used for imaging measurements on human prostate tissue samples. The results show that small objects hidden inside the host prostate tissues at depths of up to 8.5 mm can be identified using the NIR spectral polarization imaging methods [8].

Similar to the digital rectal examination through the rectum for checking an abnormal prostate in clinical, the best way to optically image prostate tumors is illuminating and imaging the prostate gland through rectum. For this reason, we have imaged objects hidden inside prostate tissues through rectum-membrane-prostate tissues.

In this paper, we present our results on spectral polarization imaging studies for four model human rectum-membrane-prostate tissue samples in the NIR range from 650 to 900 nm. The model rectum-membrane-prostate samples were made with a small piece of absorber or prostate tissue stained with indocyanine green dye embedded inside a large piece of prostate tissues in a rectum-membrane-prostate structure. The measurements show that the longer wavelength NIR light scattered or emitted from tissues and contrast agents are preferred for detecting objects hidden in prostate tissues in rectum-membrane-prostate structures.

## II. SAMPLES AND EXPERIMENTAL METHODS

Human rectum-membrane-prostate tissue samples were obtained from autopsy cases at Hackensack University Medical Center (HUMC) and used for the NIR spectral polarization imaging measurements under the Institutional Review Board approvals from both HUMC and City College of New York. The prostate glands were cut into pieces with thickness from  $\sim 1$  to  $\sim 3$  mm. The slices of the prostate tissue used are uniform. Four model rectum-membrane-prostate tissue samples were made with a small piece of an object such as an absorber as shown in Fig. 1(a), or a tiny piece of prostate tissue dyed with a contrast agent (indocyanine green) embedded inside a large host piece of prostate tissue in a rectum-membrane-prostate tissue structure as shown in Fig. 1(b). The depth of the objects beneath the surface of the rectum-membrane-prostate tissue structure was varied by using different prostate tissue slices to obtain the critical imaging depth.

Manuscript received December 6, 2002; revised February 12, 2003. This work was supported in part by the U.S. Army Medical Research and Materiel Command Grant DAMA17-01-1-084 (CUNY RF 47462-00-01), in part by the Department of Energy Center for Laser Imaging and Cancer Diagnosis at CCNY, and in part by the New York State Technology Foundation.

W. B. Wang, J. H. Ali, and R. R. Alfano are with the Institute for Ultrafast Spectroscopy and Lasers, and New York State Center for Advanced Technology for Ultrafast Photonic Materials and Applications, Department of Physics, City College, City University of New York, New York, NY 10031 USA (e-mail: wwang@sci.cuny.cuny.edu).

J. H. Vitenson is with the Urology Department, Hackensack University Medical Center, Hackensack, NJ 07601 USA.

J. M. Lombardo is with the Pathology Department, Hackensack University Medical Center, Hackensack, NJ 07601 USA.

Digital Object Identifier 10.1109/JSTQE.2003.813301

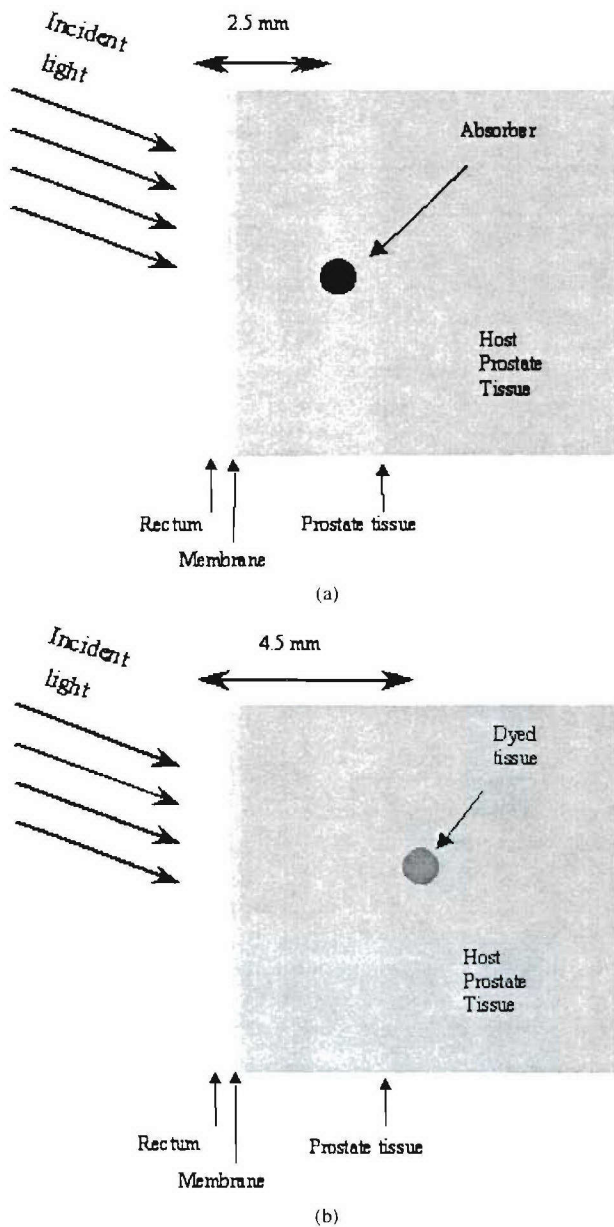


Fig. 1. Layer structures of model rectum-membrane-prostate tissue samples made of (a) a small dot piece of black absorber and (b) a tiny piece of prostate tissue dyed with indocyanine green embedded inside a larger piece of host prostate tissue in a rectum-membrane-prostate structure.

The NIR spectral polarization imaging setup used for the imaging measurements was presented elsewhere [8]. Light from a white light source is used to illuminate a sample with an average power of  $\sim 50 \mu\text{W}/\text{cm}^2$ , which is much lower than the critical illumination level given by FDA. The illumination and detection wavelengths are selected by wide-band pass filters placed on two multiple filter wheels, which are located in the illumination and detection paths, respectively, and can be rotated to the desired filter position controlled by a computer. The wavelengths of the wide-band pass filters change from 550 to 900 nm with full-width at half-maximum = 40 nm for each filters. A charge coupled device (CCD) camera records the images formed by light scattered or emitted from the samples. Polarizers  $P_1$  placed in the illumination path, and  $P_2$  placed in front of the CCD, are used to choose the polarization configuration

of the illumination and detection. The images can be recorded when the detection polarization is parallel or perpendicular to that of illumination.

Different imaging methods, which include scattered light imaging, tissue emission wing imaging, and contrast agent fluorescence imaging, were performed and compared to image objects inside rectum-membrane-prostate tissue structures. For scattered light imaging, the same illumination and detection band pass filters are used. For emission light imaging, the band pass wavelengths of the detection (imaging) filter are longer than that of the illumination so that the pump light is blocked, and only the light emitted from the sample is collected by the CCD camera. Since the scattering, absorption, and emission properties of the hidden foreign objects and prostate tissues are different, both scattered and emitted NIR light images can be used to identify the objects hidden inside prostate tissues.

### III. EXPERIMENTAL RESULTS

#### A. Scattered Light Imaging

The sample used for the scattered light imaging measurements consisted of a small piece of absorber ( $\sim \phi 1 \text{ mm}$ ) embedded inside a large slice of prostate tissue ( $\sim 30 \times 20 \text{ mm}$ ) in a rectum-membrane-prostate structure with a depth of  $\sim 2.5 \text{ mm}$  from the surface of the rectum-membrane-prostate tissue structure [see Fig. 1(a)]. During the measurements, the illumination and detection wavelengths were synchronously changed so that the detection wavelengths were always kept the same as that of illumination. In this way, the emission light is blocked, and the CCD camera only collects the light scattered from the sample.

The scattered light images recorded at the wavelengths of 600, 700, and 800 nm with the detection polarization perpendicular to that of illumination are shown in Fig. 2(a)–(c). It can be seen that the object (absorber) cannot be distinguished by the 600 nm image, but it can be clearly identified as a dark point by the 800 nm image. As the wavelength increases from 600 to 800 nm, the visibility of the object improves. The wavelength dependence of the image quality of the scattered light images can be explained by the relative absorption spectra of the prostate and rectum tissues shown in Fig. 3. The relative absorptions of the prostate and rectum tissues decrease when the wavelength increases from 400 nm to NIR. The short wavelength (such as 600 nm) light was absorbed and scattered strongly by the surface and near surface layers of the rectum-membrane-prostate tissues, and could not reach the object deeply embedded in the host prostate tissue. In this case, the scattered light images are formed by the light scattered only from the surface and near surface tissue layers with almost no contribution from the object, and therefore, the object cannot be identified. In contrast, the larger penetration of the longer wavelength NIR light in rectum-membrane-prostate tissues enables them to reach the deeper object. Once the NIR light reaches the object, the difference of scattering and absorption properties between the foreign object and the surrounding tissues is reflected in the image, and therefore, the foreign object can be identified by the NIR scattering images.

The scattered light imaging measurements were extended to other rectum-membrane-prostate tissue samples with objects embedded at a depth greater than 2.5 mm. The results show that the image measurements were repeatable for different prostate

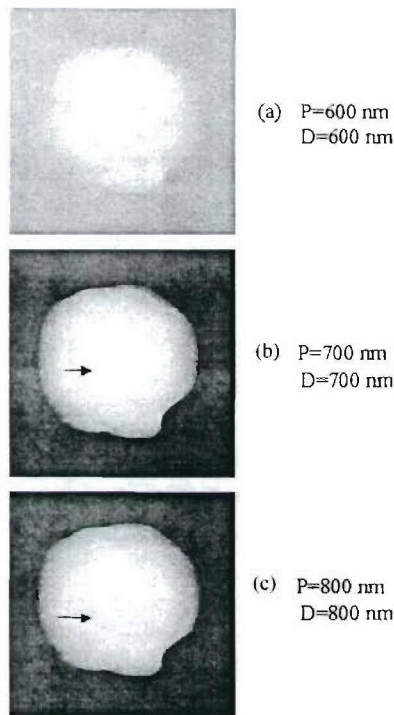


Fig. 2. Scattered light images recorded at wavelengths of (a) 600, (b) 700, and (c) 800 nm, respectively, where *P*: pump, *D*: detection. The sample consists of a small dot piece of a black absorber hidden inside a large host prostate tissue in a human rectum-membrane-prostate structure at depth of 2.5 mm from the surface of the rectum.

slices with the same thickness of  $\sim 2.5$  mm, but, at the same low illumination intensity of  $\sim 50 \mu\text{W}/\text{cm}^2$ , the object could not be observed with depth more than 2.5 mm even from the images obtained at longer wavelengths of 750 nm–850 nm.

*B. Tissue Emission Wing Imaging*

The sample used for the tissue emission wing imaging measurements consisted of a small piece of absorber ( $\sim \phi 1$  mm) embedded inside a large slice of prostate tissue ( $\sim 30 \times 20$  mm) in a rectum-membrane-prostate structure as shown in Fig. 1(a) with a depth of  $\sim 4.0$  mm from the surface of the rectum-membrane-prostate tissue structure. The tissue emission wing images are formed by the light emitted, not scattered, from the rectum-membrane-prostate sample tissues at the NIR emission wing range. In tissue emission wing imaging measurements, the detection wavelengths used were longer than that of the illumination so that the pump light was blocked, and the images recorded by CCD camera were formed only by light emitted from tissues.

The tissue emission images recorded at the wavelengths of 650, 700, and 800 nm with pump wavelengths of 550, 600, and 700 nm, are shown in Fig. 4(a)–(c), respectively. It can be seen that the object (absorber) cannot be observed by the 650 and 700 nm images, but can be identified by the 800 nm image. In order to determine the critical detection depth of the tissue emission wing imaging, the measurements were extended to the sample with object hidden at depth greater than 4.0 mm at the detection wavelength of 800 nm and the illumination wavelength of 700 nm. The results show that the object cannot be observed with depth more than 4.0 mm.

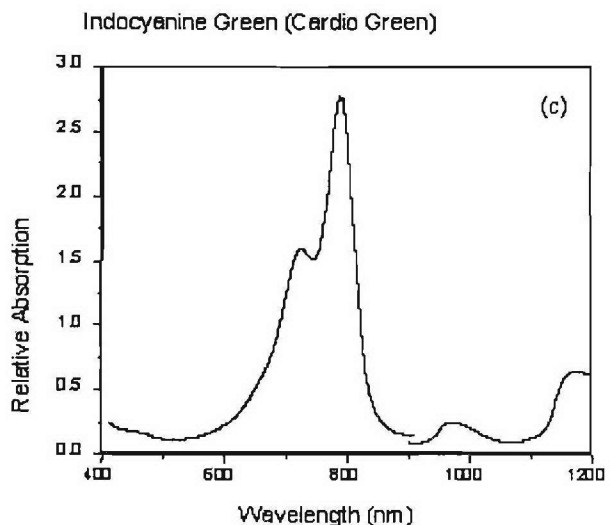
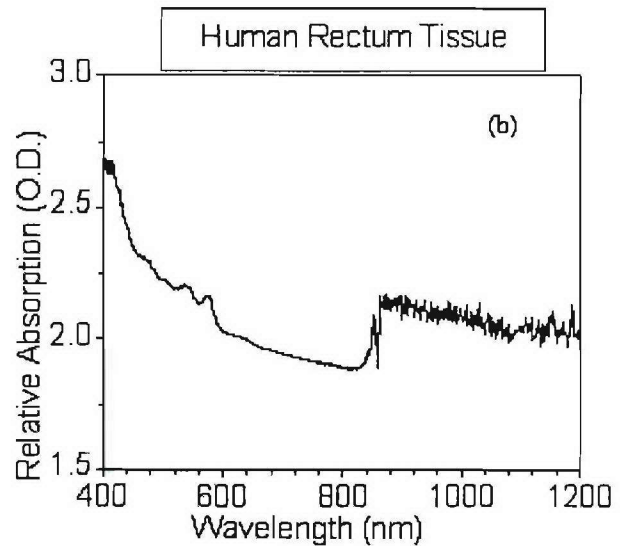
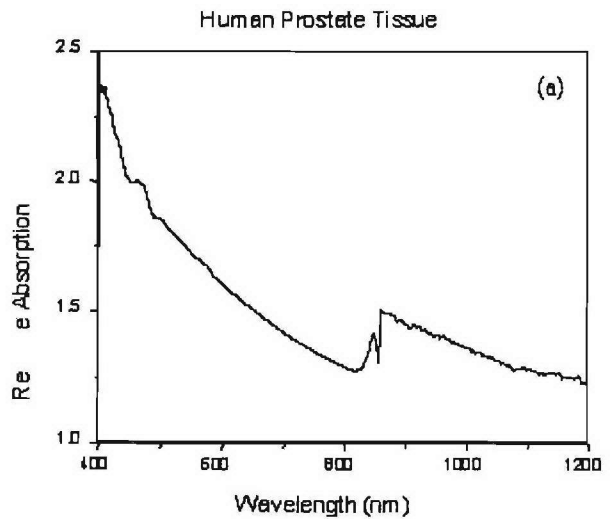


Fig. 3. Relative absorption spectrum for (a) human prostate tissue, (b) human rectum tissue, and (c) indocyanine green dye.

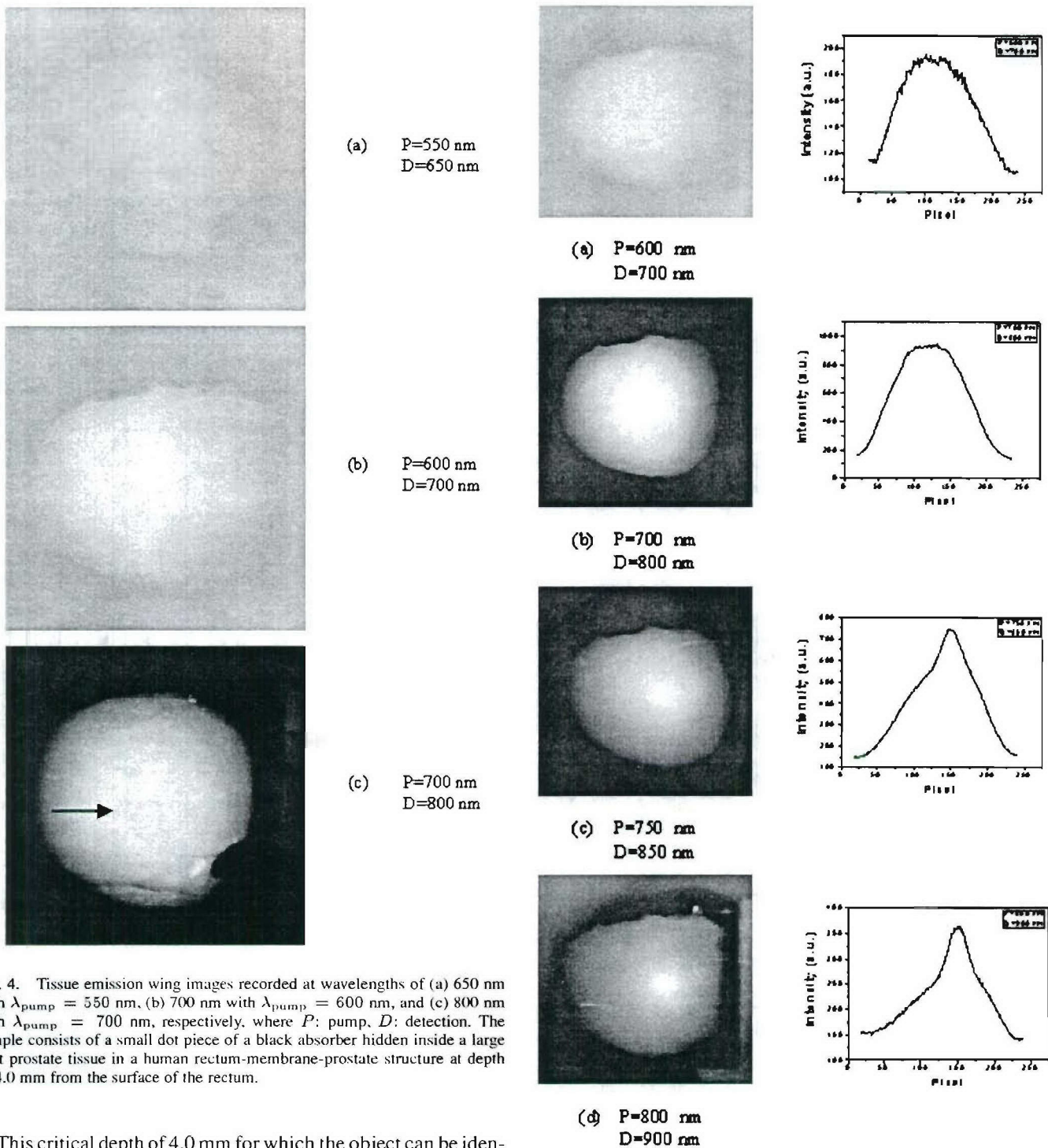


Fig. 4. Tissue emission wing images recorded at wavelengths of (a) 650 nm with  $\lambda_{\text{pump}} = 550\text{ nm}$ , (b) 700 nm with  $\lambda_{\text{pump}} = 600\text{ nm}$ , and (c) 800 nm with  $\lambda_{\text{pump}} = 700\text{ nm}$ , respectively, where  $P$ : pump,  $D$ : detection. The sample consists of a small dot piece of a black absorber hidden inside a large host prostate tissue in a human rectum-membrane-prostate structure at depth of 4.0 mm from the surface of the rectum.

This critical depth of 4.0 mm for which the object can be identified from the tissue emission wing imaging is larger than that from the scattered light imaging. This improvement of detection depth can be understood because the signal light in the tissue emission wing imaging travels a much shorter distance than that in the scattering light imaging.

### C. Contrast Agent Fluorescence Light Imaging

The sample used for the contrast agent emission light imaging measurements consists of a tiny piece ( $\Phi \sim 1.0\text{ mm}$ ) of prostate tissue dyed with indocyanine green (cardio green) embedded inside a large piece of host prostate tissue ( $\sim 25 \times 15\text{ mm}$ ) in a rectum-membrane-prostate structure about 4.5 mm deep from

Fig. 5. Contrast agent fluorescence images recorded with (a)  $\lambda_P = 600\text{ nm}$  and  $\lambda_D = 700\text{ nm}$ , (b)  $\lambda_P = 700\text{ nm}$  and  $\lambda_D = 800\text{ nm}$ , (c)  $\lambda_P = 750\text{ nm}$  and  $\lambda_D = 850\text{ nm}$ , and (d)  $\lambda_P = 800\text{ nm}$  and  $\lambda_D = 900\text{ nm}$ , where  $P$ : pump,  $D$ : detection. The curves on the right side show cross-section intensity distributions of corresponding images shown on the left side. The cross sections were taken from a same number row of the different images. The sample consists of a tiny piece of tissue dyed by indocyanine green in a human rectum-membrane-prostate tissue structure at a depth of 4.5 mm from the surface of the rectum-membrane-prostate tissue structure.

the surface of the rectum-membrane-prostate tissues as shown in Fig. 1(b). Since the emission from the contrast agents is much stronger and more polarized than tissue emission, introducing

contrast agents to the NIR spectral polarization imaging technique is expected to further improve the imaging depth and resolution [5]–[8].

The contrast agent emission light images for the sample described in Fig. 1(b) recorded at different pump and detection wavelengths varied from 600 to 900 nm are shown in Fig. 5. The salient feature of the images is that the dyed object cannot be distinguished by images obtained with short pump wavelengths (600 and 700 nm), while the object can be clearly identified by the images obtained with longer pump wavelengths (750 and 800 nm). When the pump wavelength increases, the visibility of the dyed object increases dramatically. This improvement can be seen more clearly by their image intensity distribution of a cross section taken from a same row number of the different images as shown by curves on the right side of Fig. 5. Using the data from these curves, the image contrasts for images with detection wavelengths of 800 [Fig. 5(b)], 850 [Fig. 5(c)], and 900 nm [Fig. 5(d)] were calculated to be 0%, 17.7%, and 19.3%, respectively. This pump wavelength dependence of the image quality can be explained from the measured relative absorption spectra of prostate and rectum tissues and indocyanine green shown in Fig. 3. With longer wavelengths (750 and 800 nm) pump, the light can penetrate the rectum-membrane-prostate tissues and reach the dyed object. In addition, the absorption of indocyanine green at 750 and 800 nm is stronger than that at short wavelengths, and the emission from the dye is much stronger than that of native emission from prostate tissues [5]–[8]. As a result, the dyed object can be clearly distinguished by those contrast agent emission light images.

The good contrast of the image shown in Fig. 5(d) indicates the possibility of observing the dyed object at a depth greater than 4.5 mm, i.e., the object hidden inside the prostate tissue at a certain depth greater than 4.5 mm should be observed. In order to obtain critical depth for the contrast agent fluorescence light imaging, measurements were extended to the samples with the dyed tissue embedded at depths of more than 4.5 mm using the detection wavelength of 900 nm and the illuminating wavelength of 800 nm. The results show that the dyed dot tissue with a diameter of  $\sim 1$  mm embedded at depth of 7.5 mm inside a large host prostate tissue in a rectum-membrane-prostate structure can be distinguished even illumination power was only  $\sim 50$  w/cm<sup>2</sup>.

#### IV. CONCLUSION

We have performed and compared different spectral polarization imaging methods on human rectum-membrane-prostate samples using light scattered or emitted from tissues and light emitted from contrast agents. The small foreign objects with a diameter of  $\sim 1$  mm hidden inside the host prostate tissues in rectum-membrane-prostate structures at depths of 2.5, 4.0, and 7.5 mm were imaged and identified using the scattered light imaging, tissue emission wing imaging, and contrast agent fluorescence imaging methods, respectively.

These results show that, through rectum tissues, small objects hidden inside the host prostate tissues in a rectum-membrane-prostate structure can be imaged and identified at a certain depth using the NIR spectral polarization imaging technique, in particular, by the contrast agent fluorescence imaging methods.

Our results indicate the possibility of the spectral polarization imaging technique for detecting small objects and structural changes in prostate tissues through rectum-membrane-prostate tissues and the potential of imaging and detecting prostate cancers through the rectum in real time without removing tissues using the NIR spectral polarization imaging.

#### ACKNOWLEDGMENT

The authors would like to thank Department of Pathology, HUMC for their help on preparation of rectum-membrane-prostate model samples.

#### REFERENCES

- [1] D. J. Tindall and P. T. Scardino, "Defeating prostate cancer: Crucial directions for research—Except from the report of the Prostate Cancer Progress Review Group (Review)," *Prostate*, vol. 38, no. 2, pp. 166–171, 1999. P. T. Scardino, "Prostate cancer: Detection, treatment, and prevention," *Newsweek*, Nov. 1, 1999, PP 11-12.
- [2] J. M. Schmitz, A. H. Gandjbakhele, and R. F. Bonner, "Use of polarization light to discriminate short-path photons in a multiply scattering medium," *Appl. Opt.*, vol. 31, pp. 6535–6546, 1992.
- [3] G. Porter, P. J. Sadkowski, and C. J. Tredwell, "Picosecond rotational diffusion in kinetic and steady state fluorescence spectroscopy," *Chem. Phys.*, vol. 49, pp. 416–420, 1977.
- [4] S. G. Demos and R. R. Alfano, "Optical polarization imaging," *Appl. Optics*, vol. 36, pp. 150–155, 1997.
- [5] W. B. Wang, S. G. Demos, J. Ali, and R. R. Alfano, "Imaging fluorescent objects embedded inside animal tissues using polarization difference technique," *Opt. Commun.*, vol. 142, pp. 161–166, 1997.
- [6] W. B. Wang, S. G. Demos, J. Ali, J. Gang Zhang, and R. R. Alfano, "Visibility enhancement of fluorescent objects hidden in animal tissues using spectral fluorescence difference method," *Opt. Commun.*, vol. 147, pp. 11–15, 1998.
- [7] S. G. Demos, W. B. Wang, and R. R. Alfano, "Imaging objects hidden in scattering media with fluorescence polarization preservation of contrast agents," *Appl. Opt.*, vol. 37, pp. 792–797, 1998.
- [8] W. B. Wang, J. H. Ali, J. H. Vitenson, J. M. Lombardo, and R. R. Alfano, "Spectral polarization imaging of human prostate tissues," *Proc. SPIE*, vol. 3917, pp. 75–78, 2000.



Wubao Wang received the B.S. degree in physics from the Northwestern University, Xian, P. R. China, and the M.S. and Ph.D. degrees in physics from the City College of New York, New York.

He is currently a Senior Scientist at the Institute for Ultrafast Spectroscopy and Lasers, City College of New York. He has published over 50 papers in referred journals, over 45 conference abstracts, and holds four U.S. patents. His research areas include picosecond and femtosecond time-resolved spectroscopy and lasers, ultrafast phenomena in semiconductors, quantum well-based semiconductor devices, optical imaging in turbid media for medical and nonmedical application, and nonlinear optics.



Jamal H. Ali received the B.S. degree in physics from Yarmouk University, Irbid, Jordan, in 1990. He is currently pursuing the Ph.D. degree at the City College and Graduate School, City University of New York, New York.

He has published over ten papers and holds one U.S. patent. His work focuses on structural and molecular changes in biological and nonbiological highly scattering media using IR spectral polarization and confocal imaging techniques.



**Robert R. Alfano** (M'87–SM'89–F'01) received the B.S. and M.S. degrees in physics from Fairleigh Dickinson University, Teaneck, NJ, in 1963 and 1964, respectively, and the Ph.D. degree in physics from New York University, New York, in 1972.

He is a Distinguished Professor of Science and Engineering at the City College of the City University of New York, New York, and the Director of the Institute for Ultrafast Spectroscopy and Lasers, the NASA Center for Optical Sensing and Imaging, the DoD Nanophotonic Center, and the New York State

Center for Advanced Technology in Ultrafast Photonics. Prior to joining the City College, he was a Research Physicist at General Telephone Research. He has published over 680 papers and holds 88 patents. His research during the past 35 years has been in the areas of ultrafast time-resolved spectroscopy, lasers, photonics, biomedical optics, condensed matter physics, and nonlinear optics. He has been one of the prime movers in optical biopsy and mammography. His group introduced fluorescence and Raman scattering to detect cancer and ballistic and snake photons for imaging in turbid media.

Prof. Alfano is a Fellow of the American Physical Society, the Optical Society of America, and the New York Academy of Sciences. He is a recipient of the Leonardo Da Vinci Award, the Lifetime Achievement Award in Biophotonics from Coherent, and was an Alfred P. Sloan Fellow.

**Jack H. Vitenson** received the M.D. degree from New York Medical College, New York, in 1965.

He is a Urology Physician at the Department of Urology, Hackensack University Medical Center (HUMC), Hackensack, NJ, a Chairman of the Medical Board and a Member of Board of Governors, HUMC. His research includes prostate cancers and other urology diseases.

**Joseph M. Lombardo** received the M.D. and Ph.D. degrees from the Downstate Medical Center, State University of New York, Brooklyn, in 1981.

He is a Chairman of the Pathology Department and a Director of Laboratories, Hackensack University Medical Center, Hackensack, NJ. His research includes neuroblastoma, immunodeficiency, HIV, and prostate cancers.

1  
2  
3  
4  
5  
6  
7  
8  
9  
10  
11  
12  
13  
14  
15  
16  
17  
18  
19  
20  
21  
22  
23  
24  
25  
26  
27  
28  
29  
30  
31  
32  
33  
34  
35  
36  
37

**APPLICATION FOR UNITED STATES  
LETTERS PATENT**

**DETECTING HUMAN CANCER THROUGH SPECTRAL OPTICAL IMAGING  
USING KEY WATER ABSORPTION WAVELENGTHS**

Inventor(s):  
**Robert R. ALFANO  
Jamal H. ALI  
Wubao WANG  
Manuel ZEVALLOS**

# Near Infrared Imaging of Human Prostate Cancerous and Normal Tissues Based on Water Absorption

W. B. Wang, J. H. Ali, M. Zevallos, and R. R. Alfano

Institute for Ultrafast Spectroscopy and Lasers, and New York State Center for Advanced Technology for Ultrafast Photonic Materials and Applications, Department of Physics, The City College of the City University of New York, New York, NY 10031  
Tel. 212-650-5531; Fax 212-650-5530; e-mail: [wwang@sci.ccnycuny.edu](mailto:wwang@sci.ccnycuny.edu)

**Abstract** – Near-infrared imaging measurements were performed on human prostate cancerous and normal tissues. The absorption of water fingerprints in cancerous and normal tissues were studied, and used to distinguish prostate cancerous tissue from the surrounding normal tissues.

© 2003 Optical Society of American

**OCIS codes:** (170.6510) Spectroscopy and Tissue Diagnostics; (110.3080) Infrared Imaging;

## Introduction

Prostate cancer is one of the most common and dangerous forms of cancer affecting the male population. It is the second most deadly cancer in men after lung cancer. The detection and treatment of early small prostate cancers are most important to prevent death attributable to prostate cancers.<sup>1</sup> The standard diagnostic methods for prostate cancer screening are prostate-specific antigen (PSA) test, digital rectal examination (DRE), and transrectal ultrasound (TRUS). The PSA tests and DRE exams frequently result in false positives. The positive predictive value of the TRUS is low - estimated from 7% to 57.5% with a poor spatial resolution. These inaccurate diagnoses can lead to unnecessary and invasive biopsy.<sup>2</sup>

To develop optical noninvasive technique for early small prostate cancer detection, we have been investigating spectral and polarization properties of the light scattered and emitted from tissues and contrast agents, and performed imaging measurements on human prostate tissue samples through normal prostate tissues<sup>3</sup> and rectum-membrane-prostate tissues.<sup>4</sup>

In this report, a new approach to detect prostate cancerous tissue based on the differences of water contents and absorption spectra between prostate cancerous and normal tissues is presented. The absorption fingerprints of cancerous and normal tissues at water absorption peaks were studied. Near infrared (NIR) imaging measurements using the fingerprint wavelengths were performed to detect the prostate cancerous tissues from the normal tissues. The results indicate that the NIR imaging using the fingerprint wavelengths of water absorption in prostate cancerous and normal tissues is a potential approach for monitoring the physiological change of the prostate tissues, and identifying the prostate tumor tissues from the surrounding normal tissues.

## Experimental method and samples

The schematic diagram of the NIR transmission / backscattering imaging set up used to image cancerous and normal prostate tissues is shown in Fig.1. A NIR light source was used to illuminate a model prostate cancerous-normal tissue sample, and an InGaAs-based NIR CCD camera equipped with a zoom lens working in the spectral range of 0.9  $\mu\text{m}$  to 1.7  $\mu\text{m}$  was used to record the images formed by light back-scattered or transmitted from the samples. NIR wide band filters are used to vary the illuminating and detection polarization and wavelengths of the images. The first NIR polarizer,  $P_1$  was located in the incident light beam pathway to obtain a linearly polarized illumination light, and the second NIR polarizer,  $P_2$  was positioned in front of the CCD camera for selecting the detection polarization direction (parallel or perpendicular to the polarization orientation of the illumination beam).

The human prostate normal and cancerous tissues were obtained from National Disease Research Institute (NDRI), and used for absorption-spectral and NIR imaging measurements under the Institutional Review Board (IRB) approval from City College of New York (CCNY). The cancerous-normal prostate tissue samples for imaging measurements were arranged such that the right hand side of the specimen was mostly cancerous tissue, while the left hand side was mostly normal tissue. The thickness and area of the modeling samples were  $\sim 330 \mu\text{m}$  and  $\sim 2 \times 3 \text{ cm}^2$ , respectively. Five prostate cancerous and normal tissue samples obtained from different surgical cases and different areas of prostate glands were investigated to ensure the spectral and NIR imaging differences of prostate cancerous and normal tissues.

# Published in OSA 2004 Biomedical Topical Meeting on CD-ROM (OSA, Washington DC, 2004), MF 38

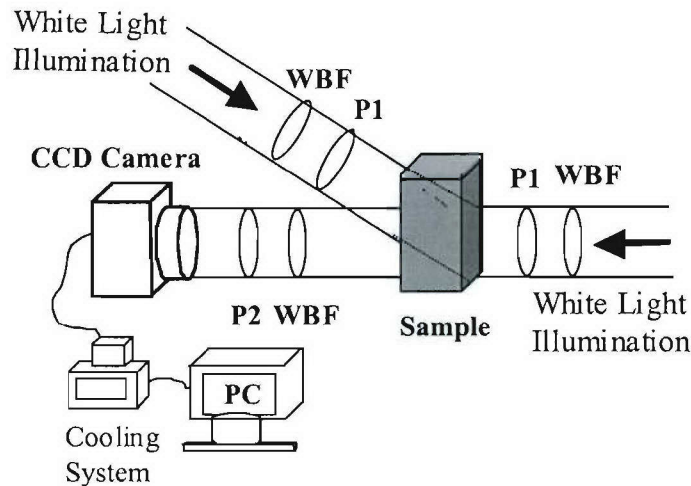


Fig.1. Schematic diagram of the NIR transmission / back-scattering imaging set up used for prostate cancerous and normal tissue measurements, where P: polarizer; WBF: wide band filter.

### Experimental results:

#### 1. Absorption spectra of prostate cancerous and normal tissues

The absorption spectra of the normal and cancerous prostate tissues were measured using Perkin-Elmer Lambda 9 UV/VIS/NIR Spectrometer with accompanied software. The absorption spectra of normal and cancer prostate tissues with a thickness of  $\sim 330 \mu\text{m}$  at the spectral range from 400 nm to 2400 nm are shown in Fig.2. As a reference, absorption spectrum of water with a thickness of  $\sim 200 \mu\text{m}$  is also plotted in Fig.2. The salient feature of the curves is that the absorption of prostate cancerous tissue is less than that of normal prostate tissue at several absorption peaks, in particular, at 1195 nm, 1450 nm and 1930 nm. These peaks are located exactly at the overtone fingerprint absorption peaks of water.

The lower water absorption in prostate cancerous tissues indicates lower content of water in the cancerous tissues than that in the prostate normal tissues. This difference of water contents and the corresponding absorption spectra between prostate cancerous and normal tissues can be used as fingerprints to distinguish prostate cancerous tissues from normal tissues.

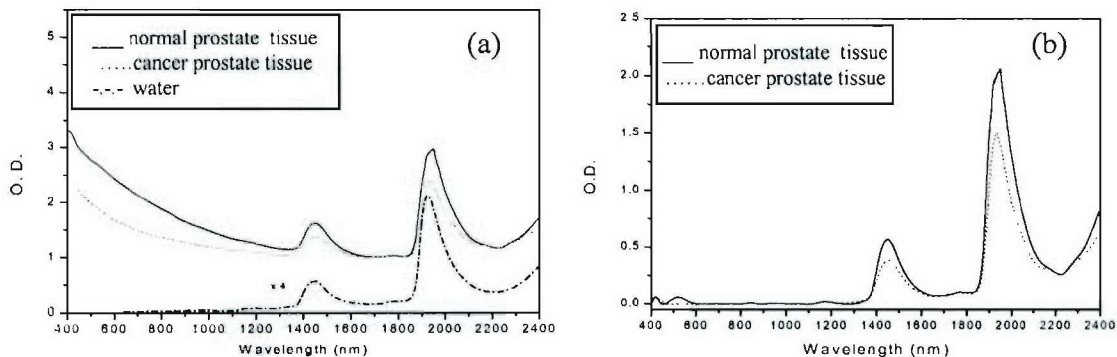


Fig.2 (a) Relative absorption spectra of prostate cancerous tissue (dashed line), normal tissue (solid line) and water (dash-dot-dash line) in the spectral range of 400 nm to 2400 nm, and (b) absorption spectra of prostate cancer tissue (dashed line), and normal tissue (solid line) after removing the scattering contribution by subtracting the scattering wing obtained from the fitting. It can be seen that there is less absorption in prostate cancerous tissues than that in normal tissues at all of the water absorption peaks.

#### 2. Imaging identification of prostate cancerous and normal tissues

NIR imaging measurements for prostate cancerous and normal tissue samples were performed using an InGaAs NIR CCD imaging system. A prostate cancerous-normal tissue sample consists of a piece of a prostate cancerous tissue

on the right side, and a piece of a prostate normal tissue on the left side. The cancerous tissue cannot be distinguished visually or from a photograph taken using a conventional digital camera as shown in Fig.3(a).

Figs.3(b) and 3(c) show back-scattering images of a prostate cancerous and normal tissue sample recorded at the fingerprint wavelengths of 1200 nm and 1450 nm, respectively.

These two NIR back-scattering images show that the high intensity areas (right side) correspond to the cancerous tissue areas, while the low intensity areas (left) correspond to the normal tissue areas. The cancer segment scatters more light than the normal because its lower absorption for water. The cancerous tissues can be clearly identified in both 1200 nm and 1450 nm images from their image intensity distributions. The image contrast of the 1450 nm image was found better than that of the 1200 nm image, which can be understood because the difference of absorption between prostate cancerous and normal tissues at the fingerprint wavelength of 1450 nm is much larger than that at 1200 nm.

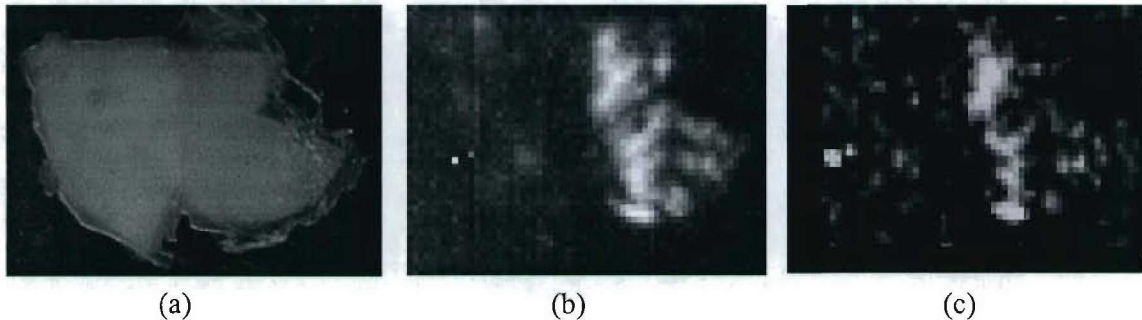


Fig.3 (a) a photograph of a model prostate cancerous and normal tissue sample taken using a conventional digital camera. The sample consists of a piece of prostate normal tissue on the left side and a piece of prostate cancer tissue on the right side. The total sample area is  $2 \times 3 \text{ cm}^2$  and the thickness is  $\sim 330 \mu\text{m}$ ; (b) a back-scattering image of the sample recorded at a wavelength of 1200 nm; and (c) a back-scattering image at 1450 nm. The prostate cancerous tissues (right half) are clearly identified by the bright areas from both of the two NIR images.

### Conclusion

The absorption spectral results clearly show that there is lower content and absorption of water in prostate cancerous tissues than that in normal tissues. This result can be used as fingerprints to distinguish prostate cancerous tissues from normal tissues in the body. The imaging results indicate that the NIR imaging using the fingerprint wavelengths of water absorption of prostate cancerous and normal tissues is a potential approach for screening, monitoring and identifying the prostate tumor tissues from the surrounding normal tissues.

### References

1. D. J. Tindall and P. T. Scardino, "Defeating prostate cancer: Crucial directions for research --- except from the report of the Prostate Cancer Progress Review Group (Review)", *Prostate*, **38**(2), 166-171 (1999).
2. Dan Harvey, "The fallibility of the prostate-specific antigen test and the prevalence of prostate cancer in men necessitate a more reliable screening tool", *Radiology Today*, Vol.4, No.14, July 7, 2003.
3. W. B. Wang, J. H. Ali, J. H. Vitenson, J. M. Lombardo, and R. R. Alfano, "Spectral polarization imaging of human prostate tissues", in *Proceedings of optical biopsy III*, SPIE, Vol. **3917**, 75 (2000).
4. W. B. Wang, J. H. Ali, J. H. Vitenson, J. M. Lombardo, and R. R. Alfano, "Spectral polarization imaging of human rectum-membrane-prostate tissues", *IEEE Journal of Selected Topics in Quantum Electronics*, **9**, No. 2, 288-293 (2003).

# **Time-resolved fluorescence kinetics and optical image of Cybesin: a prostate cancer receptor-targeted contrast agent**

Y. Pu<sup>a</sup>, W. B. Wang<sup>b</sup>, B. B. Das<sup>b</sup>, G. C. Tang<sup>b</sup>, V. Sriramoju<sup>b</sup>, S. Achilefu<sup>c</sup>, and R. R. Alfano<sup>b\*</sup>

<sup>a,b</sup>Institute for Ultrafast Spectroscopy and Lasers, and New York State Center for Advanced Technology for Ultrafast Photonic Materials and applications, <sup>a</sup>Department Electrical Engineering and <sup>b</sup>Department of Physics, The City College of the City University of New York, 138<sup>th</sup> street, Convent Avenue, New York, NY10031

<sup>c</sup>Washington University School of Medicine, 4525 Scott Avenue, St. Louis. Missouri 63110

## **Abstract**

Time-resolved polarization-dependent fluorescence spectra of Cybesin were measured using a Ti:Sapphire femto-second laser and a streak camera, showing the polarization preservation property of Cybesin. The relative fluorescence intensity and the fluorescence kinetics and polarization anisotropy of the stained cancerous and normal tissue indicate that prostate cancerous tissue takes-up more Cybesin than normal tissue does. The experimental data obtained from Cybesin solution were fitted using a time-dependent fluorescence depolarization model. An empirical model was developed to describe the time-resolved fluorescence kinetics and polarization anisotropy from Cybesin in human prostate tissue. This empirical model can be explained by the mechanism of preferential uptake of Cybesin in human prostate cancerous tissue. The fluorescence polarization difference imaging (FPDI) technique based on polarization preservation of Cybesin was used to enhance image contrast between prostate cancerous and normal tissue area.

**Key words:** time-resolved fluorescence kinetics, time-resolved fluorescence polarization anisotropy, relative fluorescence intensity, polarization preservation, fluorescence polarization difference imaging (FPDI) technique, prostate cancer, receptor-targeted contrast agent, peptide analogue conjugate

Submitted to “.....”, IUSL # 2005-xxx

\* The corresponding author (R. R. Alfano) may be reached by phone at (212) 650-5531, by fax at (212) 650-5530, by email at [alfano@sci.cuny.cuny.edu](mailto:alfano@sci.cuny.cuny.edu), or by regular mail at the address shown above.

**\*\* This is the first draft of the manuscript. It is still being revised for publication.**

## 1. Introduction:

Prostate cancer has a high incidence and mortality rate for men. Every year, nearly 180,000 new prostate cancer cases are diagnosed, and about 37,000 deaths annually are caused by it in U.S [1]. Since Alfano and his team revealed that fluorescence spectroscopy could be applied to detect cancer in tissues [2], fluorescence spectroscopy is rapidly gaining acceptance as an important diagnostic tool in the imaging of cancerous tissue [3]. The diagnostic fluorescence signal can be induced in such a medium by the introduction of a fluorescent contrast agent or by stimulating the endogenous chromophores in the tissues. The use of intrinsic chromophores to differentiate the optical properties of diseased and healthy human tissues is limited by the most of their ultraviolet emission bands [4], which are occasion leading to cancer and are not in the tissue “optical window” [5].

In order to enhance the differentiation of cancer from normal tissue, optical contrast agents were designed and synthesized to increase sensitivity and specificity for the tumor detection by studying the molecular specificity [6, 7]. Among these specific optical contrast agent, a small ICG-derivative dye-peptide, Cypate-Bombesin Peptide Analogue Conjugate (Cybesin) was synthesized and proved to detect the human prostate cancer successfully *in vitro* due to its targeting the over-express bombesin receptor [8] on the membranes of human prostate cancer cells [9], by using optical spectral fluorescence imaging technique [10].

The fluorescent contrast agent in solution, absorbing photon at time  $t$ , can undergo a rotation by virtue of local forces before emitting fluorescence at a certainly later time [11]. The rotational motions of excited state molecules can be studied by probing the anisotropy of the excited state distribution [12]. The kinetic fluorescence depolarization technique has been proposed to model these transition dipoles in various solutions. It was suggested that the rotation of the fluorescent contrast agent changes the angle between the polarization vectors of absorption and emission, and is most sensitively detected when linearly polarization light is used to excite the molecule and when a particular component of polarization is observed in emission [11, 12]. And the solvent viscosity also plays an important role in determining the rotation kinetics of molecules in solution [11, 12].

The pico-second fluorescence and polarization anisotropy measurements of the *Streptocarpus* flower and the anthocyanin pigments extracted from *Streptocarpus holstii* and *Anthurium andreaenum* were performed in our lab [13]. The results show that the pigments in the flowers exhibit both different polarization anisotropy and decay time in comparison with its pigment extract in solution [13]. Instead of the random distributions of dipoles in solution, the fluorescent dipoles of the pigment in the flowers present a normalized orientational distribution, which make the anisotropy dropped

[13]. The time-resolved polarization properties of fluorescence from ICG have been also measured in our lab [14]. The results show that the temporal intensity profiles of light emitted at polarized directions parallel ( $\parallel$ ) and perpendicular ( $\perp$ ) to the polarization direction of a linearly polarized excitation are different [11.1]. This polarization preservation property of ICG fluorescence makes it possible to be used as a polarization contrast agent to enhance the image quality.

In this study, the time-resolved fluorescence polarization profiles of Cybesin in solution and the Cybesin stained prostate cancerous and normal tissues were investigated. Both the measured relative fluorescence intensity and the calculated fluorescence polarization anisotropy of the stained cancerous and normal tissue using the accurately measured data recorded by the streak camera, suggest a mechanism of preferential uptake of Cybesin in human prostate cancerous tissue. Results also show the polarization preservation property of Cybesin similar to ICG. The experimental data obtained from Cybesin solution was fitted using the time-dependent fluorescence depolarization model described in [11] and [12]. The result shows good agreement with the theoretical anisotropy value at  $t=0$  for random distribution dipoles. The rotation time of Cybesin in solution was calculated using this model. Base on this model and the previous research works of our lab [13], an empirical model was developed to describe the time-resolved fluorescence kinetics and polarization anisotropy from the contrast agent, Cybesin, in human prostate tissue. The calculated parameters using this model and our measured data also verify the more uptake of Cybesin in prostate cancer tissue. Prostate samples consisting of a small piece of normal prostate tissue and a small piece of prostate cancer tissues stained with Cybesin were imaged. The improvement of the image contrast between cancerous and normal area was achieved compared with the conventional optical imaging approach.

## **2. Experimental method and samples**

The experimental arrangement of the time-resolved fluorescence measurements for the Cybesin and Cybesin-stained prostate tissue is schematically shown in Fig. 1. Pulses of 130 fs at 800 nm with repetition rate of 82 MHz from a Coherent Mira 900 Modelocked Ti:Sapphire laser were used to pump the samples (Cybesin and Cybesin-stained prostate cancerous or normal tissue). The fluorescence was collected by a large diameter lens with a focus length of 5 cm and directed onto a synchroscan streak camera with temporal resolution of 10 ps. An 830 nm long pass filter was used to cut off the illuminating light so that only the emission from the sample was recorded. Two polarizers ( $P_1$  and  $P_2$ ) were used.  $P_1$  was used to ensure the linear polarization of the input laser pulses and  $P_2$  used as an analyzer. The polarization of  $P_2$  was rotated between  $0^\circ$  and  $90^\circ$  with respect to that of  $P_1$  to record the intensities profiles of the parallel and perpendicular polarization components of the fluorescence. The temporal profiles recorded by a silicon intensified target (SIT) vidicon camera were analyzed to obtain temporal and polarization information of fluorescence.

The Cybesin solution used for time-resolved fluorescence study is solvated in 20% aqueous Dimethyl Sulfoxide (DMSO). Cybesin was prepared by professor Achilefu's group at the Washington University School of Medicine. The molecular structure and synthesis of this contrast agent was reported elsewhere [8]. It is mainly composed of ICG and the bombesin receptor ligand, which delivers the contrast agent to the corresponding receptor presented in the tumor [8]. The absorption band of Cybesin ranges from 680 nm to 830 nm with a shoulder peak at 720 nm and a strong peak at 792 nm. The fluorescence spectrum of Cybesin covers from 800 nm to 950 nm with a main peak at 825 nm and a weak peak at 925 nm [10].

Six (6) in-vitro prostate cancer-and-normal tissue samples obtained from the National Disease Research Interchange (NDRI) were used for the time-resolved fluorescence and optical imaging measurements under IRB approvals at CCNY (City College of New York). Samples were not chemically treated and they were not frozen prior our experiment. The samples were kept in the refrigerator at temperature 2-4°C. The prostate cancerous and normal tissues used for the fluorescence temporal measurements were cut into  $\sim 2 \times \sim 1 \times \sim 0.5$  cm (length  $\times$  width  $\times$  thickness) pieces. Both of them were soaked in the same Cybesin-DMSO (20% aqueous Dimethyl Sulfoxide) solution with a Cybesin concentration of  $\sim 3.2 \times 10^{-6}$  M for the same period of time. Then the samples were put into sodium phosphate buffer (Sigma-Aldrich) to wash off the unbound Cybesin. All the measurements and processes were performed at room temperature.

The spectral polarization imaging set up used for imaging Cybesin-stained prostate cancerous and normal tissue has been described in our early work [10]. Light from a white light source is used to illuminate the prostate tissue sample with average power of about  $50 \mu\text{W}/\text{cm}^2$ . The wavelengths of the pump and detection are selected by wide-band pass filters varying from 550 nm to 900 nm with FWHM=40 nm. A CCD camera records images formed by light emitted from the sample. Polarizers were used to obtain parallel and perpendicular image relative to the illuminating light.

A typical prostate cancerous-normal tissue sample used for the imaging measurements consists of a small piece of prostate cancer tissue and a small piece of prostate normal tissue. They were first soaked in the same Cybesin-DMSO (20% aqueous Dimethyl Sulfoxide) solution with a Cybesin concentration of  $\sim 3.2 \times 10^{-6}$  M for the same period of time, and then put into sodium phosphate buffer (Sigma-Aldrich) to wash off the unbound Cybesin. The stained normal and cancer tissues were then sandwiched between large pieces of prostate normal tissue.

### **3. Experimental results and Discussion**

### 3. 1. Time-resolved fluorescence polarization anisotropy from Cybesin in 20% aqueous DMSO

The measured temporal profiles of the fluorescence emitted from Cybesin for two polarization orientations parallel and perpendicular to the polarization direction of the excitation at 800 nm are shown in Fig. 2 (a). The thick- and thin-line profiles are  $I_{\parallel}(t)$  the parallel and  $I_{\perp}(t)$  the perpendicular component, respectively. The main difference for these two components is that  $I_{\parallel}$  is greater than  $I_{\perp}$  at all of the decay time, in particular, at the peak position, the parallel component  $I_{\parallel}(0)$  is almost three (3) times stronger than that of the perpendicular one  $I_{\perp}(0)$  at peak position. This indicates the polarization preservation nature of Cybesin.

The time-dependent polarization anisotropy can be calculated using the measured  $I_{\parallel}(t)$  and  $I_{\perp}(t)$  [11, 12]:

$$r(t) = \frac{I_{\parallel}(t) - I_{\perp}(t)}{I_{\parallel}(t) + 2I_{\perp}(t)} \quad (1)$$

The temporal profile of the polarization anisotropy  $r(t)$  of Cybesin was shown as the thin line in Fig. 2 (b). The decay behavior of  $r(t)$  reflects the type of the dipole reorientation of Cybesin in solvent. In this simple possible case where the Cybesin molecule undergoes Brownian rotation as an Einstein sphere, the time-resolved fluorescence kinetics and polarization anisotropy from Cybesin in 20% aquatic DMSO can be modeled using the following equation [11, 12]:

$$r(t) = r(0) \exp\left(-\frac{t}{\tau_{rot}}\right) \quad (2)$$

where the rotation time  $\tau_{rot}$  can be expressed in terms of the diffusion coefficient ( $D$ ), or the solvent viscosity ( $\eta$ ) and the molecular radius ( $a$ ):

$$\tau_{rot} = (6D)^{-1} = \frac{4\pi\eta a^3}{3kT} \quad (3)$$

where  $k$  is the Boltzmann constant and  $T$  is the absolute temperature of the solvent [12]. And theoretically the emission anisotropy at  $t=0$  can be given by:

$$r(0) = \left( \frac{2 \langle P_2^2 \rangle + \langle P_2 \rangle}{1 + 2 \langle P_2 \rangle} \right) P_2(\cos \delta) \quad (4)$$

where  $\langle P_2 \rangle$  is the expectation value of the second order Legendre polynomial for the distribution function  $f(\theta)$  [13, 15], and is given by:

$$\langle P_2 \rangle = \langle P_2(\cos \theta) \rangle = \int_0^\pi \sin \theta d\theta f(\theta) P_2(\cos \theta) \quad (5)$$

and where the  $\theta$  is the angle between the long axis of the molecule and the major symmetry axis of the system, and  $\delta$  is the angle between the absorption and emission dipole [13, 15].

For randomly oriented fluorescent molecules in solution, the distribution function is  $f(\theta)=1/2$ . Using this function and the above equations, the theoretically  $r(0)$  is calculated to be 0.4. The calculated measured  $r(0)$  shown as the thin line in fig. 2 (b) is 0.39 at the peak position, that is very close to the theoretical value. This indicates that the transitions dipole moments of molecules in Cybesin solution are randomly oriented and, thus the depolarization effects of Cybesin in 20% DMSO solvent can be confined to molecular rotation and to trivial effect of initial randomness [9], thus the decay behavior of Cybesin solution can be modeled using equation (2).

Since the time-resolved fluorescence polarization anisotropy was calculated from the accurately measured data by the streak camera, the rotation time  $\tau_{rot}$  of Cybesin in solution can be obtained using the equation (2) fitting our calculated experimental data of  $r(t)$  in Fig. 2 (b).

The Hough transform is a general algorithm for mapping from an observation space into a parameter space. The detail mathematics of Hough Transform is described in many textbooks [16]. It is easy and simple to program in a parameter space less than 4. In our case, observation space should be the  $r$ - $t$  space used to display the experimental calculated polarization anisotropy  $r(t)$ , and there are two parameters needed to be defined in equation (2). Therefore the Hough transform is used for defining the polarization anisotropy peak value  $r$  at time 0 [17], and the rotation time of Cybesin in 20% aquatic DMSO:  $\tau_{rot}$ .

The results are  $r(0)=0.389\pm 0.028$  and  $\tau_{rot}=359\pm 19.65$  ps, in good agreement with both theoretical and the measured peak value  $r(0)$ . The fitting curve using these calculated data and model of equation (2) shown as the thick-dark line in Fig. 2 (b) displays reasonable agreement with our experimental data.

### 3. 2. Time-resolved fluorescence polarization anisotropy from Cybesin contained in stained prostate cancerous and normal tissue

For the time-resolved fluorescence measurements of Cybesin-stained cancerous and normal tissues, six (6) cancerous tissues and six (6) normal tissues samples were performed. The averaging time-resolved fluorescence intensity profiles over six (6) samples from the cancerous and normal prostate tissues stained with Cybesin calculated from the measured data are displayed in Fig. 3 (a). The thick-solid- and thin-dash-line profiles are the parallel and perpendicular components emitted

from stained cancerous tissue, respectively. The thin-solid- and thin-dot-line profiles display the parallel and perpendicular components emitted from stained normal tissue, respectively.

The most obvious features of Fig. 3 (a) is that the emission intensities from stained cancerous tissue is bigger than those of stained normal tissue within all the life time of Cybesin emission. The emission peak of dyed cancerous tissue is much stronger than that of the dyed normal tissue. Under parallel polarization configuration, the ratio of peak fluorescence intensity of Cybesin stained cancerous tissue to that of the normal is found to be  $\sim 3.63$ , while under perpendicular the ration of that is  $\sim 3.23$ . The results indicate that the prostate cancerous tissue takes-up more Cybesin than the normal does.

The mechanism of preferential uptake of Cybesin in prostate cancerous tissue can be more verified by the statistics of the measured data used for computation of the relative fluorescence intensity. The average peak value of stained cancerous tissue  $2408.98 \pm 507.51$ , is more than three (3) times larger than that of stained normal tissue,  $663.10 \pm 107.35$  under parallel configuration. Almost same results were obtained under perpendicular configuration:  $1531.26 \pm 302.46$  for cancer and  $471.09 \pm 73.81$  for normal. The peak fluorescence intensities of perpendicular component emitted from Cybesin stained prostate cancerous tissue are also about three (3) times larger than that of normal. This indicates that the ratio of the Cybesin uptake in cancerous tissue to that in normal tissue is about three (3) times larger in this case.

Another important feature from Fig. 3 (a) is that  $I_{\parallel}$  is greater than  $I_{\perp}$  for both cancerous and normal tissue at all of the decay time. At the peak position,  $I_{\parallel}^{\text{cancer}}(0)$  is  $\sim 1.57$  times stronger than  $I_{\perp}^{\text{cancer}}(0)$ , and the ratio of  $I_{\parallel}^{\text{normal}}(0)$  to  $I_{\perp}^{\text{normal}}(0)$  is  $\sim 1.40$ . This indicates the measured fluorescence emitted from Cybesin-stained prostate cancerous and normal tissue still show the polarization preservation property, although this property dropped. Another inapparent but valuable feature is that the polarization anisotropy of stained cancerous tissue is always larger than that of normal within the emission life-time of Cybesin. Using measured  $I_{\parallel}(t)$  and  $I_{\perp}(t)$  shown in Fig. 3 (a), the temporal profile of the polarization anisotropy  $r(t)$  of the fluorescence emitted from Cybesin in stained prostate cancerous (thin-solid line) and normal (thin-dash line) tissue is calculated with the equation (1) and displayed in Fig. 3 (b).

The features of  $r(t)$  curves shown in Fig. 3 (b) are (1) The profiles of Cybesin-stained tissue show flatter decay in comparison with Cybesin solution; (2) the values of polarization anisotropy of Cybesin in the stained cancerous tissue are always bigger than that of stained normal tissue at all the

decay time. This property can be more confirmed by statistics of the peak intensity values of the calculated  $r(t)$  (at  $t \approx 0$  ps) for different samples:  $r_{(0)}^{\text{cancer}}=0.163\pm0.014$  and  $r_{(0)}^{\text{normal}}=0.120\pm0.012$ .

It is now well established that biological living tissues mimic the behavior of viscous liquid [14, 15]. This property of tissue was investigated and modeled by many groups, and usually the viscosities of biological tissues were reported to be  $10^7$  times higher than the water viscosity, which is 1 centiPoise under room temperature [18]. The viscosity of prostate tissue was also reported to be above 50,000 Poise by Dresner *et al* [19].

Previous research in our lab shows that for viscosity greater than 3,000 Poise, the values for the polarization anisotropy at  $t=0$  were found to be  $\sim 0.11\pm 0.01$ , and transitions dipole moments of fluorescent molecules are not randomly oriented in such case [21]. A normalized orientational distribution function was taken as a model for the orientational order of fluorescent molecules in this condition [18]. In particular, by taking the distribution function  $f(\theta) = 3/2 \cos^2 \theta$  and using equation (4) and (5), a calculated value of 0.1039 is obtained for emission anisotropy at  $t=0$  [21].

Base on the above work, an empirical model was developed to describe the time-resolved fluorescence kinetics and polarization anisotropy from the contrast agent, Cybesin, in human prostate tissues. We describe the cell-bonding mechanism and reorientation of Cybesin in prostate tissue as the schematic diagram shown as Figs. 4.

The time-resolved fluorescence polarization anisotropy  $r(t)$  from Cybesin contained in stained human prostate tissues can be considered as two components: (1) static component caused by the high scattering of tissue to the fluorescent cell-bonded Cybesin molecules; (2) the decay of  $r(t)$  contributed by the rotation unbonded Cybesin molecules remained in the body liquid of prostate tissue. These assumptions are reasonable because the weight of cell to that of Cybesin molecule is not comparable and cell is too huge to rotation. So we describe the temporal fluorescence polarization anisotropy  $r(t)$  from Cybesin contained in stained human prostate tissues as:

$$r(t) = r_1 + r(0) \exp\left(-\frac{t}{\tau_{rot}}\right) \quad (6)$$

Since the time-resolved fluorescence polarization anisotropy from Cybesin contained in stained human prostate tissues was calculated from the accurately measured data by the streak camera, the rotation time:  $\tau_{rot}$ , kinetic polarization peak value of anisotropy  $t=0$ :  $r(0)$  and the static polarization anisotropy of Cybesin contained in stained human prostate tissues can be obtained using the equation (6) fitting our calculated experimental data of  $r(t)$  in Fig. 3 (b).

To corresponding the numerical method used for computation with Cybesin in solution, 3-peremeters dimension Hough transform [17] is used for defining  $r(0)$ ,  $r_1$  and  $\tau_{rot}$  of Cybesin in contained in stained human prostate tissues.

The results are  $r(0)=0.105\pm 0.01$ ,  $\tau_{rot}=700\pm 150$  ps and  $r_1=0.056\pm 0.01$  for stained Cybsein in prostate cancer tissue; and for Cybsein in normal tissue:  $r(0)=0.103\pm 0.01$ ,  $\tau_{rot}=600\pm 200$  ps and  $r_1=0.005\pm 0.01$ . These are in good agreement with both theoretical peak value  $r(0)$ . The fitting curve for Cybesin stained prostate cancer (thick-solid line) and normal (thin-solid line) tissue using these calculated data and model of equation (6) shown in Fig. 3 (b) displays reasonable agreement with our experimental data.

The good agreement of our empirical model fitting with the experimental data indicates that the fluorescence kinetics of the contrast agent, Cybesin in human prostate tissues can be regarded the rotation of free Cybesin molecules remained in the liquid of tissue and the high scattering of tissue to the fluorescence of static cell-bonded Cybesin. The approximately close value of rotation time for cancer and normal tissue suggests the decay of  $r(t)$  can be explained as the rotation of free Cybesin molecules.

The close to zero value of  $r_1$  for Cybesin in normal tissue indicates very few Cybesin molecules were bonded with prostate normal cells because of the much low level bombesin receptor expressed on prostate normal cells. The larger static anisotropy value  $r_1$  of Cybesin-stained cancerous tissue than that of normal tissue also suggests more uptake of Cybesin in prostate cancerous tissue. The excitation wavelength of 800 nm used for pumping is close to the strong absorption peak of Cybesin [8]. Since prostate cancerous tissue takes up more Cybesin than the normal, the stained cancerous tissues will absorb much more photons than the stained normal, thus the Cybesin contained in the deep layer of the stained cancerous tissue will have less opportunity to be excited by the laser than those in the normal. The perpendicular component of the fluorescence emitted from the Cybesin contained in the stained tissue is mainly contributed by the photons undergoing multiply scattering. The light emitted from stained normal tissue undergoes more distance and more multiple scattering than that from the stained cancerous tissue, thus the  $r_1$  values of the stained cancerous tissue are much larger than those of the stained normal tissue.

Both the relative fluorescence intensity and the fluorescence kinetic polarization anisotropy of the stained cancerous and normal tissue indicate that prostate cancerous tissues adsorb Cybesin more than the normal. These can be understood because Cybesin targets the over-expressed bombesin

receptors of human prostate cancer cells [9]. It is well known that prostate cancer forms when cells in the prostate begin to grow out of control. According the Gleason Grade system, cell intensity increases as cancer stage advances. In grade 1 and 2, the cancerous cells are much loosely. In Gleason Grade 3 cells are starting to group together into clumps. Gleason Grade 4 is identified by more pronounced clumping together of cancerous cells. Gleason Grade 5 means that the cells have essentially merged together into cancerous islands of cells [22]. We believe that both high adsorption of Cybesin by over-expressed bombesin receptor on cancer and density of cancer cells contribute to the large fluorescence intensity in the cancerous tissue, and make Cybesin a good candidate as a marker to differentiate prostate cancerous tissue from the normal.

### 3. 3. Optical Imaging

A small piece of prostate cancer tissue and a small piece of prostate normal tissue stained with Cybesin sandwiched between large pieces of prostate normal tissue were imaged. The polarized fluorescence images of a Cybesin-stained cancerous and a normal prostate tissue sample recorded at  $\lambda_{\text{pump}}=750$  nm and  $\lambda_{\text{detection}}=850$  nm is shown in Figs. 5. Fig. 5 (a) displays the parallel image recorded when the polarization direction of  $P_2$  in front of CCD is parallel ( $\parallel$ ) to that of the illuminating beam. Fig. 5 (b) displays the perpendicular image recorded when the polarization direction of  $P_2$  is perpendicular ( $\perp$ ) to that of the illuminating beam. Fig. 5 (c) displays the difference image obtained by subtracting the perpendicular image (Fig. 5 (b)) from the parallel image (Fig. 5 (a)). Fig. 5 (d), 5 (e) and 5 (f) show the digital spatial cross section intensity distributions of the images shown in Figs. 5 (a), 5 (b) and 5 (c), respectively.

It can be seen from the images that the cancerous area is much brighter than that of the normal area. Using the digital data shown in Figs. 5 (d) and (e), the ratio of imaging intensity of cancerous to normal areas is found to be  $\sim 3.5$  under parallel polarization, and  $\sim 3.09$  under perpendicular configuration. These are in good agreement with that obtained from the time-resolved fluorescence measurements.

The improvement of the FPGDI image quality can be shown from the intensity distribution in Fig. 5 (f) clearly shows a higher spatial resolution. The resolution of full width at half maximum (FWHM) for the peak of cancerous area is reduced by a factor of 2.4 with respect to that of the conventional image; and that of normal reduced 2.6.

The other salient feature of these images and their intensity distributions is that the relative contrast of cancerous to normal areas in the polarization difference image shown in Figs. 5 (c) is obviously higher than those in the individual polarization images shown in Figs. 5 (a) and 5 (b). In

order to confirm the improvement of the image quality of the fluorescence polarization difference image over the individual polarization image, the contrasts (C) of the cancerous area to the normal area for all of images shown in Figs. 5 were calculated using.

$$C = \frac{I_c - I_n}{I_c + I_n} \quad (7)$$

where  $I_c$  and  $I_n$  are the local maximum intensities of the dyed cancerous and normal tissue area raised subtracting background intensity, respectively. Using the digital data shown in Figs. 5 (d), (e) and (f), the contrasts for these parallel, perpendicular and polarization difference images are calculated to be 0.55, 0.48 and 0.63, respectively.

These results show that Cybesin has a polarization preservation property similar to ICG, and the polarization difference image displayed in Fig. 5 (c) has a better image quality than that of the individual polarization images. The image of the Cybesin dyed prostate cancerous and normal tissues hidden inside the host tissue is formed by photons emitted from Cybesin that have undergone coherent scattering (ballistic photon), less scattering (snake photon) and multiple scattering (diffusive photon) [23]. Since most of the photons emitted by the contrast agent undergo multiple scattering, only small percentage of the photons retain their polarization information while they propagate in tissue, the intensities of the two image components  $I_{\parallel}$  and  $I_{\perp}$  have only small difference. When the two image components are subtracted ( $I_{\parallel} - I_{\perp}$ ), the strong diffusive image component is canceled out. Only ballistic photon and partial snake photon contribute to the formation of the FPDI image. So the surrounding area to fluorescent dot is moved out. Therefore the spatial resolution becomes better.

The contrast enhancement between cancerous and normal area is due to the higher polarization anisotropy of Cybesin contained in cancerous tissue. Higher polarization anisotropy means higher polarization degree. So value of  $I_{\parallel} - I_{\perp}$  in the Cybesin stained cancer image is expected larger than the value in normal image. Thus, the contrast is increased.

#### **4. Conclusion:**

Time-resolved fluorescence kinetics and polarization anisotropy of a receptor-targeted contrast agent, Cybesin, were investigated. The time-resolved fluorescence polarization profiles of Cybsin solution, and Cybesin stained human prostate cancerous and normal tissues were measured. The experimental results indicate that prostate cancerous tissue takes up more Cybesin than normal tissue and Cybesin has polarization preservation property. These properties make Cybesin a potential marker for prostate cancer and can be used as a polarization contrast agent to enhance image quality.

The experimental data obtained from Cybsein solution was fitted using a time-dependent fluorescence depolarization model. An empirical model was developed to describe the time-resolved fluorescence kinetics and polarization anisotropy from the contrast agent, Cybesin, in human prostate tissue. Both show good agreement with our experimental measured data and can be explained by the mechanism of preferential uptake of Cybesin in human prostate cancerous tissue. Optical imaging of prostate cancerous and normal tissue stained with Cybesin was investigated. The fluorescence-polarization-difference-imaging technique was used to enhance the contrast between cancerous and normal tissue areas greatly.

### **5. Acknowledgement:**

This research is supported by U. S. Army Medical Research and Material Command grant numbered DAMD17-01-1-0084 (CUNY RF 47462-00-01). The authors acknowledge the help of NDRI for providing normal and cancer prostate tissue samples.

### **Reference**

- [1] D. J. Tindall and P. T. Scardino, "Defeating prostate cancer: Crucial direction for research --- except from the report of the Prostate Cancer Progress Review Group (Review)", *Prostate*, 38(2), 166-171 (1999)
- [2] R. R. Alfano, D. Tata, J. Cordero, P. Tomashefsky, F. Longo, and M. Alfano, "Laser Induced Fluorescence Spectroscopy from Native Cancerous and Normal Tissue", *IEEE J. Quantum Electron*, 20, 1507-1511 (1984).

- [3] M Sadoqi, P Riseborough and S Kumar, "Analytical models for time resolved fluorescence spectroscopy in tissues". *Phys. Med. Biol.*, 46, 2725-2743 (2001).
- [4] "The science of photobiology" by Kendric C. Smith, 2<sup>nd</sup> edition, Plenum press, 1989.
- [5] Donna J. Dean and Brenda J. Korte, "Biomedical Imaging and Bioengineering", *Optics & Photonics News*, October 2003, [http://ultra.bu.edu/papers/2003\\_10\\_OPN.pdf](http://ultra.bu.edu/papers/2003_10_OPN.pdf).
- [6] M. A. Clause and R. K. Jain, "Interstitial Transport of Rabbit and Sheep Antibodies in Normal and Neoplas Tic Tissue", *Cancer Res.*, 50, 3487-3492 (1990).
- [7] D. J. Bornhop, C. H. Contag, K. Licha and C. J. Murphy, "Advances in contrast agents, reporters, and detection", *J. Biomed. Opt.*, 6, 106-110 (2001).
- [8] J. E. Bugaj, S. Achilefu, R. B. Dorshow, R. Rajagopalan, "Novel Fluorescent contrast agents for optical imaging of *in vivo* tumor based on a receptor-targeted dye-peptide conjugate platform", *Journal of Biomedical Optics* 6(2), 122-133 (2001).
- [9] Jean Claude Reubi, Sandra Wenger, Jacqueline Schmuckli-Maurer, Jean-Claude Schaer, and Mathias Gugger, "Bombesin Receptor Subtypes in Human Cancers: Detection with the Universal Radioligand (125) I-[D-TYR(6), beta-ALA(11), PHE(13), NLE(14)] bombesin (6-14)", *Clinical Cancer Research*, Vol. 8, 1139-1146 (2002).
- [10] Y. Pu, W. B. Wang, G. C. Tang, F. Zeng, S. Achilefu, J. H. Vitenson, I. Sawczuk, S. Peters, J. M. Lombardo and R. R. Alfano, "Spectral polarization imaging of human prostate cancer tissue using a near-infrared receptor-targeted contrast agent", *Technology in Cancer Research & Treatment*, Volume 4 429-436, (2005).
- [11] G. R. Fleming, J. M. Morris and G. W. Robinson, "Direct observation of rotational diffusion by picosecond spectroscopy", *Chemical Physics*, 17, 91-100, (1976).
- [12] G. Porter, P. J. Sadkowski and C. J. Tredwell, "Picosecond rotational diffusion in kinetic and steady state fluorescence spectroscopy", *Chemical Physics Letter*, 49, 416-420, (1977).
- [13] F. Pellegrino, P. Sekuler and R. R. Alfano, "Picosecond fluorescence kinetics and polarization anisotropy from anthocyanin pigment", *Photobiochemistry and Photobiophysics*, 2, 15-20, (1981).
- [14] W. B. Wang, S. G. Demos, J. Ali and R. R. Alfano, "Imaging fluorescence objects embedded inside animal tissue using polarization difference technique", *Optical Communications*, 142, 161-166, (1997).
- [15] A. Szabo, "Theory of polarization fluorescent emission in uniaxial liquid crystals", *J. Chem. Phys.* 72(8), 4620-4626, (1980) .

- [16] Ramesh Jain, Rangchar Kasturi and Brian G. Schunck, “*Machine Vision*”, Chapter 6, P218-223, Co-published by MIT Press and McGraw-Hill Inc, ISBN 0-07-032018-7, Copyright@1995 by McGraw-Hill Inc.
- [17] Y. Pu, The Matlab code for the computing the parameters:  $r(0)$ ,  $r_1$  and rotation time can be obtained by reaching the author Y. Pu at [puyang@sci.ccny.cuny.edu](mailto:puyang@sci.ccny.cuny.edu)
- [18] D. A. Beysens, G. Forgacs, J. A. Glazier, “Cell sorting is analogous to phase ordering in fluids”, *Proc. Natl. Acad. Sci. USA.* 97, 9467–9471. (2000).
- [19] Jean Paul Rieu<sup>1</sup> and Yasuji Sawada, “Hydrodynamics and cell motion during the rounding of two dimensional hydra cell aggregates”, *Eur. Phys. J. B.* 27, 167-172 (2002)
- [20] M. A. Dresner, P. J. Rossman, S. A. Kruse and R. L. Ehman, “MR Elastography of the Prostate”, *ISMRM 99 CDs*, <http://cds.ismrm.org/ismrm-1999/PDF2/526.pdf>
- [21] F. Pellegrino, “Energy transfer in the primary stages of the photosynthetic process investigated by picosecond time resolved fluorescence spectroscopy”, A dissertation thesis of the City University of New York, Chapter 9, 270-315, (1981)
- [22] Prostate Cancer Foundation, “Gleason Grade - Prostate Cancer Overview”, [http://www.prostatecancerfoundation.org/site/c.itIWK2OSG/b.47290/k.FC08/Screening\\_Diagnosis\\_and\\_the\\_Gleason\\_Grade.htm](http://www.prostatecancerfoundation.org/site/c.itIWK2OSG/b.47290/k.FC08/Screening_Diagnosis_and_the_Gleason_Grade.htm)
- [23] L. Wang, P. P. Ho, C. Liu, G. Zhang and R. R. Alfano, "Ballistic 2-D imaging through scattering wall using an ultrafast Kerr gate," *Science* 253, 769-771 (1991).

## Figure Captions

Fig. 1. Schematic diagram of the experimental set up used for the time-resolved fluorescence measurements. P<sub>1</sub>, P<sub>2</sub>: polarizers; BS: beam splitter; LP: long pass filter of 830 nm; SIT: silicon intensified target.

Fig. 2. Temporal polarization profiles and polarization anisotropy of fluorescence emitted from Cybesin in 20% aqueous DMSO under a linear polarized 800 nm laser illumination. (a) The profiles of the time-resolved emission components have polarization directions parallel (thick line) and perpendicular (thin line) to the polarization direction of excited light. (b) Calculated time-dependent polarization anisotropy (thin line) using the measured data shown in (a) and equation (1) shown in the text and the fitting curve (thick line) using equation (2) and calculated parameters using Hough transform and the calculated data of polarization anisotropy of Cybesin solution.

Fig. 3. (a) The averaging time-resolved fluorescence intensity emitted from the Cybesin stained cancerous (thick solid line) and normal (thin solid line) prostate tissues when the detection polarization direction is parallel, and cancerous (thin dash line) and normal (thin dot line) prostate tissues when the detection polarization direction is perpendicular to that of excited light at  $\lambda_{\text{pump}}=800$  nm. (b) Calculated time-dependent polarization anisotropy using equation (1) shown in the text and the measured data of temporal polarized fluorescence intensity emitted from the cancerous (thin solid line) and normal (thin dash line) prostate tissues stained by Cybesin under a linear polarized 800 nm laser illumination, and the fitting curves for Cybesin in cancer tissue (thick solid line) and Cybesin in normal tissue (thin solid line) using equation (6) and calculated parameters using Hough transform and the calculated data of polarization anisotropy of Cybesin in cancerous and normal tissue, respectively.

Figs. 4. The schematic diagrams of physical basis of the cell-bonding mechanism and reorientation of Cybesin contained in stained prostate cancer (a) and normal (b) tissues. Cybesin molecules with their absorption transition vectors (arrows) aligned parallel to linearly polarized light (along the vertical page axis) are selectively excited. For free Cybesin molecules, the rapidly rotations contribute fluorescence depolarization. Conversely, Cybesin conjugating to prostate cells show static property. The preferential uptake of Cybesin in human prostate cancerous tissue results in the larger static anisotropy value  $r_1$  of Cybesin-stained cancerous tissue than that of normal tissue.

Figs. 5. Polarization dependence of contrast agent fluorescence emission images of a cancerous and normal prostate tissue sample recorded at  $\lambda_{\text{pump}}=750\text{nm}$  and  $\lambda_{\text{detection}}=850\text{nm}$  when the polarization direction of P<sub>2</sub> is parallel (a) and perpendicular (b) to that of the illuminating light. Fig. 5 (c) is the polarization difference image obtained by subtracting Fig. 5 (b) from Fig. 5 (a). Figs. 5 (d), (e) and (f)

are the digital spatial cross section intensity distributions of the images shown in Figs. 5 (a), (b) and (c) at the row crossing the areas of the stained cancer (C) and normal (N) tissues, respectively.

Fig. 1. Pu, et al

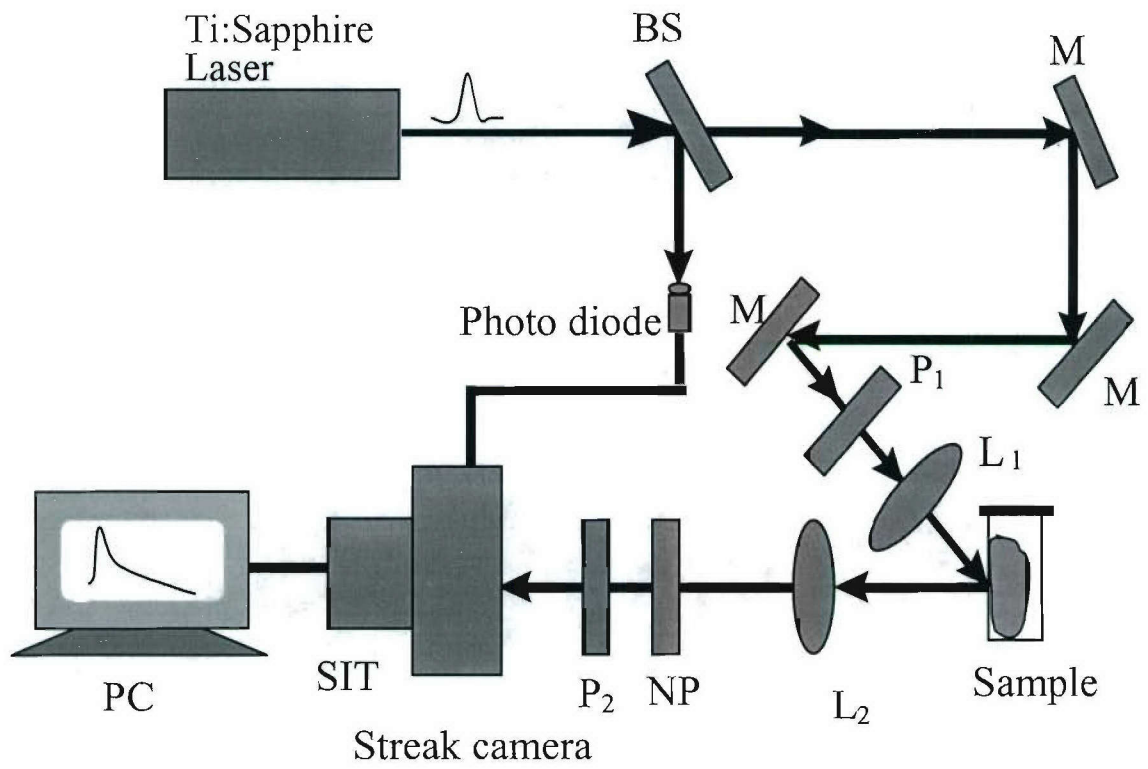
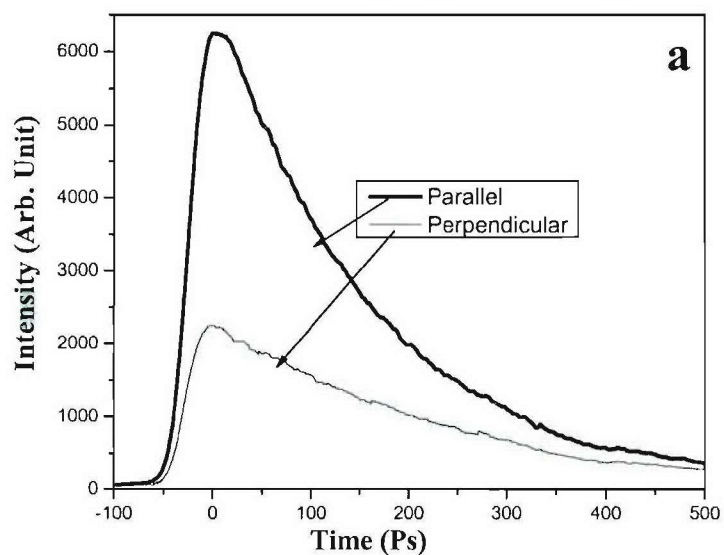


Fig. 2. Pu, et al

Time-resolved fluorescence intensity of Cybesin in 20% aquatic DMSO



Time Resolved Polarization Anisotropy of Cybesin in 20% aquatic DMSO

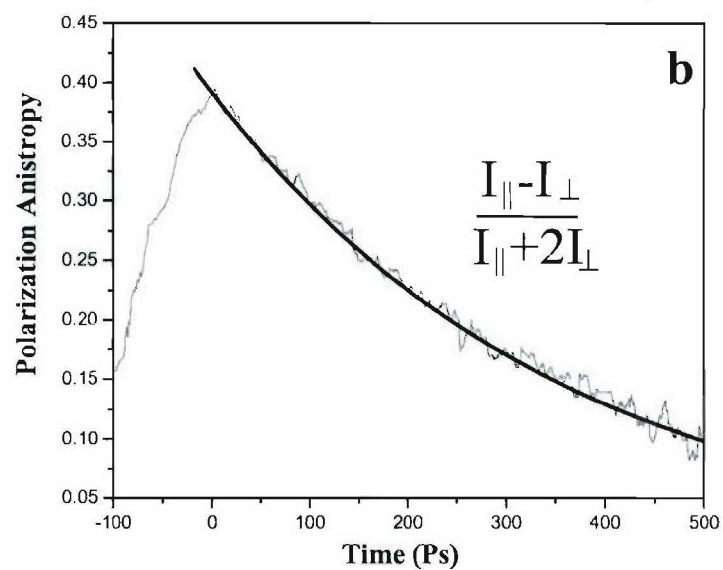
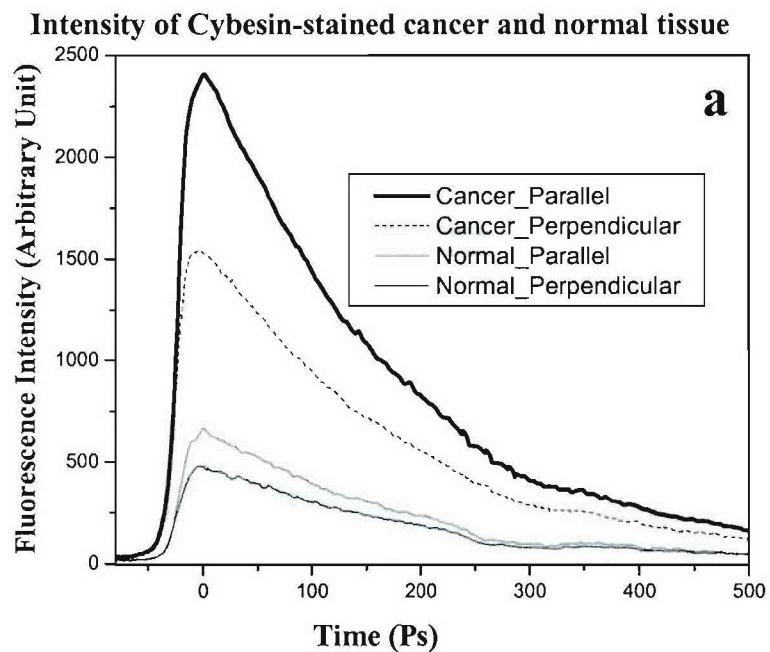
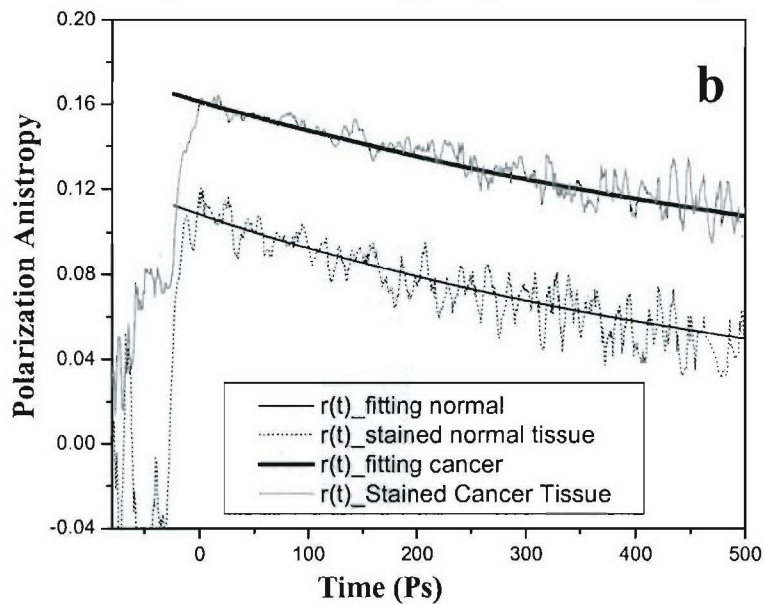


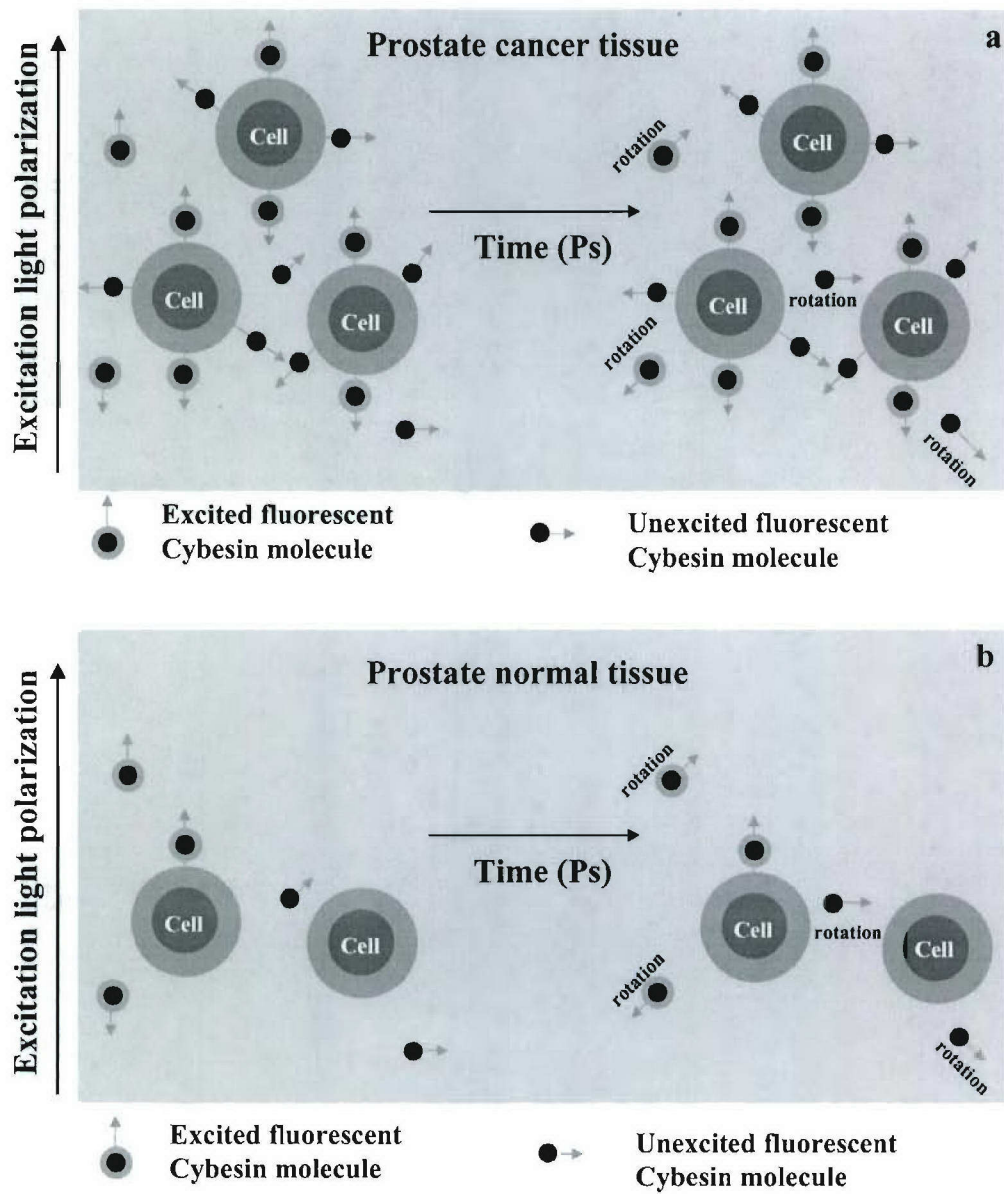
Fig. 3. Pu, et al



**Time-resolved polarization anisotropy of Cybesin stained with prostate tissue**



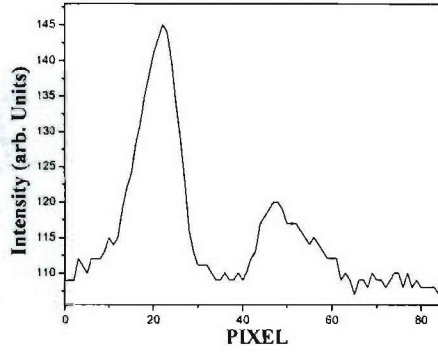
Figs. 4. Pu, et al



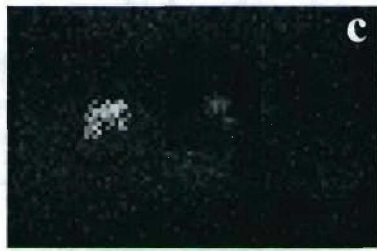
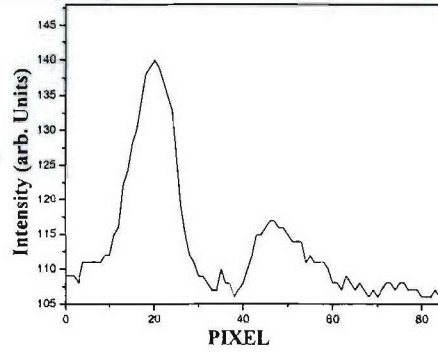
Figs. 5. Pu, et al



Intensity of Spatial Distribution of parallel Emission



Intensity of Spatial Distribution of Perpendicular Emission



Intensity of Spatial Distribution of Polarization Difference

